UNIVERSIDAD COMPLUTENSE DE MADRID
FACULTAD DE MEDICINA
Departamento de Oftalmología y Otorrinolaringología

TESIS DOCTORAL

Estudio de la coroides de la población sana mediante tomografía de coherencia óptica swept-source

Study of the choroid of healthy population using swept-source optical coherence tomography

MEMORIA PARA OPTAR AL GRADO DE DOCTOR

PRESENTADA POR

Jorge Ruiz Medrano

Directores

José María Ruiz Moreno
Julián García Feijóo
Francine Behar-Cohen

Madrid, 2018

UNIVERSIDAD COMPLUTENSE DE MADRID

FACULTAD DE MEDICINA

PROGRAMA DE DOCTORADO

EN CIENCIAS DE LA VISIÓN

DEPARTAMENTO DE OFTALMOLOGÍA

Y OTORRINOLARINGOLOGÍA

ESTUDIO DE LA COROIDES DE LA POBLACIÓN SANA MEDIANTE

TOMOGRAFÍA DE COHERENCIA ÓPTICA SWEPT-SOURCE

STUDY OF THE CHOROID OF HEALTHY POPULATION USING

SWEPT-SOURCE OPTICAL COHERENCE TOMOGRAPHY

JORGE RUIZ MEDRANO

MADRID, 2017

UNIVERSIDAD COMPLUTENSE DE MADRID

FACULTAD DE MEDICINA

PROGRAMA DE DOCTORADO

EN CIENCIAS DE LA VISIÓN

DEPARTAMENTO DE OFTALMOLOGÍA

Y OTORRINOLARINGOLOGÍA

ESTUDIO DE LA COROIDES DE LA POBLACIÓN SANA MEDIANTE

TOMOGRAFÍA DE COHERENCIA ÓPTICA SWEPT-SOURCE

STUDY OF THE CHOROID OF HEALTHY POPULATION USING

SWEPT-SOURCE OPTICAL COHERENCE TOMOGRAPHY

JORGE RUIZ MEDRANO

DIRECTORES:

JOSÉ MARÍA RUIZ MORENO

JULIÁN GARCÍA FEIJÓO

FRANCINE BEHAR-COHEN

MADRID, 2017
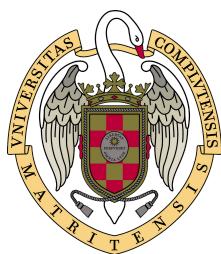
D. JOSÉ MARÍA RUIZ MORENO, Catedrático de Oftalmología de la Facultad de Medicina de Albacete de la Universidad de Castilla La Mancha

CERTIFICA:

Que la presente tesis doctoral titulada "ESTUDIO DE LA COROIDES DE LA POBLACIÓN SANA MEDIANTE TOMOGRAFÍA DE COHERENCIA ÓPTICA SWEPT-SOURCE/STUDY OF THE CHOROID OF HEALTHY POPULATION USING SWEPT-SOURCE OPTICAL COHERENCE TOMOGRAPHY" ha sido realizada bajo nuestra dirección por Don Jorge Ruiz Medrano, Licenciado en Medicina y Cirugía y que reúne las condiciones y requisitos necesarios y suficientes para ser defendida en público y poder acceder al grado de Doctor en Medicina y Cirugía.

Y para que así conste, firmo la presente Certificación en Albacete, a 15 de Diciembre de 2016.

Fdo. Prof. José María Ruiz Moreno

D. JULIAN GARCIA FEIJOO, Catedrático de Oftalmología de la Facultad de Medicina de la Universidad Complutense de Madrid

CERTIFICA:

Que la presente tesis doctoral titulada "ESTUDIO DE LA COROIDES DE LA POBLACIÓN SANA MEDIANTE TOMOGRAFÍA DE COHERENCIA ÓPTICA SWEPT-SOURCE/STUDY OF THE CHOROID OF HEALTHY POPULATION USING SWEPT-SOURCE OPTICAL COHERENCE TOMOGRAPHY" ha sido realizada bajo nuestra dirección por Don Jorge Ruiz Medrano, Licenciado en Medicina y Cirugía y que reúne las condiciones y requisitos necesarios y suficientes para ser defendida en público y poder acceder al grado de Doctor en Medicina y Cirugía.

Y para que así conste, firmo la presente Certificación en Madrid, a 15 de Diciembre de 2016.

Fdo. Prof. J. Garcia Feijoo.

Hôpital ophtalmique
Jules-Gonin
Service universitaire d'ophtalmologie
Fondation Asile des aveugles

UNIL | Université de Lausanne

Au service de
votre santé visuelle

Avenue de France 15 - case postale 133
CH-1000 Lausanne 7

To whom it may concern

Mrs. FRANCINE BEHAR-COHEN, Professor of Ophthalmology at the University of Lausanne,

CERTIFIES:

That the PhD entitled "**STUDY OF THE CHOROID OF HEALTHY POPULATION USING SWEPT-SOURCE OPTICAL COHERENCE TOMOGRAPHY**" has been developed under our supervision by Mr. Jorge RUIZ MEDRANO, MD, and that it gathers the necessary conditions and criteria to be presented and defended in public to grant access to the Degree of Doctor in Medicine and Surgery.

For that purpose, I hereby sing this certification in Lausanne, on December 15th 2016.

Prof. Francine Behar-Cohen

Francine Behar-Cohen, MD, PhD
Chairman of the University Eye Clinic of Lausanne
Medical Director of the Jules Gonin Eye Hospital
Director of the INSERM, UMRS 872, Team 17
Avenue de France 15, CP 133
1000 Lausanne 7 - Switzerland

Informe del Director de la Tesis Doctoral

DATOS DE LA TESIS DOCTORAL	
Nombre del Doctorando	**Jorge Ruiz Medrano**
Título de la Tesis	**"ESTUDIO DE LA COROIDES DE LA POBLACIÓN SANA MEDIANTE TOMOGRAFÍA DE COHERENCIA ÓPTICA SWEPT-SOURCE"** **"STUDY OF THE CHOROID OF HEALTHY POPULATION USING SWEPT-SOURCE OPTICAL COHERENCE TOMOGRAPHY"**
Facultad o Centro	**UCM. FACULTAD DE MEDICINA. HCSC.**

DATOS DEL DIRECTOR DE LA TESIS DOCTORAL	
Nombre Completo	**José María Ruiz Moreno**
Centro al que pertenece en la actualidad	**Facultad de Medicina.** **Universidad de Castilla La Mancha** **02006. Albacete.**
D.N.I/Pasaporte	**16517923J**
e-mail	**josemaria.ruiz@uclm.es**

VALORACIÓN DE LA TESIS				
	Muy Buena	**Buena**	**Suficiente**	**Deficiente**
Originalidad	x			
Definición Objetivos	x			
Metodología	x			
Relevancia Resultados	x			
Discusión / Conclusiones	x			

INFORME (en caso necesario se podrán añadir más hojas):

El trabajo de la Tesis Doctoral puede ser calificada de excelente. Ha sido realizada de acuerdo con la metodología científica y siguiendo los principios éticos de la investigación biomédica. Los objetivos planteados se han completado. La calidad de los resultados obtenidos de gran originalidad y novedosos están avalados por las cinco publicaciones realizadas en revistas de alto factor de impacto. Por ello cuenta con la calidad suficiente para proceder a su defensa.

- Macular choroidal thickness in normal paediatric population measured by Swept-Source optical coherence tomography. **Invest Ophthalmol Vis Sci** 2013;54:353-359
- Macular choroidal thickness profile in a healthy population measured by swept-source optical coherence tomography. **Invest Ophthalmol Vis Sci** 2014;55:3532-42
- Morphologic features of the choroidoscleral interface in a healthy population using swept-source optical coherence tomography. **Am J Ophthalmol** 2015;160:596-601
- Asymmetry in macular choroid thickness profile between both eyes in a healthy population measured by Swept-Source optical coherence tomography. **Retina 2015;**35:2067–2073
- Analysis of age-related Choroidal Layers thinning in Healthy Eyes Using Swept-Source Optical Coherence Tomography. **Retina** 2016; Oct 10. [Epub ahead of print] PMID: 27755379

Fdo.:

RUIZ MORENO
JOSE MARIA –
16517923J

Firmado digitalmente por
RUIZ MORENO JOSE MARIA
- 16517923J
Fecha: 2016.12.29 17:28:02
+01'00'

Albacete, a 15 de diciembre de 2016

Este impreso deberá entregarse a la Comisión Académica responsable del Programa de Doctorado, para su estudio y aprobación en la admisión a trámite de la tesis doctoral, con el fin de que se incluya junto con la documentación enviada a la Comisión de Doctorado para la aprobación, si procede, y designación del Tribunal que ha de juzgar la Tesis Doctoral en el acto de defensa.

Informe del Director de la Tesis Doctoral

DATOS DE LA TESIS DOCTORAL	
Nombre del Doctorando	Jorge Ruiz Medrano
Título de la Tesis	"ESTUDIO DE LA COROIDES DE LA POBLACIÓN SANA MEDIANTE TOMOGRAFÍA DE COHERENCIA ÓPTICA SWEPT-SOURCE" "STUDY OF THE CHOROID OF HEALTHY POPULATION USING SWEPT-SOURCE OPTICAL COHERENCE TOMOGRAPHY"
Facultad o Centro	UCM. FACULTAD DE MEDICINA. HCSC.

DATOS DEL DIRECTOR DE LA TESIS DOCTORAL	
Nombre Completo	Julián García Feijoó
Centro al que pertenece y dirección	UCM. FACULTAD DE MEDICINA. Hospital Clínico San Carlos de Madrid. C/ Profesor Martín Lagos 28040, Madrid
D.N.I/Pasaporte	05273573H
e-mail	jgarciafeijoo@hotmail.com

	VALORACIÓN DE LA TESIS			
	Muy Buena	Buena	Suficiente	Deficiente
Originalidad	x			
Definición Objetivos	x			
Metodología	x			
Relevancia Resultados	x			
Discusión / Conclusiones	x			

INFORME (en caso necesario se podrán añadir más hojas):

La Tesis Doctoral puede ser calificada de excelente. Ha sido realizada de acuerdo con la metodología científica y siguiendo los principios éticos de la investigación biomédica. Los objetivos planteados se han completado. La calidad de la TD está avalada por las dos publicaciones realizadas en revistas de impacto como consecuencia de la TD. Por ello cuenta con la calidad suficiente para proceder a su defensa.

- Macular choroidal thickness in normal paediatric population measured by Swept-Source optical coherence tomography. **Invest Ophthalmol Vis Sci** 2013;54:353-359

- Macular choroidal thickness profile in a healthy population measured by swept-source optical coherence tomography. **Invest Ophthalmol Vis Sci** 2014;55:3532-42

- Morphologic features of the choroidoscleral interface in a healthy population using swept-source optical coherence tomography. **Am J Ophthalmol** 2015;160:596-601

- Asymmetry in macular choroid thickness profile between both eyes in a healthy population measured by Swept-Source optical coherence tomography. **Retina** 2015;35:2067–2073

- Analysis of age-related Choroidal Layers thinning in Healthy Eyes Using Swept-Source Optical Coherence Tomography. **Retina** 2016; Oct 10. [Epub ahead of print] PMID: 27755379

Madrid, a 29 de diciembre de 2016

Fdo.:

PhD Director Report

PhD Information	
PhD Candidate	Jorge Ruiz Medrano
PhD Title	"ESTUDIO DE LA COROIDES DE LA POBLACIÓN SANA MEDIANTE TOMOGRAFÍA DE COHERENCIA ÓPTICA SWEPT-SOURCE" "STUDY OF THE CHOROID OF HEALTHY POPULATION USING SWEPT-SOURCE OPTICAL COHERENCE TOMOGRAPHY"
Centre	UCM. FACULTAD DE MEDICINA. HCSC.

PhD Director Information	
Complete Name	Francine Behar-Cohen
Centre and Adress	Université de Lausanne Hôpital Ophthalmique Jules Gonin, Fondation Asile des Aveugles. Avenue de France 15, 1000, Lausanne, VAUD (Switzerland)
Passeport	14DF 67 874
e-mail	francine.behar@gmail.com

	EVALUATION			
	Very Good	**Good**	**Pass**	**Fail**
Originality	X			
Objective definition	X			
Methods	X			
Results relevance	X			
Discussion / Conclusions	X			

REPORT:

This PhD work can be classified as excellent. It has been done following scientific methodology and the tenets of biomecical investigation. All objectives set were completed. The quality of the results obtained is backed by the 5 papers published in international journals with high impact factor. It has enough quality to procedd with its defense.

- Macular choroidal thickness in normal paediatric population measured by Swept-Source optical coherence tomography. Invest Ophthalmol Vis Sci 2013;54:353-359
- Macular choroidal thickness profile in a healthy population measured by swept-source optical coherence tomography. Invest Ophthalmol Vis Sci 2014;55:3532-42
- Morphologic features of the choroidoscleral interface in a healthy population using swept-source optical coherence tomography. Am J Ophthalmol 2015;160:596-601
- Asymmetry in macular choroid thickness profile between both eyes in a healthy population measured by Swept-Source optical coherence tomography. Retina 2015;35:2067–2073
- Analysis of age-related Choroidal Layers thinning in Healthy Eyes Using Swept-Source
Optical Coherence Tomography. Retina 2016; Oct 10. [Epub ahead of print] PMID: 27755379.

Lausanne, 19th December 2016

Signed:
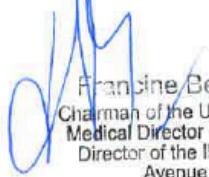
Francine Behar-Cohen, MD, PhD
Chairman of the University Eye Clinic of Lausanne
Medical Director of the Jules Gonin Eye Hospital
Director of the INSERM, UMRS 872, Team 17
Avenue de France 15, CP 133
1000 Lausanne 7 - Switzerland

COPYRIGHT

1. Ruiz-Moreno JM, Flores-Moreno I, Lugo F, Ruiz-Medrano J, Montero JA, Akiba M. Macular choroidal thickness in normal pediatric population measured by swept-source optical coherence tomography. Invest Ophthalmol Vis Sci. 2013;54:353-9. doi: 10.1167/iovs.12-10863.
2. Ruiz-Medrano J, Flores-Moreno I, Peña-García P, Montero JA, Duker JS, Ruiz-Moreno JM. Macular choroidal thickness profile in a healthy population measured by Swept-Source Optical Coherence Tomography. Invest Ophthalmol Vis Sci. 2014;55:3532-42. doi: 10.1167/iovs.14-13868.
3. Ruiz-Medrano J, Flores-Moreno I, Montero JA, Duker JS, Ruiz-Moreno JM. Morphological features of the choroidoscleral interface in a healthy population using Swept-source Optical Coherence Tomography. Am J Ophthalmol 2015;160:596-601. doi: 10.1016/j.ajo.2015.05.027.
4. Ruiz-Medrano J, Flores-Moreno I, Peña-García P, Montero JA, Duker JS, Ruiz-Moreno JM. Asymmetry in macular choroidal thickness profile between both eyes in a healthy populations measured by Swept-Source optical coherence tomography. Retina 2015;35:2067-73. doi: 10.1097/IAE.0000000000000590.
5. Ruiz-Medrano J, Flores-Moreno I, Peña-García P, Montero JA, García-Feijóo J, Duker JS, Ruiz-Moreno JM Analysis of age-related Choroidal Layers thinning in Healthy Eyes Using Swept-Source Optical Coherence Tomography. Retina 2016 (epub ahead of print).
6. Ruiz-Medrano J, Ruiz-Moreno JM, Goud A, Vupparaboina KK, Jana S, Chhablani J. Age-related changes in choroidal vascular density of healthy subjects based on image binarization of Swept-Source Optical Coherence Tomography. Retina 2017 (accepted).

A mi familia,

AGRADECIMIENTOS

Me gustaría aprovechar estas líneas para poder dar las gracias a todas las personas que han colaborado en este trabajo y me han ayudado de una manera directa o indirecta a poder hacerlo posible.

Mi decisión de realizar un proyecto de tesis doctoral viene de muy lejos, motivada por el hecho de haber crecido con dos doctores en medicina en casa, que me han servido siempre de ejemplo y motivación para tratar de ser mejor en todos los aspectos. Como me han dicho siempre: "las cosas, si se hacen, se hacen bien".

Este trabajo comenzó justo antes de empezar la residencia, hace ya cinco años, cuando tuve la oportunidad de colaborar en el primer trabajo de esta línea de investigación y me enseñaron a medir la primera coroides. Gracias de corazón al **Dr. Ignacio Flores Moreno** por la ayuda durante esas largas tardes de mediciones, por todas las vitrectomías, las ganas que tiene de enseñar y los ratos fuera del trabajo.

Gracias a **Pablo Peña García** por todo el trabajo estadístico que ha llevado a cabo durante estos años y por las largas explicaciones telefónicas para tratar de hacerme ver todo lo que se podía sacar de las tablas y gráficas que nos proporcionó.

A mis compañeros de residencia, muchos de los cuales han llegado a ser para mí no sólo compañeros de trabajo, sino grandes amigos. A mis compañeros de promoción, en especial a los **Dres. Jorge Peraza y Pilar Cifuentes**, porque sinceramente creo que hemos hecho un gran equipo y de verdad espero que volvamos a tener la suerte de trabajar juntos en el futuro.

A mis amigos los **Dres. José Fernández-Vigo y Gabriel Arcos**, por todas esas horas de guardias que pasamos juntos, y que gracias a ellos no fueron tan largas; los congresos, los partidos de fútbol, el Tour de Francia y los largos en la piscina.

Al **Dr. Jay S Duker** por sus valiosas revisiones y comentarios que tanto han ayudado a la hora de conseguir estas publicaciones.

Considero fundamental dar las gracias a mis directores de tesis: Gracias al **Profesor Julián García Feijóo**, mi Jefe de Servicio durante la residencia, por toda la ayuda durante estos años y las facilidades a la hora de ampliar fronteras con la formación, que me han permitido ver cómo se trabaja en Milán, Barcelona, Albacete, Manchester y Lausana. A la **Profesora Francine Behar-Cohen** por darme la gran oportunidad de la que ahora estoy disfrutando, con este puesto de Fellow de Retina y Oncología en el Hospital Oftálmico Jules Gonin de Lausana y por sus ganas de transmitir a todo el mundo su pasión por la investigación.

Al **Dr. Luis Arias Barquet** y a su equipo, por los dos meses increíbles que pasé en la sección de retina del Hospital Universitario de Bellvitge, por la confianza que mostró en mí todos los miércoles en quirófano permitiéndome operar sin importarle la dificultad del caso, por su calma y por todo lo que me enseñó en tan poco tiempo.

A mis hermanos, **Guillermo y Magali**, porque a pesar de que no puede haber tres hermanos tan diferentes, tampoco los puede haber mejores.

Un agradecimiento muy especial para **Rosa**, por estos cinco años fantásticos y los que nos quedan por delante, por todos los ratos robados para llevar a cabo este trabajo y por estar SIEMPRE ahí para mí. Gracias.

A mi madre. Por ser la persona más fuerte que conozco y enseñarme cosas mucho más importantes que las que te puedan enseñar en una Facultad de Medicina. Gracias.

Y principalmente **a mi padre, el Profesor José María Ruiz Moreno**, director de este proyecto de tesis, sin el cual esto no habría sido posible. Gracias por haberme transmitido el amor por esta profesión desde niño. Por su esfuerzo constante, por su dedicación, por su entrega, su increíble capacidad de trabajo, su apoyo constante y su ayuda inestimable. Por su comprensión y sobre todo por su ejemplo. MUCHAS GRACIAS.

LISTADO DE ABREVIATURAS

AFG: Angiografía fluoresceínica

AVI: Angiografía con verde de indocianina

CSC: Coriorretinopatía serosa central

CT: Choroidal thickness

D: Dioptrías / Diopters

DMAE: Degeneración macular asociada a la edad

EDI-OCT: Enhanced depth imaging optical coherence tomography

EE: Equivalente esférico

EPR: Epitelio pigmentario de la retina

ICGA: Indocyanine Green Angiography

MCT: Macular choroidal thickness

MM: Miopía magna/miope magno

NVC: Neovascularización coroidea

OA-OCT: Óptica adaptativa OCT

OCT: Tomografía de coherencia óptica

OCTa: Angiografía OCT

PIO: Presión intraocular

RPE: Retinal pigment epithelium

SD-OCT: Tomografía de coherencia óptica de dominio espectral

SE: Spherical equivalent

SS-OCT: Tomografía de coherencia óptica Swept-Source

TD-OCT: Tomografía de coherencia óptica de dominio tiempo

US: Ultrasonidos

VEGF: Factor de crecimiento vascular endotelial

ÍNDICE:

1. INTRODUCCIÓN

1. INTRODUCCIÓN

1.1 DEFINICIÓN

La coroides es un tejido pigmentado y densamente vascularizado que forma parte de la úvea, la capa media del ojo y que se sitúa entre la esclerótica y la retina. Alcanza desde el nervio óptico hasta la *ora serrata*, continuándose en su parte más anterior con el cuerpo ciliar y la raíz del iris. Entre sus funciones encontramos el aporte de oxígeno y nutrientes a la retina externa, así como la absorción de luz gracias a su alta densidad de pigmento, imprescindible para la visión. Mide 0,22 mm en el polo posterior y entre 0,1 y 0,15 mm en la zona más anterior en estudios anatomopatológicos *post-mortem*,[1] aunque alcanzada la vejez puede reducirse hasta entorno a las 80 μm.[2]

Está compuesta de vasos derivados de la anastomosis de las arterias ciliares posteriores, que proceden a su vez de la arteria oftálmica. Éstas atraviesan la esclerótica posteriormente en un número que se sitúa entorno a 15-20 y a una distancia de 5-6 mm del nervio óptico. Las arterias se ramifican en arteriolas que terminan en los lóbulos coriocapilares. Éstos drenan su contenido hacia las vénulas, que convergen y salen del ojo a nivel del ecuador en forma de 4-5 venas vorticosas.[3] Ocasionalmente es posible encontrar una vena vorticosa que denominamos ciliovaginal, que está localizada en el polo posterior y que sale del globo ocular cerca del nervio óptico o a través del mismo. Las venas vorticosas atraviesan la esclerótica en un trayecto oblicuo para acabar uniendo a las venas oftálmicas superior o inferior.

La coroides es un tejido derivado de la cresta neural y el mesénquima periocular. La coriocapilar empieza su desarrollo entorno a la 4ª-5ª semana de gestación. Su endotelio se reduce a un espesor de una sola célula y da lugar a sus típicas fenestraciones alrededor de la 9ª semana. Una vez alcanzado el final del primer trimestre la coriocapilar es prácticamente idéntica a la forma adulta. El resto de capas comienzan su desarrollo en la semana 15, momento en que arteriolas y vénulas empiezan a formarse, siento identificables a las 22 semanas.[4]

1.2   EMBRIOLOGÍA E HISTOLOGÍA

La vesícula óptica se forma a partir de una protrusión del neuroectodermo y se invagina sobre sí misma para formar una copa óptica de doble pared. La más externa dará lugar al EPR mientras que la interna está destinada a convertirse en el resto de capas de la retina. La parte más inferior muestra dos bordes donde se une el tejido que es la fisura coroidea y es por ahí por donde la arteria hialoidea penetra en el ojo. La úvea se forma a partir del mesodermo y del tejido neuro-ectodérmico que rodean a la copa óptica. Las células mesodérmicas que la rodean se diferencian en vasos al mismo tiempo que se desarrolla el EPR. La capa coriocapilar comienza a formarse entorno a la 5ª o 6ª semana de desarrollo embrionario y es entorno a la semana 6 que la membrana de Bruch empieza a ser reconocible.[4,5] La coriocapilar se organiza con anterioridad al desarrollo del resto de la coroides. Las arterias ciliares posteriores penetran en el tejido coroideo entorno a la 8ª semana de gestación y no maduran hasta la semana 22.

Los precursores de los melanocitos migran hacia la úvea en formación desde la cresta neural a finales de la 4ª semana y empiezan el proceso de diferenciación hacia el séptimo mes. La pigmentación de la coroides empieza de atrás hacia delante, desde el nervio óptico hasta la ora serrata y se completa entorno al mes 9.[6]

Histológicamente la coroides puede dividirse en 5 capas diferentes: La membrana de Bruch; la coriocapilar; la capa de medianos vasos o capa de Sattler; la capa de grandes vasos o capa de Haller; y el espacio supracoroideo.[7]

La membrana de Bruch es una matriz extracelular localizada en el límite entre la retina y la coroides. Se extiende anteriormente hasta la *ora serrata* y se continúa por un tejido que se le asemeja hasta el cuerpo ciliar. Cumple funciones importantes como sustrato del EPR por un lado y de las paredes vasculares de la coriocapilar por otro. Está compuesta en su mayoría de fibras elásticas y fibras de colágeno y tiene un espesor de entre 2 y 4 µm y puede ser dividida a su vez en 5 capas: La membrana basal del EPR, capa colágena interna, capa de tejido elástico, capa colágena externa y membrana basal del endotelio coriocapilar.

La membrana basal del EPR es un entramado de fibras de colágeno tipo IV, semejante al resto de membranas basales del cuerpo. Contiene el mismo tipo de colágeno IV que las membranas basales del glomérulo renal, con funciones de filtro y transporte.[8] La capa colágena interna contiene fibras de colágeno de tipo I, III y V que se cruzan en un plano paralelo a la membrana de Bruch y que se relacionan con condroitin sulfato y dermatan sulfato mayoritariamente.[8] La capa de tejido elástico está compuesta por colágeno tipo VI, fibronectina y una serie de capas de 0,8 µm apiladas de fibras elásticas entrecruzadas, que dejan espacios de aproximadamente

1 μm.[9] Tiene un papel mecánico y como función de barrera antiangiogénica. La capa colágena externa, cuyo grosor oscila entre 1 y 5 μm, muestra una composición similar a la capa colágena interna, pero a diferencia de ésta, presenta una serie de protrusiones en los espacios intervasculares de la coriocapilar llamadas columnas intercapilares.[2] Por último la membrana basal del endotelio de la coriocapilar es una membrana de 0,07 μm cuya función teórica sería inhibir la migración celular endotelial hacia la membrana de Bruch al igual que hacen las láminas basales asociadas a los capilares retinianos.

La coriocapilar es la más interna de las capas vasculares de la coroides. Está compuesta por un entramado de capilares fenestrados que cumplen la importante función del aporte de nutrientes y oxígeno para el EPR, la capa de fotorreceptores, la capa plexiforme externa y la parte más externa de la capa nuclear interna. La fenestración de esta red vascular es la que permite la libre circulación e intercambio entre coroides y retina, mayoritariamente moléculas pequeñas y solutos que son capaces de atravesar los poros de entorno a 60-70 nm que se sitúan en sus paredes. Asimismo, la mayoría de las fenestraciones así como los tres tipos de receptores del factor de crecimiento vascular endotelial (VEGF) se sitúan de cara a la retina principalmente, mientras que la densidad de pericitos es mayor del lado más escleral.[10] Según algunos autores, esta red es más densa en la zona situada bajo la fóvea, alcanzando un espesor teórico de unas 10 μm, en comparación con las 7 μm de zonas más periféricas.[11]

La capa de medianos vasos o capa de Sattler está formada por las pequeñas arteriolas que suministran a la coriocapilar, formando una red capilar de distribución

lobular semejante a los glomérulos renales. Estos lóbulos varían en forma, tamaño y densidad vascular dependiendo de dónde se sitúen y de la localización relativa de las arteriolas nutricias y de las vénulas de drenaje. La capa de Haller, más externa, está formada por vasos de un calibre mayor y no guarda un patrón claro. El estroma en que están embebidos estos vasos está formado en su mayoría por fibroblastos, células musculares lisas, mastocitos, linfocitos, macrófagos, melanocitos y células nerviosas. Las arterias y las venas coroideas no siguen un curso estrictamente paralelo de forma que una sección que recibe aporte sanguíneo de una arteria no tiene por qué corresponder exactamente con la sección que drena a una vena. Siempre hay cierta superposición entre segmentos arteriales adyacentes.[5]

El espacio supracoroideo constituye la capa más externa de la coroides, siendo una capa de transición entre ésta y la esclerótica.[7] Este espacio no es visible utilizando las técnicas de imagen habituales, que después veremos en mayor detalle, en el caso de pacientes normales, pero sí en el caso de determinadas patologías. Por el contrario, en el caso de las muestras histológicas aparece artefactada, viéndose mucho más grande tras el procesado de las muestras

Los vasos que constituyen la coroides están rodeados por un plexo nervioso que recibe inervación de los sistemas simpático y parasimpático. Asimismo, se han hallado células ganglionares en la proximidad de los vasos coroideos de mayor calibre. La función de esta inervación coroidea no está clara hoy en día, pero dado que estas fibras muestran una tinción positiva para óxido nítrico sintasa y péptido intestinal vasoactivo, los hay que defienden la teoría de que cumplen una función reguladora del flujo sanguíneo.[11,12]

28

1.3   FUNCIONES

La retina es uno de los tejidos con mayor actividad metabólica del cuerpo humano y recibe oxígeno de dos vías diferentes: la circulación retiniana y la coroides, siendo el aporte del mismo su función principal.

Los dos tercios más internos de la retina dependen de la circulación retiniana, cuyo origen se encuentra en la arteria central de la retina. Es una red vascular con capacidad de autorregulación ya que es capaz de responder a las variaciones en los niveles de oxígeno y de esta forma mantener unos niveles relativamente constantes en el tejido retiniano. La retina externa y el epitelio pigmentario, por otra parte, dependen en exclusiva del aporte de oxígeno por parte de la circulación coroidea. Asimismo, la coroides peripapilar juega un papel importante en lo que se refiere al aporte sanguíneo de la parte más anterior del nervio óptico.[13]

La creencia generalizada es que a diferencia de la vascularización retiniana, los vasos de la coroides no poseen capacidad de autorregulación, de manera que los niveles de oxígeno de estas estructuras dependen directamente de los niveles de oxígeno sistémico.[14] Los hay, sin embargo, que creen que la coroides podría tener cierta capacidad de autorregulación, basándose en la ya descrita presencia de células ganglionares y de mastocitos en proximidad a los grandes vasos coroideos.[11,12]

Hayreh explica en sus trabajos como el flujo coriocapilar está en función de diferentes gradientes de presión, lo que permite que las regiones que hayan sufrido un descenso de aporte sanguíneo por problemas en su arteria nutricia reciban lo necesario. La práctica totalidad de los tejidos corporales muestran algún tipo de autorregulación, pero como acabamos de explicar, el caso de la coroides es

controvertido. Mientras que algunos defienden que la coroides no puede autorregularse cuando la perfusión se reduce a causa de un aumento de presión intraocular (PIO),[15] otros han demostrado que el flujo coroideo varía con la PIO,[16] la producción endógena de óxido nítrico y la acción de las células ganglionares coroideas.[12]

Otra de las explicaciones propuestas para justificar que la autorregulación de la coroides no es completa es el hecho de que a pesar de que el flujo coroideo es mucho mayor que el de otros tejidos, la extracción de oxígeno se mantiene baja. La autorregulación debería ajustar el flujo sanguíneo a las necesidades del tejido concreto. En el caso que nos ocupa, la elevada presión parcial de oxígeno y la baja extracción del mismo implican que el flujo coroideo se mantiene a un nivel mucho mayor de lo que en teoría dictarían las necesidades de la coroides o el EPR. Además, se hace difícil pensar que pueda existir una comunicación o una autorregulación directa entre los elipsoides de los fotorreceptores, donde se encuentran las mitocondrias que consumen la gran mayoría del oxígeno empleado, y la capa coriocapilar, ya que existen enfermedades que afectan directamente a la retina externa y no se asocian con una reducción del espesor coroideo.[17]

Otra de las funciones clásicas atribuidas a la coroides es la de mejorar la función óptica. Al ser un tejido altamente pigmentado puede la absorción de la luz dispersada, mientras que protege indirectamente del estrés oxidativo. Hay autores que defienden que el hecho de vivir en un medio con una presión parcial de O_2 elevada junto con la exposición permanente a la luz pueden ser factores de riesgo para la transformación maligna en melanomas. Hay autores que han propuesto otras

teorías para el alto flujo de sangre que recibe la coroides. Entre ellas se incluye una función de refrigeración del calor que se genera por el gran rendimiento metabólico de la retina externa, pero estas hipótesis están en duda, ya que la teórica vasodilatación que debería tener lugar en condiciones de aumento de temperatura no se ha demostrado en ojos normales.[5]

1.4   MÉTODOS DE ESTUDIO

El estudio de la coroides se ha disparado en la pasada década gracias a varios descubrimientos en técnicas de imagen que han permitido una visualización y medición más rápidas y precisas.

1.4.1   ULTRASONOGRAFÍA

En 1956 las técnicas ultrasónicas (US) fueron utilizadas por primera vez para el diagnóstico de enfermedades oculares.[18] Algunos utilizaron las llamadas técnicas de modulación de intensidad (modo B) que requerían la inmersión de los ojos en agua, mientras se obtenía una tomografía acústica del ojo gracias a un movimiento de barrido de un cristal frente a la estructura a examinar. Otros usaban métodos de amplitud-tiempo (modo A), en los que el eje *x* de la pantalla conforma el eje tiempo y el eje *y* conforma el eje de amplitud del eco.[19]

A pesar de que la coroides normal no podía ser medida, y algunos autores afirmaron que lesiones de menos de 4,0 mm de altura no podían ser completamente evaluadas,[20] los melanomas coroideos y desprendimientos de retina podían encontrarse en casos en los que penetraban en la cavidad vítrea en al menos entre

1,5 y 2,0 mm. La sangre sub-retiniana coagulada suponía un difícil diagnóstico diferencial en aquel momento. Las sondas ultrasónicas de contacto fueron introducidas en los años setenta, con evoluciones continuas y mejoras en la sensibilidad.

A lo largo de las dos últimas décadas la revolución de la tecnología en formato digital ha traído cambios en las técnicas de exploración y almacenamiento de datos, junto con grandes mejoras en la calidad de imagen.[21]

El melanoma coroideo es el tumor intraocular maligno más común, y a pesar de la aparición de nuevas técnicas de imagen, la ecografía es todavía de gran utilidad. Antes de su aparición, los melanomas tan sólo se sospechaban cuando una masa visible podía ser apreciada a través de medios transparentes, e incluso en casos en los que una masa es visible, el diagnóstico puede que no sea tan evidente.[22] Pero es en casos de medios opacos cuando el US es de mayor utilidad. Los patrones ultrasónicos de masas coroideas son aún cruciales para establecer un buen diagnóstico diferencial.[22]

1.4.2   ANGIOGRAFÍA

La angiografía con fluoresceína (AFG) y la angiografía con verde indocianina (AVI) se han practicado durante décadas para obtener información clínica útil sobre la retina y la coroides.[23,24]

La AFG se desarrolló en los años 60 para el estudio de tumores coroideos,[25,26] y se utilizó fundamentalmente para estudiar la vascularización retiniana, por lo que algunos de los primeros autores en utilizar este contraste estudiaron la circulación

coroidea a lo largo de las primeras fases del angiograma o a través de áreas de atrofia retiniana, que hacían más visibles y más fáciles de distinguir a los vasos coroideos.[24,25]

Mientras tanto, la AVI fue el primer colorante utilizado en la industria fotográfica y fue aplicado por primera vez con fines clínicos en 1972 cuando Flower intentó describir y captar en imagen la vascularización coroidea.[23] La indocianina es una sustancia lipofílica e hidrofílica con una alta capacidad de unión a proteínas plasmáticas (hasta un 98%).[27] Éstas muestran un mayor peso molecular que la albúmina, lo que otorga a la indocianina una menor permeabilidad vascular y penetración en tejidos. Esto la diferencia de la fluoresceína, y nos permite realizar un mejor estudio de la vascularización coroidea. Se metaboliza por el hígado y se excreta vía biliar.

Se inyecta vía intravenosa utilizado concentraciones de 5 mg/ml y para capturar su circulación son necesarios filtros de excitación y de barrera con picos de 805 y 835 nm respectivamente. Las imágenes se toman normalmente desde 8-10 hasta 40 minutos después de la inyección del colorante.[28] Estudios posteriores sugirieron que estadios más tempranos de la AVI podían ser útiles para localizar los vasos nutricios de los complejos de neovascularización coroidea (NVC) y así ayudar a guiar tratamientos focales de los mismos.[29]

Fue de hecho la degeneración macular asociada a la edad (DMAE) la que centró la gran mayoría de los estudios realizados usando AVI, pero también ha resultado de ayuda para los investigadores en la fisiología de ciertas alteraciones inflamatorias coriorretinianas, así como patologías del segmento anterior.[27]

La mejor forma de visualizar la vascularización coroidea es mediante la AVI, y no está limitado a casos en los que puedan encontrarse zonas de atrofia del EPR y la coriocapilar como en el caso de AFG.[30] Teniendo en cuenta que la coroides es un tejido tridimensional y que las imágenes que se obtienen son reproducidas en dos dimensiones, es importante tener un apropiado conocimiento de la anatomía de la coroides para poder levar a cabo una interpretación precisa de la angiografía. Variaciones anatómicas normales del drenaje sanguíneo, entre otras cosas, muestran un patrón asimétrico en hasta el 50% de los pacientes, con preferencia por una de las venas vorticosas, que puede llevar a interpretaciones erróneas.[31]

La AVI resulta ser especialmente útil para la detección de NVC recurrente en casos difíciles, como desprendimientos del epitelio pigmentario (DEP) o áreas adyacentes a cicatrices de láser.[32,33] Es más precisa que el AFG para la localización de NVC debajo de hemorragias subretinianas o sub-EPR debido a la mayor capacidad de penetración que otorga la luz infrarroja.[34]

La AVI se ha convertido en la herramienta más útil para la detección de pólipos maculares, extramaculares o peripapilares.[11] También es utilizada para localizar los puntos de fuga en la coroides o los vasos coroideos dilatados en pacientes con coroidopatía serosa central (CSC).[35,36]

1.4.3   TOMOGRAFÍA DE COHERENCIA ÓPTICA

Desde su desarrollo original hace más de veinte años, la tomografía de coherencia óptica (OCT) se ha convertido en una herramienta casi indispensable en el día a día del estudio del paciente con patología retiniana, ya que permite el estudio del

paciente de una manera rápida, "in vivo" y no invasiva. Esta tecnología comenzó su desarrollo en los años 80, siendo las primeras imágenes similares a las ecografías en modo A.[37] En 1992, fueron desarrolladas las imágenes transversales en dos dimensiones, con los primeros escáneres de retina para humanos "in vivo" viendo la luz en 1993.[38]

La OCT se basa en el principio de la interferometría de baja coherencia. Se dirige un haz de luz de baja coherencia al tejido objetivo (habitualmente el área macular o el nervio óptico) y la luz que se refleja en el tejido de manera dispersa es combinada con un haz de luz de referencia produciendo un patrón de interferencia. Éste es utilizado para construir un A-scan axial que no es sino la representación de las propiedades dispersivas de los tejidos que han sido alcanzado por la luz. De la combinación de diferentes A-scans con distintos puntos de incidencia podemos generar un B-scan, que es la representación en dos dimensiones de un corte transversal de la zona estudiada.[38]

Los primeros modelos de OCT fueros denominados OCT de dominio tiempo (TD-OCT). Esta tecnología utilizaba un único detector y los A-scans eran generados a base de mover un espejo para modificar el haz de referencia y así estudiar el tejido en diferentes planos de profundidad. El principal inconveniente era la velocidad de exploración, que junto con la falta de resolución y de penetrancia en los tejidos hicieron que esta tecnología quedara rápidamente obsoleta.[38,39]

A continuación en el año 2006 apareció el OCT de dominio espectral o de dominio Fourier que utiliza múltiples detectores en lugar de múltiples rayos de referencia generado a partir de un espejo en movimiento para obtener los A-scans.

Su velocidad es aproximadamente de unos 30000 A-scans por segundo, llegando a alcanzar los 100000. La resolución axial de estos aparatos se sitúa entorno a las 5 μm y la resolución lateral, limitada por la difracción de la pupila es de unas 20 μm. La velocidad de el SD-OCT nos ha permitido también obtener imágenes de una mayor calidad al reducir el ruido en las mismas, que es el responsable del aspecto poco definido de algunos B-scans. Al adquirir, guardar y combinar múltiples tomas de un mismo B-scan situado en una misma posición conseguimos una imagen promedio, con mínimo ruido y una definición mucho más alta.[39] Poco después fue desarrollado el software para el "eye-tracking" ocular, que nos ayudó a asegurarnos de que las imágenes se obtienen en la misma localización exacta en diferentes exploraciones. Sin embargo, a pesar de las obvias ventajas sobre el TD-OCT, las distorsiones y atenuaciones en la señal debidas a la presencia de tejidos pigmentados u opacidades de medios hacían aún difícil la obtención de imágenes de la coroides con buena calidad en la mayoría de los ojos.

Más tarde, Spaide publicó los primeros artículos utilizando la nueva técnica "enhanced-depth imaging" OCT (EDI-OCT), que proporcionaba una visualización consistente de la coroides en la mayoría de los ojos y que permitió mediciones de espesor reproducibles y precisas.[5,40,41] Una de las consecuencias de utilizar una transformación Fourier para descodificar la señal de interferometría es la aparición de dos imágenes conjugadas. Sin embargo, sólo una de ellas es utilizada o mostrada en la mayoría de aparatos utilizados en la práctica clínica habitual, habitualmente la que muestra la retina hacia la parte superior de la pantalla y la coroides debajo de ésta. Si modificamos el punto de foco para ubicarlo en la esclerótica interna, las

estructuras profundas como la coroides pueden verse con mucha mayor definición. De esta forma la imagen conjugada e invertida aparece en pantalla, mientras que la imagen con orientación clásica aparece en blanco debido a la falta de información.

De esta forma ganamos unas 500-800 µm de penetrancia en los tejidos oculares, que en ciertos pacientes con coroides más delgadas como puedan ser los miopes magnos (MM) o los pacientes con DMAE, puede permitirnos visualizar la práctica totalidad de la esclerótica e incluso la grasa orbitaria. Pero con todas estas ventajas también surge un inconveniente, y es el hecho de que al obtener la máxima sensibilidad de imagen en la coroides, perdemos calidad en la visualización del vítreo.

Las técnicas más recientes para imágenes de OCT consisten en una OCT con una longitud de onda más larga y alta penetración: el OCT Swept-Source (SS-OCT).[42–44] El SS-OCT utiliza un laser sintonizable que funciona a 100000 Hz con una longitud de onda entorno a 1 mm. Estos aparatos pueden realizar un promedio de imágenes de hasta 96 B-scans en la misma posición, y en caso de utilizar el modo de exploración de una línea sencilla genera imágenes que llegan a contener un promedio de hasta 1024 A-scans y una longitud de 12 mm.[45] De acuerdo con algunas publicaciones, el espesor coroideo puede ser medido de forma fiable con este dispositivo hasta en el 100% de los pacientes.[46,47]

Los vasos de la retina tienen una apariencia hiper-reflectiva en las imágenes de OCT, al tiempo que los vasos de la coroides son hipo-reflectivos. Esta diferencia parece estar relacionada con la velocidad de las células sanguíneas que van a través de los vasos de cada tejido. La velocidad con la que fluye la sangre dentro de los

vasos de la coroides es mucho más alta que la velocidad con la que fluye en los vasos de la retina. Como ha sido explicado con anterioridad, las producción de imágenes de OCT está basada en la interferometría, donde un margen de interferencia es detectado para generar la intensidad de la señal. La alta velocidad de las células sanguíneas hace que el margen de interferencia se desvanezca, por lo que no se observa ninguna señal dentro de los vasos de la coroides. Por otro lado, la velocidad de las células sanguíneas es relativamente baja en el caso de estructuras vasculares retinianas, lo que contribuye a la señal de interferencia como una señal hipereflectiva.[48]

1.4.4   OCT "EN FACE"

Las últimas mejoras en técnicas de OCT permiten la adquisición de múltiples B-scans generando imágenes de alta resolución. La OCT en modo "*en face*" apareció recientemente como una nueva técnica de imagen que proporciona una nueva forma de visualización del polo posterior. Mientras que los nuevos "C-scans" nos proporcionan un plano coronal del polo posterior, la tecnología en face general un aplanamiento artificial de los tejidos del polo posterior usando como referencia la capa seleccionada (habitualmente el EPR) y permitiéndonos navegar a través de distintas capas al mismo tiempo que se modifica la profundidad de la imagen a través de estas capturas en tres dimensiones.[49] De esta manera, la OCT en face permite una nueva visión de la coriocapilar, la capa de Sattler y la de Haller sin necesidad de contraste de indocianina, llegando a diagnosticar incluso el vaso nutricio del algún complejo neovascular.

Los B-scans de OCT y imágenes en face muestran los vasos coroideos de forma hipo-reflectiva en comparación con lo que les rodea.[50] Pero no todas las imágenes oscuras son en realidad vasos coroideos, ya que sombras de los vasos retinianos pueden provocar imágenes que induzcan a error. Se registran imágenes del fondo al mismo tiempo en la mayoría de los aparatos actuales, lo que fácilmente ayuda a distinguir cuál es cuál.[51]

Esta tecnología se ha utilizado en patologías como la CSC, en la que ha permitido demostrar la presencia de vasos engrosados a lo largo de todas las capas de la coroides.[50] Otros estudios han permitido también la visualización de más del 90% de los pólipos diagnosticables mediante AVI o las ramificaciones vasculares de las MNV bajo la membrana de Bruch y bajo estos pópipos.[52] También ha sido utilizada para confirmar hallazgos anteriores, como la atrofia coriocapilar que encontramos en los pacientes afectados de DMAE.[53]

1.4.5 ANGIOGRAFÍA OCT

Mientras que la OCT en face ayuda a visualizar una vascularización coroidea normal, la angiografía OCT (OCTa), el último desarrollo en el campo de OCT, proporciona buenas imágenes de los vasos retinianos y complejos neovasculares sin necesidad de utilizar ningún contraste.[54,55] Esta nueva herramienta identifica los vasos en base a variaciones entre múltiples B-scans consecutivos. El tejido retiniano es estático pero la sangre está en constante movimiento, y el procesamiento informático de estas imágenes ayuda a eliminar todo el tejido estático, mostrando una imagen del contenido de los vasos retinianos, dibujando de esta manera el perfil de los mismos,

con el inconveniente de que no permite apreciar la fuga o exudación vascular.[54] Esto

limita el uso de esta técnica de imagen en lo que se refiere a las alteraciones de

permeabilidad vascular. De la misma manera, y como detecta el flujo sanguíneo, las

MNV inactivas pueden ser casi idénticas a las activas, lo cual puede llevar a una

malinterpretación. La imagen de OCTa se genera con la presentación de esta señal

en una escala de blanco y negro. El escáner de alta densidad de áreas en dos

dimensiones general un esquema volumétrico del flujo sanguíneo que nos permite

visualizar de manera directa vasos retinianos y coroideos, tanto normales como

alterados. De esta manera, esta tecnología tiene una aplicación importante para

captura de complejos neovasculares que se hallen tanto por encima como por

debajo del EPR.

Jia[56] mejoró esta tecnología introduciendo la angiografía Split-spectrum

amplitude-decorrelation (SSADA). Esta herramienta permite la mejora del índice de

señal/ruido para la detección de flujo mostrando la red microvascular y eliminando

automáticamente errores de movimiento.

Dado que la OCTa no precisa de la utilización de contrastes externos por vía

intravenosa, esta técnica se puede realizar de manera repetida y sin el riesgo de

sufrir efectos adversos.

2. JUSTIFICACIÓN

41

2. JUSTIFICACIÓN

Como se ha comentado con anterioridad, la retina, y en particular la capa de fotorreceptores presentan una demanda muy alta de oxígeno que se suple de manera casi exclusiva gracias al aporte aporte de nutrientes y de la oxigenación que le proporciona la coroides, una de las estructuras de mayor flujo sanguíneo por gramo del cuerpo humano, y ha quedado de sobra demostrado a través de numerosas publicaciones el importante papel que juega la coroides en multitud de patologías como puedan ser la CSC,[27,57–59] la DMAE y la VCP,[27,59–62] la miopía magna,[63–66] las uveítis posteriores[27,58,59,67,68] y los tumores coroideos[27,69–71] entre otras.

La suposición de que alteraciones vasculares de la coroides pudieran causar problemas de visión no es nueva. Autores como Spaide han observado envainamientos y oclusiones de los canales vasculares coroideos con la edad, en lo que se ha llamado esclerosis coroidea senil. Estudios histopatológicos de pacientes ancianos ha mostrado una importante atrofia del tejido coroideo con una marcada pérdida de los vasos de calibre pequeño y mediano, llegando al punto en que la membrana de Bruch aparece en ocasiones en una situación contigua a la esclerótica, haciendo que los vasos de mayor calibre ocupen la práctica totalidad del espesor coroideo.

Si las modificaciones de la coroides efectivamente juegan un papel o participan en la génesis de algunas enfermedades de la retina, el perfil normal de grosor coroideo y su morfología deben ser conocidos con el mayor detalle posible, para poder diferenciar las variaciones de la normalidad de los hallazgos anómalos y

poder señalar y cuantificar los cambios patológicos en el momento preciso de su

aparición lo más precozmente posible.

3. HIPÓTESIS Y OBJETIVOS

3. HIPÓTESIS Y OBJETIVOS

El objetivo principal de este trabajo se centra en el estudio del grosor y del perfil de la coroides del sujeto sano, planteando la hipótesis de que:

- No existen diferencias entre hombres y mujeres.

- No existen diferencias entre ojos derechos e izquierdos.

- Existe una reducción progresiva del grosor coroideo con la edad conservando un mismo perfil.

- No existen diferencias en el perfil coroideo entre la población infantil y la adulta.

- La densidad vascular de la coroides disminuye con la edad.

3.1. OBJETIVO 1

Evaluar el grosor coroideo de una población pediátrica sana utilizando tecnología de coherencia óptica Swept-Source.

3.2. OBJETIVO 2

Determinar el perfil de grosor coroideo macular de una población sana utilizando tecnología de coherencia óptica Swept-Source.

3.3. OBJETIVO 3

Analizar las características morfológicas de la interfaz esclero-coroidea de una población sana utilizando tecnología de coherencia óptica Swept-Source.

3.4. OBJETIVO 4

Determinar si existen diferencias en el perfil de grosor coroideo macular entre los dos ojos en una población sana utilizando tecnología de coherencia óptica Swept-Source.

3.5. OBJETIVO 5

Estudiar los cambios que la edad induce en el grosor de las diferentes capas de la coroides de una población sana utilizando tecnología de coherencia óptica Swept-Source.

3.6. OBJETIVO 6

Analizar la densidad vascular de la coroides de la población sana utilizando tomografía de coherencia óptica Swept-Source.

4. PUBLICACIONES

4.1 Macular Choroidal Thickness in Normal Pediatric

Population Measured by Swept-Source Optical Coherence

Tomography

48

Macular Choroidal Thickness in Normal Pediatric Population Measured by Swept-Source Optical Coherence Tomography

José M. Ruiz-Moreno,[1,2] Iñaki Flores-Moreno,[1] Francisco Lugo,[2] Jorge Ruiz-Medrano,[2] Javier A. Montero,[3] and Masahiro Akiba[4]

PURPOSE. To evaluate choroidal thickness in healthy pediatric population by swept-source longer-wavelength optical coherence tomography (SS-OCT).

METHODS. This was a cross-sectional comparative, noninterventional study. The macular area of 83 eyes from 43 pediatric patients (<18 years) was studied with an SS-OCT prototype system. Macular choroidal thickness was manually determined at 750-μm intervals by measuring the perpendicular distance from the posterior edge of the RPE to the choroid/sclera junction, along a horizontal 4500-μm line centered in the fovea. Three observers independently determined choroidal thickness. Pediatric choroidal thickness was compared with choroidal thickness from 75 eyes from 50 normal healthy adult volunteers (18 years or older).

RESULTS. Mean age was 10 ± 3 years (3–17) in the pediatric population versus 53 ± 16 (25–85) in the adult population (P < 0.001). Mean spherical equivalent was not different (P ¼ 0.06) between both groups. Mean subfoveal choroidal thickness was 312.9 ± 65.3 μm in the pediatric versus 305.6 ± 102.6 μm in the adult population (P ¼ 0.19). Mean macular choroidal thickness was 285.2 ± 56.7 μm in the pediatric versus 275.2 ± 92.7 μm in the adult population (P ¼ 0.08). The distribution of choroidal thickness along the horizontal line was different for both populations; the temporal choroid was thicker in the pediatric population (320, 322, and 324 μm; P ¼ 0.002, 0.001, and 0.06, respectively), followed by the subfoveal (312 μm) and nasal choroid (281, 239, and 195 μm).

CONCLUSIONS. Macular choroidal thickness in the pediatric population is not significantly thicker than that of healthy adults. Differences are more remarkable in the temporal side of the fovea. (Invest Ophthalmol Vis Sci. 2013;54:353–359) DOI: 10.1167/iovs.12-10863

Technological advances and new information about the role of the choroid in ophthalmic pathology have promoted new research on choroidal anatomy and physiology.[1]

Choroidal changes are associated with some conditions such as central serous chorioretinopathy,[2–5] age-related macular degeneration,[4–11] polypoidal choroidal vasculopathy,[4–7,10] myopic maculopathy,[12–16] posterior uveitis,[4,5,17–21] and choroidal tumors.[4,22,23] Even though indocyanine green angiography (ICGA) and optical coherence tomography (OCT) have aided in the study of the choroid, adequate morphologic examination using spectral domain OCT (SD-OCT) has not been possible until recently due to the presence of pigment cells that attenuate the incident light, and the limited depth of penetration inherent to the design of SD-OCT instruments.[1]

It has been previously reported that choroidal thickness (as determined by SD-OCT) decreases with age in healthy eyes.[24–29] However, pediatric choroidal thickness has not been previously determined.

High penetration, swept-source longer-wavelength OCT (SS-OCT) has an innovative 1-μm band light source,[30–33] longer than that of conventional machines, that provides higher penetration through the RPE, enabling deep choroidal imaging. There are no commercially available SS-OCT machines and prototypes are mainly used for research.

The aim of this study is to determine choroidal thickness in the pediatric population using a prototype SS-OCT.

PATIENTS AND METHODS

A cross-sectional comparative, noninterventional study was performed at VISSUM Alicante, Spain. All examinations were obtained in the afternoon to avoid diurnal variations.[34,35] The institutional review board of VISSUM Alicante approved the use of the prototype SS-OCT and data collection. This study followed the tenets of the Declaration of Helsinki.

The macular area of a healthy pediatric population (<18 years) was studied with an SS-OCT prototype system (Topcon Corporation, Tokyo, Japan), after their parents provided informed consent. The SS-OCT prototype used to image the full-thickness choroid and sclera is based on SS-OCT technology,[36] which uses a tunable laser as a light source operated at a 100,000-Hz A-scan repetition rate in the 1-μm wavelength region. The reference mirror is placed at the deepest position of the retina to increase sensitivity at the choroidal level in macular imaging. An OCT image contains 1024 axial scans and up to 96 images are considered for image averaging. Lateral resolution is 20 μm while axial resolution is 8 μm in the retina.[37] Lateral and axial resolution are independent.

Acquisition time was 1 second. Choroidal thickness was manually calculated as the perpendicular distance from the external surface of the RPE (hyperreflective line) to the internal surface of the sclera.
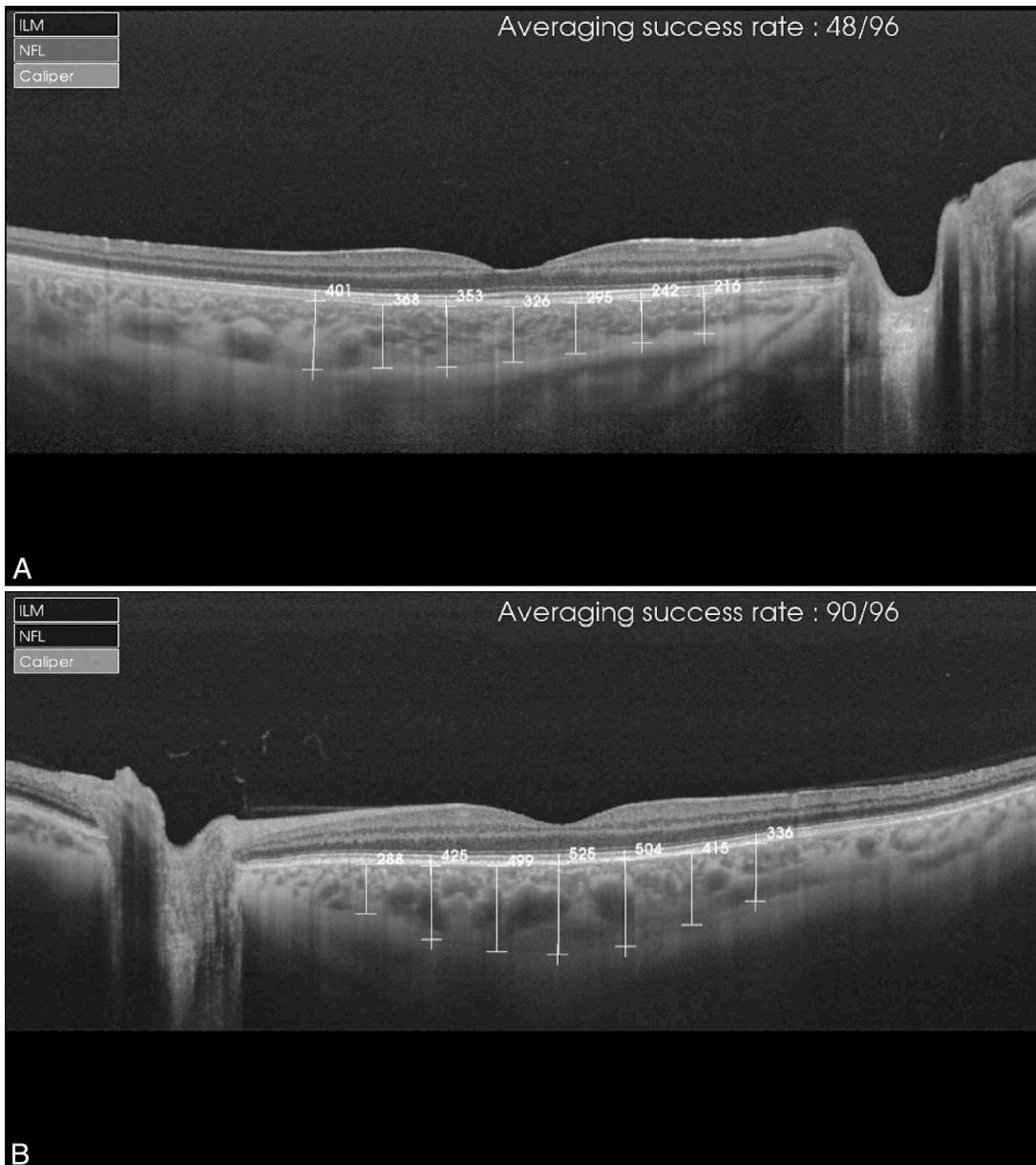
Figure 1. Choroidal thickness determinations (in 1m). (A) Pediatric eyes. (B) Adult eyes.

Choroidal thickness was determined under the fovea (subfoveal choroidal thickness); three further determinations were performed every 750 1m temporal (T1, T2, and T3) and nasal (N1, N2, and N3) to the fovea (Fig. 1). Average macular horizontal choroidal thickness was calculated as the average of these seven determinations.

An average macular profile was calculated as a line formed by the mean values of each point (T3, T2, T1, subfoveal, N1, N2, and N3) in the pediatric and adult groups.

Pediatric choroidal thickness was compared with that of normal healthy adult volunteers (18 years or older). Eyes with spherical equivalent (SE) beyond 6 diopters (D) or ocular conditions were excluded from both groups. An experienced technician determined refractive errors using an auto-refractometer (Nidek, Gamagohri, Japan) that was later checked by a certified optometrist.

Three observers determined choroidal thickness independently and the final thickness was calculated as the arithmetic mean of the

calculations of the three observers. The interobserver reproducibility was evaluated using intraclass correlation coefficient and Bland Altman plots. Pearson's correlation was calculated for choroidal thickness and age and SE; P value < 0.05 was considered statistically significant. Statistical analysis was performed using licensed statistical software (SPSS version 14.0; SPSS Inc., Chicago, IL).

RESULTS

The macular area of 83 eyes from 43 healthy pediatric individuals (<18 years) was studied with an SS-OCT prototype system and compared with 75 eyes from 50 normal healthy adult volunteers (18 years or older).

SS-OCT allowed visualization of choroidal thickness in all the cases (100%) in both groups (Fig. 1). Mean age in the pediatric population was 10 ⵹ 3 years (3–17) versus 53 ⵹ 16 years (25–85) in the adult group (P < 0.001; Student's t-test). Mean SE was similar in both groups (0.3 ⵹ 2.0 D, range þ3.75 to −5.25 in children versus 0.16 ⵹ 1.4 D, range þ3.25 to −5.0 in adults; P ¼ 0.06; Student's t-test). Mean subfoveal choroidal thickness was 312.9 ⵹ 65.3 lm (158–469) in children versus 305.6 ⵹ 102.6 lm (152–624) in adults (P ¼ 0.19; Mann-Whitney U test). Average macular horizontal choroidal thickness was 285.2 ⵹ 56.7 lm (153–399) in children versus 275.2 ⵹ 92.7 lm (132–551) in adults (P ¼ 0.08; Mann-Whitney U test; Table 1).

Pediatric choroidal thickness was highest in the temporal side (320, 322, and 324 lm for T3, T2, and T1, respectively; confidence intervals 13.2, 12.9, and 13.0 lm, respectively); then in the fovea (312 lm; confidence interval 14.1 lm); and thinnest in the nasal side (281, 239, and 195 lm for N1, N2, and N3 respectively; confidence intervals 14.1, 13.3, and 12.5 lm, respectively). Adult choroidal thickness was highest in the fovea (305 lm; confidence interval 23.3 lm); followed by the temporal (281, 290, 299 lm for T3, T2, and T1, respectively; confidence intervals 18.5, 20.3, and 21.6 lm, respectively); and the nasal side (290, 253, 205 lm for N1, N2, and N3 respectively; confidence intervals 23.8, 23.4, and 22.5 lm, respectively; Fig. 2). Differences in choroidal thickness between both groups were statistically significant at T3 and T2 (P ¼ 0.002 and P ¼ 0.01, respectively, Student's t-test) and near significance in T1 (P ¼ 0.06, Student's t-test). Differences in subfoveal and nasal choroidal thickness were not statistically significant.

The average temporal choroidal thickness within the pediatric group was lower in the group formed by children 10 to 17 years (n ¼ 35 eyes) than among children aged 3 to 9 years (n ¼ 48 eyes); but the differences between both groups were less marked in the nasal sectors (Fig. 2B).

Correlation between macular horizontal choroidal thickness and age or SE and between subfoveal choroidal thickness and SE in the pediatric group was r ¼ −0.25 (P ¼ 0.02); r ¼ 0.37 (P ¼ 0.001); and r ¼ 0.41 (P ¼ 0.000), respectively. Correlation between choroidal thickness and age in the whole population was weak or not significant at N3, N2, N1, and fovea, and significant at T1 (r ¼ −0.22, P ¼ 0.004); T2 (r ¼ −0.29, P ¼ 0.000); and T3 (r ¼ −0.33, P ¼ 0.000; Fig. 3).

The intraclass correlation coefficient for choroidal thickness for the three independent observers was between 0.91 and 0.98. The Bland-Altman plots showed small differences and narrow limits of agreement for choroidal thickness for interobserver comparison, suggesting satisfactory agreement between the observers. Most of the data points were tightly clustered around the zero line of the difference between the two choroidal thickness determinations and 95% to 97.5% of the determinations fell within limits of agreement (Fig. 4).
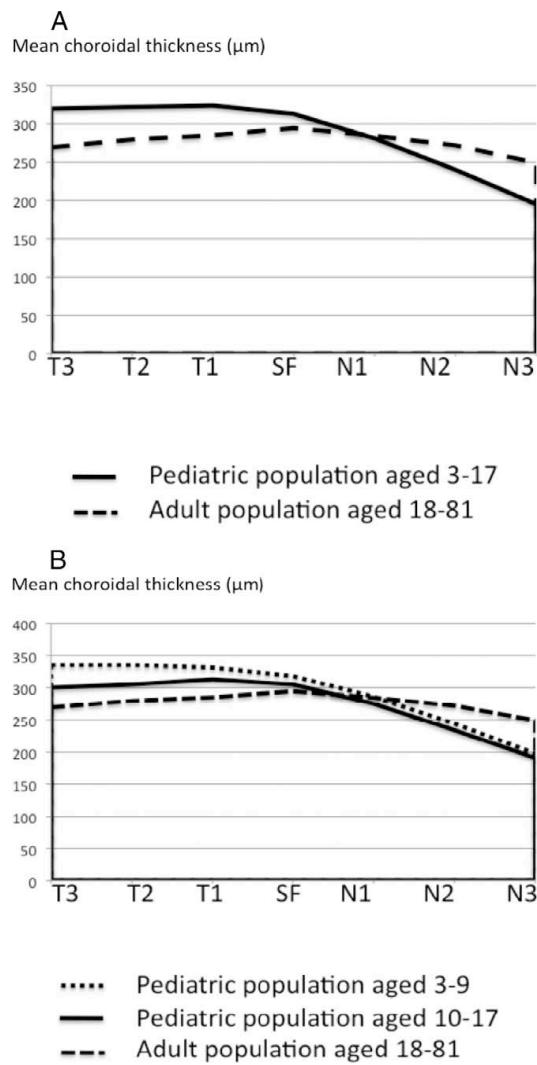
Figure 2. (A) Choroidal thickness profile in the pediatric versus the adult group. (B) The pediatric group has been split into two subgroups (aged 3–9 and 10–17 years) and the respective profiles are compared with the adult profile.

DISCUSSION

Choroidal research has always been difficult. ICGA permits visualization of choroidal vessels[4,5] and recent advances in OCT technology have added cross-sectional information about the choroid.[1] Enhanced-depth imaging provided by SD-OCT has permitted cross-sectional research of the choroid, increasing our knowledge on the pathophysiology and etiology of several ocular conditions.[2,3,6–23] Long wavelength SS-OCT prototypes (1050–1060 nm) have been used in patients improving image quality. Faster and higher quality software may overcome RPE barrier effect and movement artifacts.[11,26,38]
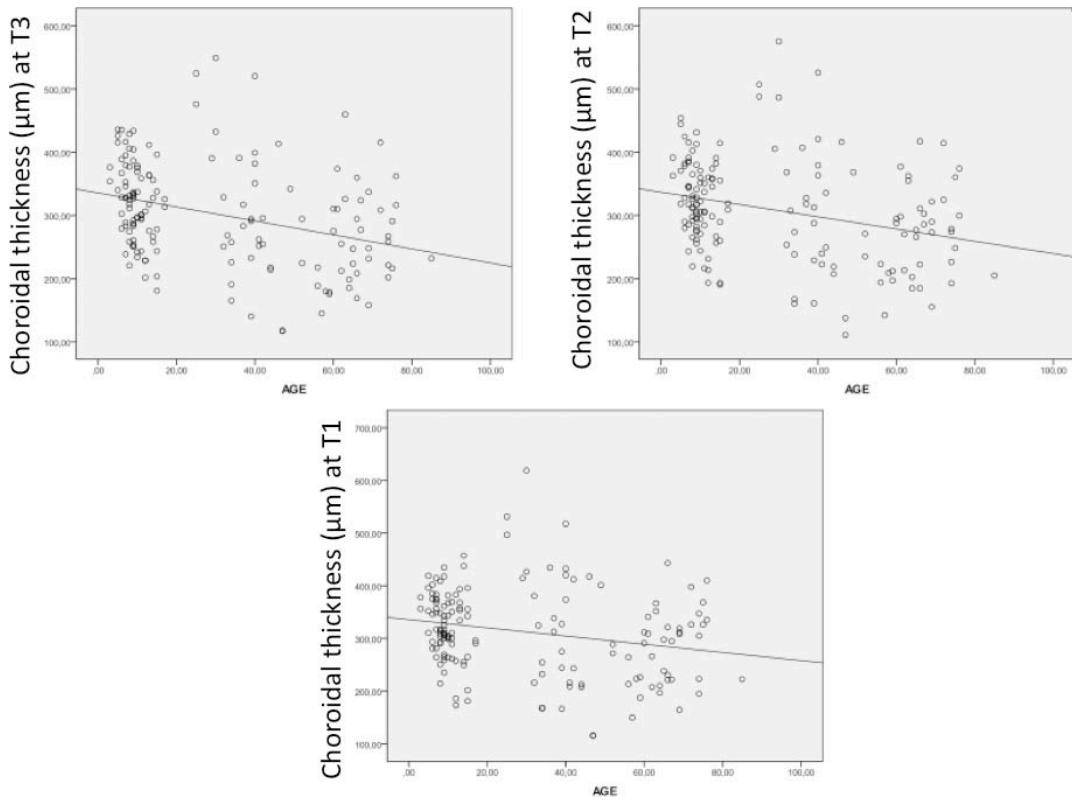
FIGURE 3. Scatterplot showing choroidal thickness at T3, T2, and T1 in the whole group. Choroidal thickness and age correlate significantly: T1 (r ¼ −0.22, P ¼ 0.004); T2 (r ¼ −0.29, P ¼ 0.000); and T3 (r ¼ −0.33, P ¼ 0.000).

Papers on choroidal thickness report a progressive choroidal thinning associated with age.[24–29] Margolis described 1.56-1m thinning for each year of life.[28] Agawa[38] and Li[39] reported that such correlation between choroidal thickness and age did not exist in eyes with axial length <25 mm. The effect of age on pediatric choroidal thickness has not been studied previously.

In our series, SS-OCT allowed visualization of the choroid in all the cases with high-quality images (Fig. 1), permitting choroidal thickness determination. Our data suggest that the temporal choroid may become thinner with age, even thinner than the subfoveal choroid in the adult population. This finding is reinforced by the significant inverse correlation between choroidal thickness and age in the whole group at T1, T2, and T3 (Fig. 3).

The average values of choroidal thickness in our adult group were in agreement with previously reported series with similar age distribution (Table 2).[25,27,28] Due to the strong correlation between age and choroidal thickness in adults,[28] the age factor should be carefully considered when comparing populations with different age distributions.[26,29,38,39] Mean subfoveal choroidal thickness in our adult group (312.9 6 65.3 1m)

TABLE 1. Patients' Demographics and CT

	Pediatric Population	Adult Population	P Value
n (eyes)	83	75	
Mean age; y	9.6 6 3.1; 3–17	53.2 6 15.6; 25–85	P < 0.001; Student's t-test
Mean SE	0.3 6 2.0 D; 3.75 to −5.25	−0.16 6 1.4 D; 3.25 to −5.0	P ¼ 0.06; Student's t-test
Mean subfoveal CT	312.9 6 65.3 1m; 158–469	305.6 6 102.6 1m; 152–624	P ¼ 0.19; Mann-Whitney U test
Mean macular CT	285.2 6 56.7 1m; 153–399	275.2 6 92.7 1m; 132–551	P ¼ 0.08; Mann-Whitney U test
Subfoveal CT 95% CI	298.7–327.3 1m	281.9–329.4 1m	
Macular CT 95% CI	272.9–297.8 1m	250.0–293.3 1m	
Definite choroid/sclera junction, %	100	100	

CT, choroidal thickness.
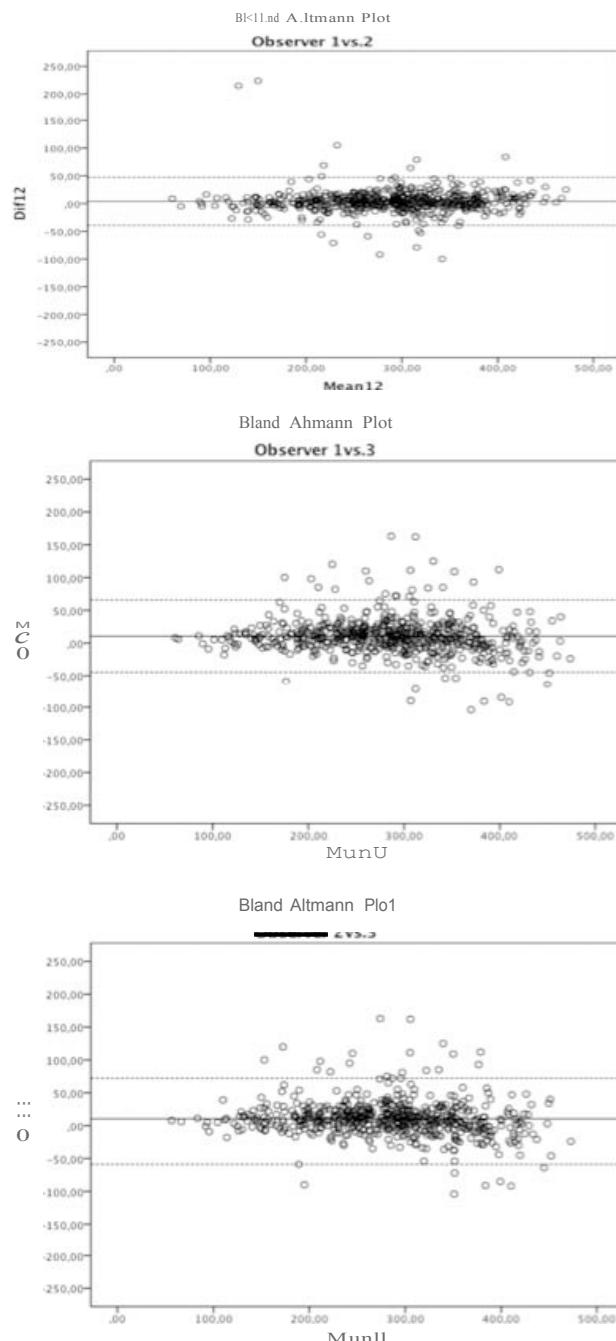
52

Bl<ll.nd A.ltmann Plot

Observer 1vs.2

Bland Ahmann Plot

Observer 1vs.3

Bland Altmann Plo1

Fl<ru u: 4.   BlandAllm2l\ plots rcpracnting the dîfl'crcncc:s in intcrobsc:l"\.":r dctCI'Tt\ÎN.tion.s of choroidal thickncs:s. *Sl:>lid tines* rcprcscnt mc:an dîfl'crcncc 2nd*dasbed lines* show the lowcr 2nd upper95% limîts of 2gr«mcnt.Moot of the d2t2points uc tightly dustcrcduound the zero Une of the dîfl'cR:ncc bctween the two choroi<Wthickness dctcrmîn2tion.s.

53

TABLE 2. Characteristics of Subfoveal CT

Study	Mean Age	Cases	Subfoveal CT	OCT System	Relation Age/CT	Definite Choroid/ Sclera Junction, %
Ruiz-Moreno adult group	53.2	75	305	SS-OCT	–	100
Margolis[28]	50.4	54	287	Spectralis	þ	
Manjunath[27]	51.1	34	272	Cirrus	þ	74
Ikuno[26]	39.4	86	354	SS-OCT	þ	
Agawa[38]	32.9	43	348	SS-OCT	–	
Li[39]	24.9	93	342			
Branchini[1]	35.2	28	337 to 347	Cirrus Spectralis RTVue		96.4
Ouyang[29]	32.8	59	297	Cirrus	–	100
Ruiz-Moreno pediatric population	9.6	83	312	SS-OCT	–/þ	100

was higher than the average values reported in other series with younger patients (Table 2).

Even though the retinal landmarks may be slightly different from those reported in the literature, most of the choroidal thickness results were very similar considering Margolis' age-correction for choroidal thickness (1.56 lm reduction per year).[28] We were unable to compare these data with those from our pediatric group since such data have not been previously reported. In our series, we have not found significant differences between adults and children except for the temporal choroid. The age at which subfoveal choroidal thickness starts to decrease, as has been suggested by some authors, is still to be determined.[28] This decline is probably related to aging vascular changes. We have found a significant correlation between macular choroidal thickness and age, macular choroidal thickness, and SE and between subfoveal choroidal thickness and SE within the pediatric group.

The topographic profile of choroidal thickness in the adult group in our series (Fig. 2) was highest in the subfoveal area, followed by the temporal and the nasal areas, as has been previously reported in other series.[1,26–29] However, this profile was different in the pediatric population: choroidal thickness was highest in the temporal choroid with 320, 322, and 324 lm, followed by the subfoveal choroid with 312 lm and the nasal choroid with 281, 239, and 195 lm; Fig. 2).

The subgroup analyses of the pediatric population showed that the profile of choroidal thickness seems to change progressively during the second decade of life, as the child grows older. These changes in choroidal thickness probably reflect vascular remodeling associated with choroidal maturation. The higher metabolic needs of the fovea compared with the surrounding retina may cause a reduction of the thickness of the temporal choroid, while sparing the subfoveal choroid.

OCT devices reported in the literature provide different qualities of imaging, permitting a more or less adequate visualization of the line delimiting the choroid and the sclera. In our series, all the patients examined by SS-OCT showed a clearly defined, measurable posterior portion of the choroid. Measurable choroidal thickness has been reported in 74%[27] to 90%[25] of the eyes examined by Cirrus HD-OCT and in 95.8% of the eyes examined by Heidelberg EDI-OCT.[40] Two papers comparing OCT equipments reported 96.4%[1] and 90.7% measurability.[41] Choroidal visualization was better in those studies using longer wavelength equipments. The high intra-class correlation coefficient (0.91–0.98) and the narrow limits of agreement of the Bland-Altman plots for the three independent observers highlight SS-OCT accuracy in choroidal thickness determination.

In the present study, we have considered SE instead of axial length determinations since previous indications from the literature show that refraction, which is more convenient to

obtain, provides equivalent modeling capability as axial length.[42]

Among the limitations of this study, we may mention that choroidal thickness has to be manually determined since there is no commercially available automated software. To our best knowledge, this is the first report of choroidal thickness determination in children using SS-OCT. A few studies have been previously performed in adults using SS-OCT[26,36,38] with different age distributions.

According to our results, macular choroidal thickness is similar in the healthy pediatric and adult population with different choroidal thickness profiles. New studies about choroidal thickness in pediatric population are required to confirm our findings. Knowledge of the normal choroidal thickness and choroidal thickness profile may aid in the understanding of normal changes and the appearance of chorioretinal conditions in pediatric eyes.

References

1. Branchini L, Regatieri CV, Flores-Moreno I, Baumann B, Fujimoto JG, Duker JS. Reproducibility of choroidal thickness measurements across three spectral domain optical coherence tomography systems. Ophthalmology. 2012;119:119–123.

2. Imamura Y, Fujiwara T, Margolis R, Spaide RF. Enhanced depth imaging optical coherence tomography of the choroid in central serous chorioretinopathy. Retina. 2009;29:1469–1473.

3. Maruko I, Iida T, Sugano Y, Ojima A, Sekiryu T. Subfoveal choroidal thickness in fellow eyes of patients with central serous chorioretinopathy. Retina. 2011;31:1603–1608.

4. Stanga PE, Lim JI, Hamilton P. Indocyanine green angiography in chorioretinal diseases: indications and interpretation: an evidence-based update. Ophthalmology. 2003;110:15–21. quiz 22–23.

5. Yannuzzi LA. Indocyanine green angiography: a perspective on use in the clinical setting. Am J Ophthalmol. 2011;151:745–751.e1.

6. Chung SE, Kang SW, Lee JH, Kim YT. Choroidal thickness in polypoidal choroidal vasculopathy and exudative age-related macular degeneration. Ophthalmology. 2011;118:840–845.

7. Koizumi H, Yamagishi T, Yamazaki T, Kawasaki R, Kinoshita S. Subfoveal choroidal thickness in typical age-related macular degeneration and polypoidal choroidal vasculopathy. Graefes Arch Clin Exp Ophthalmol. 2011;249:1123–1128.

8. Manjunath V, Goren J, Fujimoto JG, Duker JS. Analysis of choroidal thickness in age-related macular degeneration using spectral-domain optical coherence tomography. Am J Ophthalmol. 2011;152:663–668.

9. Switzer DW Jr, Mendonca LS, Saito M, Zweifel SA, Spaide RF. Segregation of ophthalmoscopic characteristics according to choroidal thickness in patients with early age-related macular degeneration. Retina. 2012;32:1265–1271.

10. Ueta T, Obata R, Inoue Y, et al. Background comparison of typical age-related macular degeneration and polypoidal choroidal vasculopathy in Japanese patients. Ophthalmology. 2009;116:2400–2406.

11. Wood A, Binns A, Margrain T, et al. Retinal and choroidal thickness in early age-related macular degeneration. Am J Ophthalmol. 2011;152:1030–1038.e2.

12. Chen W, Wang Z, Zhou X, Li B, Zhang H. Choroidal and photoreceptor layer thickness in myopic population. Eur J Ophthalmol. 2012;22:590–597.

13. Fujiwara T, Imamura Y, Margolis R, Slakter JS, Spaide RF. Enhanced depth imaging optical coherence tomography of the choroid in highly myopic eyes. Am J Ophthalmol. 2009;148: 445–450.

14. Fureder W, Krauth MT, Sperr WR, et al. Evaluation of angiogenesis and vascular endothelial growth factor expression in the bone marrow of patients with aplastic anemia. Am J Pathol. 2006;168:123–130.

15. Ikuno Y, Tano Y. Retinal and choroidal biometry in highly myopic eyes with spectral-domain optical coherence tomography. Invest Ophthalmol Vis Sci. 2009;50:3876–3880.

16. Wang NK, Lai CC, Chu HY, et al. Classification of early dry-type myopic maculopathy with macular choroidal thickness. Am J Ophthalmol. 2012;153:669–677.e2.

17. Aoyagi R, Hayashi T, Masai A, et al. Subfoveal choroidal thickness in multiple evanescent white dot syndrome. Clin Exp Optom. 2012;95:212–217.

18. Channa R, Ibrahim M, Sepah Y, et al. Characterization of macular lesions in punctate inner choroidopathy with spectral domain optical coherence tomography. J Ophthalmic Inflamm Infect. 2012;2:113–120.

19. Fong AH, Li KK, Wong D. Choroidal evaluation using enhanced depth imaging spectral-domain optical coherence tomography in Vogt-Koyanagi-Harada disease. Retina. 2011; 31:502–509.

20. Maruko I, Iida T, Sugano Y, et al. Subfoveal choroidal thickness after treatment of Vogt-Koyanagi-Harada disease. Retina. 2011; 31:510–517.

21. Nakai K, Gomi F, Ikuno Y, et al. Choroidal observations in Vogt-Koyanagi-Harada disease using high-penetration optical coherence tomography. Graefes Arch Clin Exp Ophthalmol. 2012; 250:1089–1095.

22. Say EA, Shah SU, Ferenczy S, Shields CL. Optical coherence tomography of retinal and choroidal tumors. J Ophthalmol. 2011;2011:385058.

23. Shields CL, Perez B, Materin MA, Mehta S, Shields JA. Optical coherence tomography of choroidal osteoma in 22 cases: evidence for photoreceptor atrophy over the decalcified portion of the tumor. Ophthalmology. 2007;114:e53–e58.

24. Ding X, Li J, Zeng J, et al. Choroidal thickness in healthy Chinese subjects. Invest Ophthalmol Vis Sci. 2011;52:9555–9560.

25. Ho J, Branchini L, Regatieri C, Krishnan C, Fujimoto JG, Duker JS. Analysis of normal peripapillary choroidal thickness via spectral domain optical coherence tomography. Ophthalmology. 2011;118:2001–2007.

26. Ikuno Y, Kawaguchi K, Nouchi T, Yasuno Y. Choroidal thickness in healthy Japanese subjects. Invest Ophthalmol Vis Sci. 2010;51:2173–2176.

27. Manjunath V, Taha M, Fujimoto JG, Duker JS. Choroidal thickness in normal eyes measured using Cirrus HD optical coherence tomography. Am J Ophthalmol. 2010;150:325–329.e1.

28. Margolis R, Spaide RF. A pilot study of enhanced depth imaging optical coherence tomography of the choroid in normal eyes. Am J Ophthalmol. 2009;147:811–815.

29. Ouyang Y, Heussen FM, Mokwa N, et al. Spatial distribution of posterior pole choroidal thickness by spectral domain optical coherence tomography. Invest Ophthalmol Vis Sci. 2011;52: 7019–7026.

30. Huber R, Adler DC, Srinivasan VJ, Fujimoto JG. Fourier domain mode locking at 1050 nm for ultra-high-speed optical coherence tomography of the human retina at 236,000 axial scans per second. Opt Lett. 2007;32:2049–2051.

31. Lim H, de Boer JF, Park BH, Lee EC, Yelin R, Yun SH. Optical frequency domain imaging with a rapidly swept laser in the 815-870 nm range. Opt Express. 2006;14:5937–5944.

32. Unterhuber A, Povazay B, Hermann B, Sattmann H, Chavez-Pirson A, Drexler W. In vivo retinal optical coherence tomography at 1040 nm - enhanced penetration into the choroid. Opt Express. 2005;13:3252–3258.

33. Yasuno Y, Hong Y, Makita S, et al. In vivo high-contrast imaging of deep posterior eye by 1-micron swept source optical coherence tomography and scattering optical coherence angiography. Opt Express. 2007;15:6121–6139.

34. Brown JS, Flitcroft DI, Ying GS, et al. In vivo human choroidal thickness measurements: evidence for diurnal fluctuations. Invest Ophthalmol Vis Sci. 2009;50:5–12.

35. Tan CS, Ouyang Y, Ruiz H, Sadda SR. Diurnal variation of choroidal thickness in normal, healthy subjects measured by spectral domain optical coherence tomography. Invest Ophthalmol Vis Sci. 2012;53:261–266.

36. Ikuno Y, Maruko I, Yasuno Y, et al. Reproducibility of retinal and choroidal thickness measurements in enhanced depth imaging and high-penetration optical coherence tomography. Invest Ophthalmol Vis Sci. 2011;52:5536–5540.

37. Hirata M, Tsujikawa A, Matsumoto A, et al. Macular choroidal thickness and volume in normal subjects measured by swept-source optical coherence tomography. Invest Ophthalmol Vis Sci. 2011;52:4971–4978.

38. Agawa T, Miura M, Ikuno Y, et al. Choroidal thickness measurement in healthy Japanese subjects by three-dimensional high-penetration optical coherence tomography. Graefes Arch Clin Exp Ophthalmol. 2011;249:1485–1492.

39. Li XQ, Larsen M, Munch IC. Subfoveal choroidal thickness in relation to sex and axial length in 93 Danish university students. Invest Ophthalmol Vis Sci. 2011;52:8438–8441.

40. Mwanza JC, Hochberg JT, Banitt MR, Feuer WJ, Budenz DL. Lack of association between glaucoma and macular choroidal thickness measured with enhanced depth-imaging optical coherence tomography. Invest Ophthalmol Vis Sci. 2011;52: 3430–3435.

41. Yamashita T, Shirasawa M, Arimura N, Terasaki H, Sakamoto T. Repeatability and reproducibility of subfoveal choroidal thickness in normal eyes of Japanese using different SD-OCT devices. Invest Ophthalmol Vis Sci. 2012;53:1102–1107.

42. Nishida Y, Fujiwara T, Imamura Y, Lima LH, Kurosaka D, Spaide RF. Choroidal thickness and visual acuity in highly myopic eyes. Retina. 2012;32:1229–1236.

4.2 Macular Choroidal Thickness Profile in a Healthy

Population Measured by Swept-Source Optical Coherence

Tomography

Macular Choroidal Thickness Profile in a Healthy Population Measured by Swept-Source Optical Coherence Tomography

Jorge Ruiz-Medrano,[1] Ignacio Flores-Moreno,[2] Pablo Peña-García,[3] Javier A. Montero,[4] Jay S. Duker,[5] and José M. Ruiz-Moreno[2,6]

[1]Clínico San Carlos University Hospital, Ophthalmology Unit, Madrid, Spain
[2]Department of Ophthalmology, Castilla La Mancha University, Albacete, Spain
[3]Division of Ophthalmology, Miguel Hernández University, Alicante, Spain
[4]Pío del Río Hortega University Hospital, Ophthalmology Unit, Valladolid, Spain
[5]New England Eye Center, Tufts Medical Center, Boston, Massachusetts, United States
[6]Alicante Institute of Ophthalmology, Vissum, Vitreo-Retinal Unit, Alicante, Spain

Correspondence: Jorge Ruiz-Medrano, c/ Meléndez Valdés, 38, 28015 Madrid, Spain;
jorge.ruizmedrano@gmail.com.

PURPOSE. To determine choroidal thickness (CT) profile in a healthy population using swept-source optical coherence tomography (SS-OCT).

METHODS. This was a cross-sectional, noninterventional study. A total of 276 eyes (spherical equivalent ≤3 diopters [D]) were scanned with SS-OCT. Horizontal CT profile of the macula was created measuring subfoveal choroidal thickness (SFCT) from the posterior edge of retinal pigment epithelium (RPE) to the choroid–sclera junction. Three determinations were performed at successive points 1000 μm nasal and five more temporal to the fovea. Subjects were divided into five age groups.

RESULTS. The mean SFCT was 301.89 ± 80.53 μm (95% confidence interval: 292.34–311.43). The mean horizontal macular choroidal thickness (MCT) was 258.69 ± 64.59 μm (95% confidence interval: 251.04–266.35). No difference in CT was found between men and women. Mean SFCT of the different study groups was 325.6 ± 51.1 (0–10 years), 316.7 ± 90.1 (11–20 years), 313.9 ± 80.3 (21–40 years), 264.6 ± 79.3 (41–60 years), and 276.3 ± 88.8 μm in subjects older than 60 years (P < 0.001; ANOVA test). Mean horizontal MCT was 286.0 ± 43.5, 277.7 ± 68.2, 264.0 ± 61.9, 223.4 ± 62.2, and 229.7 ± 66.1 μm, respectively (P < 0.001; ANOVA test). The CT profile was different for each age group.

CONCLUSIONS. To our knowledge, this is the first population study of CT of healthy eyes across a broad range of age groups using SS-OCT. As has been determined using spectral-domain OCT, CT decreases with advancing age, especially after age 40. There were no differences due to sex. The greatest CT variation takes place in temporal sectors.

Keywords: choroidal thickness, healthy population, SS-OCT, swept-source OCT

In recent years the choroid and its role in posterior segment disease has become an increasing subject of study. Ultrasonography,[1] magnetic resonance imaging (MRI),[2] and Doppler laser have been employed to study the choroid, but due to insufficient resolution are of limited use. On the other hand, indocyanine green (ICG) angiography reveals useful clinical information but does not provide cross-sectional images of the choroid for in vivo study.[3,4]

The introduction of optical coherence tomography (OCT) and its continuous development represent a clear breakthrough in choroidal imaging as it provides deeper, higher-resolution imaging of the eye layers with brief acquisition times.[5,6] Initially, time-domain OCT (TD-OCT) was the technology available to study the posterior segment, but because of poor penetration below the retinal pigment epithelium (RPE) and relatively low resolution, TD-OCT could not be employed for choroidal imaging. In 2006, spectral-domain OCT (SD-OCT) became commercially available. Despite its obvious advantages over TD-OCT, signal roll-off with depth and signal attenuation by pigmented tissues or media opacities still precluded choroidal imaging in most eyes. Spaide et al.[7] introduced a technique to allow choroidal imaging using SD-OCT devices: enhanced depth image OCT (EDI-OCT), which provides consistent choroidal visualization in most eyes and allows quantitative and reproducible thickness measurements. The most recent innovative technology available for OCT imaging is high-penetration, swept-source longer-wavelength OCT (SS-OCT).[8–11] Copete et al.[12] and Ruiz-Moreno et al.[13] affirmed that reliable measurement of CT was possible in 100% of eyes using an SS-OCT device.

As advancements in technology allow extensive studies of the choroid to be performed, variations in CT and morphology have been associated with conditions such as central serous chorioretinopathy,[4,14–16] age-related macular degeneration,[4,16–22] polypoidal choroidal vasculopathy,[4,16–18,21] myopic maculopathy,[23–27] posterior uveitis,[4,15,16,28–31] and choroidal tumors.[4,32,33]

3532
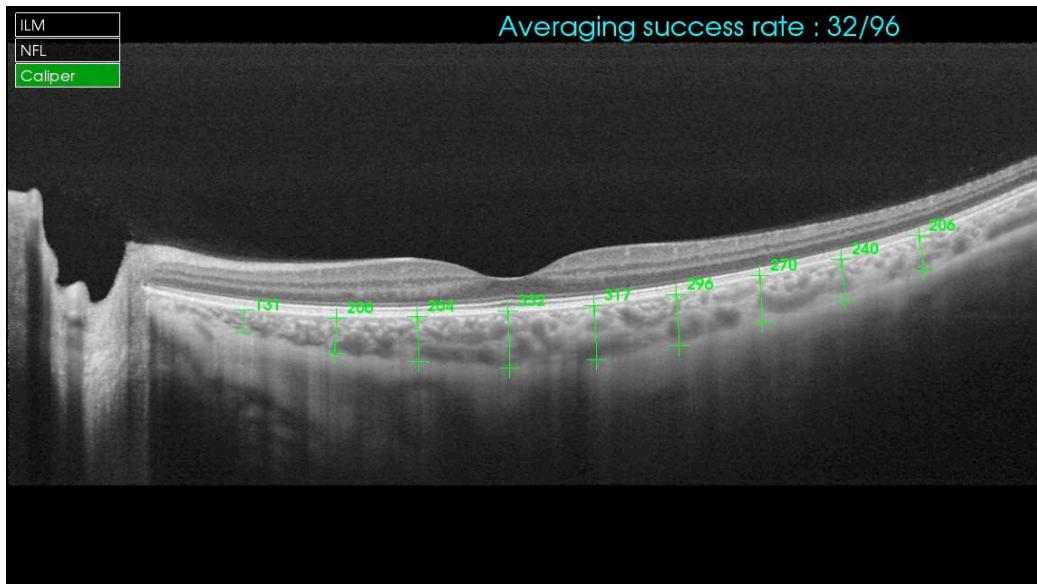
Figure 1. Example of choroidal thickness measures in all nine locations, from the posterior edge of RPE to the choroid–sclera junction; from N3 position (right) to T5 position (left).

Age-related thinning of the choroid of healthy patients studied by SD-OCT has been well documented,[34–39] as well as differences in CT between adult and pediatric eyes.[13] A paper by Ikuno et al.[36] described the CT in healthy subjects ranging from 23 to 88 years of age with SS-OCT technology and CT changes according to change in subjects' age. To our knowledge, however, no previous report has determined the age at which the choroid is thickest, or the normal evolution or changes in thickness with age or sex across a wide span of ages. If choroidal variations do play a role in retinal diseases, the normal CT profile must be known so that it is possible to point out variations as they appear. The aim of this study was to determine CT profile in a large population with healthy eyes using SS-OCT.

Patients and Methods

This was a cross-sectional, noninterventional study, performed at Vissum Alicante, Spain. The study followed the tenets of the Declaration of Helsinki. The institutional review board of Vissum Alicante approved the study. All examinations were obtained in the afternoon to avoid diurnal variations (16:00–20:00).[40–42]

We manually measured the CT in 276 eyes from 154 patients. Ninety-three patients (60.4%) were male (164 eyes, 78 right and 86 left), and 61 patients (39.6%) were female (112 eyes, 57 right and 55 left). Their macular area was studied with an SS-OCT system (Topcon Corporation, Tokyo, Japan) after they provided informed consent. Inclusion criteria were best-corrected visual acuity (BCVA) between 20/20 and 20/25, spherical equivalent (SE) between þ3 and −3 diopters (D), and no systemic or ocular diseases. Eyes with any history of any retinal disease in the fellow eye were not included. Eyes with SE beyond 63 D were excluded.

The SS-OCT device used to image the full-thickness choroid and sclera,[43] which uses a tunable laser as a light source, operated at 100,000-Hz A-scan repetition rate in the 1-lm wavelength region. The device can do image averaging of up to 96 B-scans at each location. For this study, the reference mirror was placed at the deeper position of the retina so that the sensitivity was higher at the choroidal area in macular imaging. A line scanning mode, which produces an OCT image containing 1024 axial scans with a scan length of 12 mm, was employed. This sampling space in object space corresponds to 11.7 lm/pixel. Lateral resolution is set at 20 lm with 24-mm axial eye length, while axial resolution is 8 lm in the retina.[44] Lateral and axial resolution are independent.

Acquisition time was 1 second. This allowed us to obtain good-quality images even in 3-year-old children. A horizontal CT profile of the macula was manually created measuring CT (from the posterior edge of RPE to the choroid–sclera junction) under the fovea using the prototype software. The outer aspect of the lamina fusca, rather than the outer limit of the choroidal vessels, was the landmark used to determine the most distal aspect of the choroid.

Five further determinations were performed every 1000 lm temporal (T1, T2, T3, T4, and T5) and three more nasal (N1, N2, and N3) to the fovea (Fig. 1).

An experienced technician determined refractive errors and BCVA using an autorefractometer (Nidek, Gamagohri, Japan) that was later checked by a certified optometrist.

To study the possible evolution of the CT, the study group was divided into five subgroups according to age distribution: 0 to 10 (eyes, n ¼ 75), 11 to 20 (n ¼ 48), 21 to 40 (n ¼ 50), 41 to 60 (n ¼ 40), and older than 60 years (n ¼ 63). Mean age was 33.5 6 24.9 years (from 3 to 95). Mean SE was 0.10 6 1.36 D (from þ3 to −3).

Two observers determined CT independently and in a masked fashion.

58
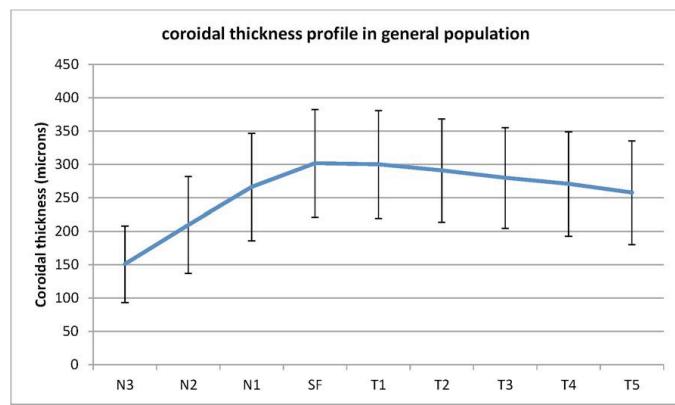
Figure 2. Choroidal thickness profile in general population (microns/measurement locations).

For statistical treatment of the data, the program used was version 17.0 of SPSS for Windows (SPSS, Chicago, IL, USA). Interobserver reproducibility was evaluated using intraclass correlation coefficient (ICC) for each variable measured (mean and 95% confidence interval), coefficient of variation between graders, and Bland-Altman plots. The means of the measures obtained by the two observers were the data used for the rest of the calculations. Kolmogorov-Smirnov test was applied for all data samples in order to check normality. Comparison between groups was performed using Student's t-test when samples were normally distributed or Mann-Whitney test when parametric statistics were not possible. The level of significance used was always the same ($P < 0.05$). Homogeneity of variances was checked using the Levene test. For comparison of several independent samples, analysis of variance (ANOVA) or Kruskal-Wallis test was used depending on whether normality could be assumed. Bivariate correlations were evaluated using Pearson or Spearman correlation coefficients, depending on whether normality could be assumed or not. For the development of predictive models, linear regression was used.

RESULTS

Swept-source OCT allowed both independent observers clear visualization of both the RPE and scleral–choroidal junction and therefore accurate measurement of CT in all eyes (100%). Mean subfoveal choroidal thickness (SFCT) was 301.89 ᛡ 80.53 ᛁm (from 99.50 to 539.50; 95% confidence interval: 292.34–311.43). Mean macular horizontal CT was 258.69 ᛡ 64.59 ᛁm (from 99.00 to 455.28; 95% confidence interval: 251.04–266.35). The horizontal CT profile can be seen in Figure 2.

No statistically significant difference in CT was found in men compared to women. The two sexes showed a similar choroidal profile (Fig. 3), although women were found to have a trend toward thinner temporal choroids. Mean SFCT was 303.9 ᛡ 70.9 ᛁm in men versus 296.4 ᛡ 94.1 ᛁm in women (P ¼ 0.483; Student's t-test). Mean horizontal MCT was 260.8 ᛡ 60.9 ᛁm in men versus 255.0 ᛡ 70.7 ᛁm in women (P ¼ 0.227; Mann-Whitney U test). Mean age was 30.39 ᛡ 25.37 in men versus 37.48 ᛡ 23.86 in women (P ¼ 0.006; Mann-Whitney test). Mean SE was 0.15 ᛡ 1.38 D in men versus 0.09 ᛡ 1.34 D in women (P ¼ 0.796; Mann-Whitney test) (Table 1).
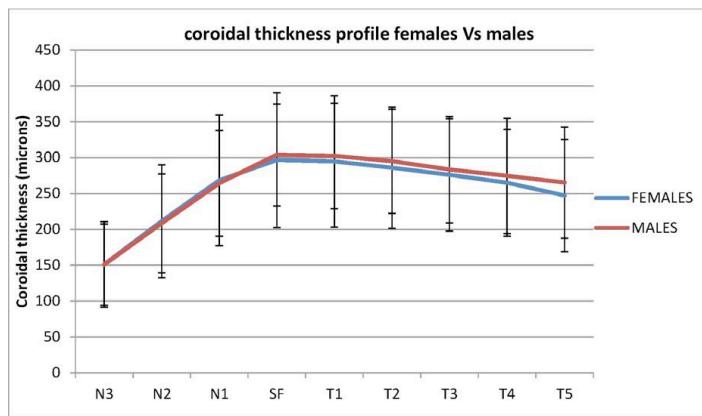

Figure 3. Choroidal thickness profile comparison, men (red) versus women (blue) (microns/measurement locations).

TABLE 1. Choroidal Thickness Comparison in Men and Women

	Male	Female	P Test
Choroidal thickness	260.8 Ƃ 60.9	255.0 Ƃ 70.7	0.227, Mann-Whitney
95% CI	251.15–269.76	242.91–267.32	
Subfoveolar thickness, MSFT	303.9 Ƃ 70.9	296.4 Ƃ 94.1	0.483, Student's t-test
95% CI	293.22–314.86	281.15–316.13	
Age, mean Ƃ SD	30.39 Ƃ 25.37	37.48 Ƃ 23.86	0.006, Mann-Whitney
95% CI	26.48–34.24	33.64–42.65	
SE, mean Ƃ SD	0.15 Ƃ 1.38	0.09 Ƃ 1.34	0.796, Mann-Whitney
95% CI	−0.07 to 0.36	−0.19 to 0.30	

TABLE 2. Choroidal Thickness Comparison in Different Age Groups

	0–10 y	11–20 y	21–40 y	41–60 y	>60 y	P, ANOVA
Mean choroidal thickness	286.0 Ƃ 43.5	277.7 Ƃ 68.2	264.0 Ƃ 61.9	223.4 Ƃ 62.2	229.7 Ƃ 66.1	<0.001
95% CI	276.04–296.08	257.90–297.54	246.41–281.64	203.54–243.34	213.11–246.42	
Subfoveal choroidal thickness	325.6 Ƃ 51.1	316.7 Ƃ 90.1	313.9 Ƃ 80.3	264.6 Ƃ 79.3	276.3 Ƃ 88.8	<0.001
95% CI	313.92–337.44	290.54–342.91	291.11–336.78	239.11–290.06	253.94–298.67	
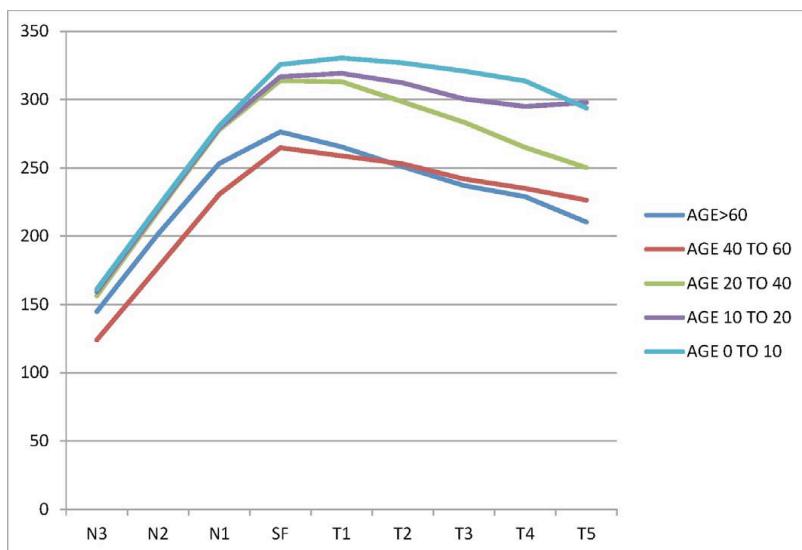
FIGURE 4. Choroidal thickness profile in different age groups (microns/measurement locations).

Mean SFCT of the different study groups (Table 2) was 325.6 Ƃ 51.1 lm in subjects 0 to 10 years, 316.7 Ƃ 90.1 lm in those 11 to 20 years, 313.9 Ƃ 80.3 lm in those 21 to 40 years, 264.6 Ƃ 79.3 lm in those 41 to 60 years, and 276.3 Ƃ 88.8 lm in those older than 60 years, differences that were statistically significant (P < 0.001; ANOVA test). Mean horizontal MCT was 286.0 Ƃ 43.5, 277.7 Ƃ 68.2, 264.0 Ƃ 61.9, 223.4 Ƃ 62.2, and 229.7 Ƃ 66.1 lm for subjects 0 to 10, 11 to 20, 21 to 40, 41 to 60, and >60 years, respectively (P < 0.001; ANOVA test). The CT profile was different in each age group (Figs. 4, 5, 6), showing an evident statistically significant difference; CT was thicker as age decreased except in the group older than 60 years, where it was thicker than among those 41 to 60 years (Table 3). However, differences in mean MCT and SFCT were not significant between subjects ages 41 to 60 versus those older than 60 years (P ¼ 0.629 and 0.502; Student's t-test, respectively).

Spherical equivalent was not different between groups except for the group 0 to 10 years (P ¼ 0.016; Kruskal-Wallis test), with 0.51 Ƃ 1.49 D in this group. Mean SE of the other groups was not different (P ¼ 0.429; Kruskal-Wallis test) (Table 3).

Correlation Analysis and Linear Regression Models

There exists a high correlation between CT and age, which is statistically significant (Table 4; Fig. 7). This correlation was found to be stronger the farther the CT was measured
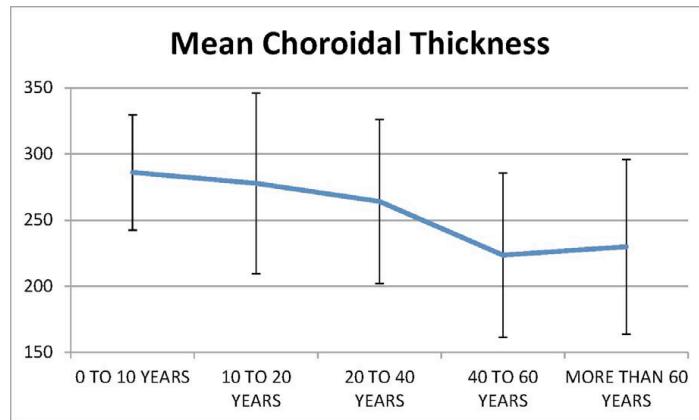
FIGURE 5. Mean choroidal thickness (microns) in different age groups.

temporally from the foveal center. Correlations between SE and CT were significant only in subfoveal and nasal measurement points (Table 4).

Macular CT multiple regression analysis including age and SE was R ¼ 0.407 (r² ¼ 0.166), showing that subtle changes appear with the variation of this parameter but with a high significance (P < 0.001). The equation predicted is as follows:

$$MCT ð microns Þ ¼ 292:484 - 1:006 * Age ð years Þ þ 5:292 * SE ð D Þ:$$

$$ð1Þ$$

Following this model, a mean reduction of 10 lm in MCT per decade (1 lm every year) and of 5.3 lm per SE diopter can be predicted. We evaluated the intereye correlation through bivariate correlations. In all measurements the correlation was strong and statistically significant (P < 0.001; Pearson correlation test), with values oscillating from r ¼ 0.680 (T5) to r ¼ 0.830 (N1) and r ¼ 0.864 for MCT. This suggests that similar results

should be obtained using one eye (randomly selected) or two eyes in the models developed. In fact, the results predicted are very similar. Evaluating only one eye per patient (taking right or left randomly), the most accurate equation to predict MCT according to age would be the following:

$$MCT \text{ in microns } ¼ 294:133 - 0:942 * Age ð years Þ$$

$$þ 3:492 * SE ð D Þ \quad ð r^2 ¼ 0:15 Þ: \quad ð2Þ$$

The SE is not statistically significant, so the equation to calculate MCT would then be

$$MCT ð microns Þ ¼ 291:847 - 0:943 * Age ð years Þ$$

$$þ 3:492 * SE ð D Þ \quad ð r^2 ¼ 0:15 Þ: \quad ð3Þ$$

The decrease in MCT is calculated to be 9.4 lm per decade (versus 10 lm when both eyes are included).
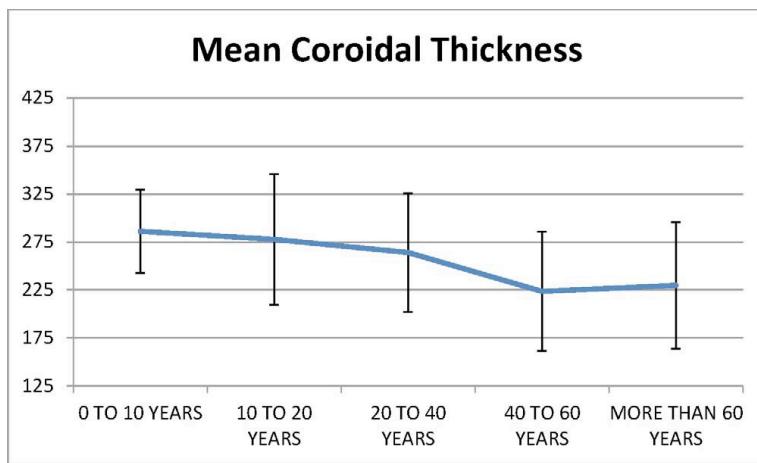
FIGURE 6. Mean subfoveolar choroidal thickness (microns) in different age groups.

Investigative Ophthalmology & Visual Science

TABLE 3. Choroidal Thickness Values According to Age Group in All Measurement Locations

Age	N3	N2	N1	SF	T1	T2	T3	T4	T5	SE, D
0–10:										
Mean	161.06	221.63	280.65	325.68	330.51	326.75	320.81	313.57	293.8	0.51
SD	45.02	49.1	54.33	51.13	54.33	56.12	59.72	63.7	60.61	1.49
95% CI	150.80–171.52	210.34–232.93	268.15–293.15	313.92–337.44	318.01–343.01	313.84–339.87	307.07–334.55	298.91–328.22	279.85–307.75	0.13–0.81
11–20:										
Mean	159.21	219.79	279.14	316.73	319.23	312.14	300.49	295.02	297.74	−0.21
SD	61.58	80.94	90.6	90.18	80.54	72.16	69.56	80.11	76.06	1.76
95% CI	141.33–177.09	196.29–243.30	252.83–305.44	290.54–342.91	295.84–342.62	291.18–333.09	280.29–320.69	271.76–318.28	275.65–319.82	−0.71 to 0.33
21–40:										
Mean	156.37	218.03	277.86	313.94	313.12	298.25	283.55	264.92	250.17	−0.15
SD	54.56	65.16	73.41	80.35	81.79	78.89	77.33	73.84	71.11	1.04
95% CI	140.87–171.88	199.51–236.55	257.00–298.72	291.11–336.77	289.88–336.36	275.83–320.67	261.57–305.53	243.94–285.90	229.96–70.38	−0.50 to 0.10
41–60:										
Mean	123.99	177.08	230.56	264.69	258.71	252.91	241.79	234.89	226.33	0.03
SD	58.35	84.35	82.25	79.34	80.8	69.42	65.11	64.75	71.46	0.94
95% CI	105.33–142.65	150.10–204.05	204.26–256.87	239.31–290.06	232.87–284.55	230.71–275.11	220.97–262.61	214.18–255.60	203.47–249.18	−0.27 to 0.33
‡60:										
Mean	144.79	201.48	253.04	276.3	265.39	250.77	236.98	228.89	210.25	0.2
SD	63.83	81.51	93.72	88.81	85.47	79.29	69.53	70.76	70.31	1.26
95% CI	128.71–160.86	180.95–222.00	229.44–276.44	253.93–298.67	243.86–286.92	230.80–270.74	219.47–254.49	211.07–246.71	192.54–227.95	−0.13 to 0.51
P test	0.001 Kruskal-Wallis	0.002 ANOVA	0.001 ANOVA	<0.001 ANOVA	<0.001 ANOVA	<0.001 ANOVA	<0.001 ANOVA	<0.001 ANOVA	<0.001 ANOVA	0.016 Kruskal-Wallis

TABLE 4. Correlations of CT With Age and Spherical Equivalent

|	N3	N2	N1	SF	T1	T2	T3	T4	T5	MCT
Age, Spearman's Rho	−0.182, $P \frac{1}{4} 0.002$	−0.180, $P \frac{1}{4} 0.003$	−0.207, $P \frac{1}{4} 0.001$	−0.287, $P \frac{1}{4} 10^{-6}$	−0.344, $P \frac{1}{4} 3\ 10^{-9}$	−0.421, $P \frac{1}{4} 3\ 3\ 10^{-13}$	−0.454, $P \frac{1}{4} 2\ 3\ 10^{-15}$	−0.447, $P \frac{1}{4} 6\ 3\ 10^{-15}$	−0.432, $P \frac{1}{4} 6\ 3\ 10^{-14}$	−0.385, $P \frac{1}{4} 3\ 3\ 10^{-11}$
Spherical equivalent, Spearman's Rho	0.178, $P \frac{1}{4} 0.003$	0.174, $P \frac{1}{4} 0.004$	0.173, $P \frac{1}{4} 0.004$	0.141, $P \frac{1}{4} 0.020$	0.104, $P \frac{1}{4} 0.086$	0.105, $P \frac{1}{4} 0.082$	0.082, $P \frac{1}{4} 0.178$	0.084, $P \frac{1}{4} 0.166$	0.064, $P \frac{1}{4} 0.294$	0.147, $P \frac{1}{4} 0.015$

62

A1

A2
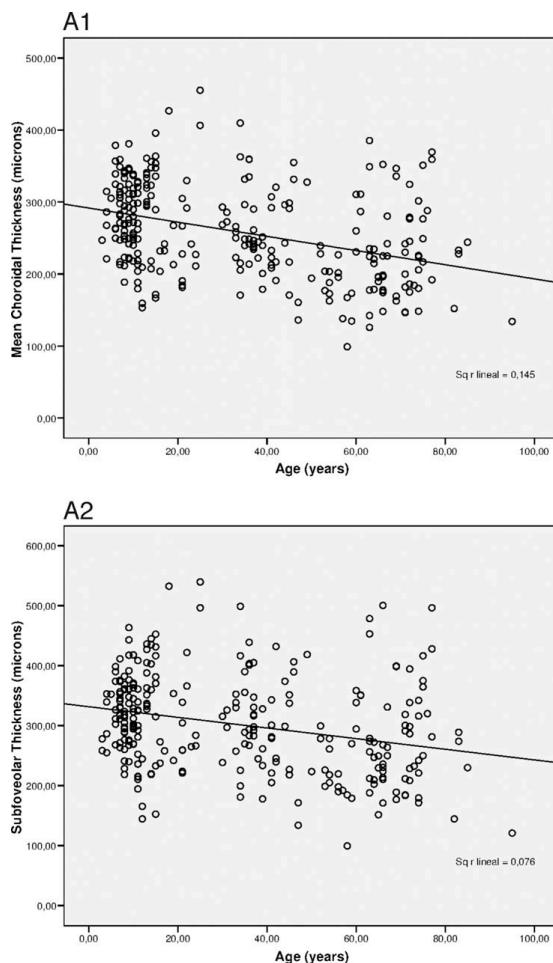
FIGURE 7. Correlation between age and mean choroidal thickness (microns, top). Correlation between age and mean subfoveolar choroidal thickness (microns, bottom).

Correlation between mean SFCT and age was R ¼ 0.275, r² ¼ 0.076. As before, the dependence found is subtle but highly significant (P < 0.001).

$$SFCT (microns) \frac{1}{4} 331:61 - 0:887*Age(years) \mathbb{P}: \qquad ð4Þ$$

This model predicts a loss of 8.87 lm of SFCT per decade.

If only one eye is evaluated per patient (taking right or left randomly), a more accurate calculation yields a SFCT in microns of 333.27 − 0.852*Age (years); R ¼ 0.266, r² ¼ 0.071. The estimated decrease in SFCT is 8.5 lm per decade (versus 8.87 lm when both eyes are included).

Intraclass correlation coefficient in CT for the two independent observers varied between 0.973 and 0.987 (Table 5). Bland-Altman plots show this good interobserver correlation (see Fig. 8). There were no statistically significant differences between the variation coefficients obtained by the two observers (Table 6; P > 0.05, Wilcoxon test).

TABLE 5. ICC in Different Measurement Locations

	ICC	95% Confidence Interval
N3	0.973	0.966, 0.978
N2	0.981	0.976, 0.985
N1	0.981	0.976, 0.985
SF	0.987	0.984, 0.990
T1	0.986	0.982, 0.989
T2	0.981	0.977, 0.985
T3	0.984	0.979, 0.987
T4	0.982	0.978, 0.986
T5	0.981	0.976, 0.985

TABLE 6. Coefficients of Variation of Each Observer at Each Measurement Point and Each Age Group Studied

	Coefficient of Variation	
	Observer 1	Observer 2
N3	0.379	0.386
N2	0.345	0.351
N1	0.302	0.303
SF	0.266	0.268
T1	0.271	0.270
T2	0.264	0.269
T3	0.269	0.273
T4	0.290	0.289
T5	0.304	0.301
MCT		
>60 y	0.287	0.289
41–60 y	0.277	0.280
21–40 y	0.237	0.234
11–20 y	0.248	0.244
0–10 y	0.152	0.153
SFCT		
>60 y	0.320	0.324
41–60 y	0.299	0.302
21–40 y	0.258	0.256
11–20 y	0.286	0.285
0–10 y	0.158	0.158

There were no statistically significant differences between the variation coefficients obtained by each observer ($P > 0.05$; Wilcoxon test).

DISCUSSION

To our knowledge, there is no previously published large study across all age groups (including pediatric patients) elucidating the normal age-related choroidal thinning that occurs in healthy eyes. Age-dependent thinning is a key factor to establish the role of the choroid in retinal pathology, something that has already been shown in several studies.[4,14–33] Although Ikuno et al.[36] performed a similar study in which they described the CT in healthy Japanese subjects, their study did not include a wide variation of ages. Furthermore, the loss of SFCT predicted by our study is 0.852 μm per year, far from the 4.32 μm per year predicted by previous papers, leading to different conclusions.

This is the largest study to date of CT measured with SS-OCT, and it confirms again the accuracy with which SS-OCT can measure the choroid. Swept-source OCT was chosen to perform this study because its characteristics allow the analysis of the choroid with more precision than previous OCT technology from a theoretical point of view. This accuracy has been shown in papers by Copete et al.[12] and Ruiz-Moreno et al.[13] using the same device. Full CT was successfully measured in 100% of the patients in those studies. Using SS-OCT we successfully measured the CT of 100% of the eyes in this study as well. Wei et al.[45] successfully measured 93.2% of 3468 patients (largest study reported to date) using Heidelberg Spectralis OCT on the EDI setting. The choice of Manjunath et al.[37] was Cirrus HD-OCT without EDI, which was able to successfully measure the choroid in only 74% of the eyes. Yamashita et al.[46] and Shin et al.[47] used Topcon SD-OCT and were able to image 63.3% and 90.7%, respectively. Copete et al.[12] compared SD-OCT and SS-OCT, obtaining good measurements in 70.4% and 100%, respectively.

Margolis et al.[38] studied a group of 54 eyes with a mean SE of −1.3 D, finding a mean SFCT of 287 μm, similar to the results of Flores-Moreno et al.[48] and those of Manjunath et al.,[37] who published a mean SFCT of 272 μm in 34 eyes of 51.1-year-old patients.

Xu et al.[49] compared diabetic with nondiabetic patients, finding a mean SFCT of 266 μm in the control group (1795 subjects).

The choroid has also been studied in pediatric population using SS-OCT. Ruiz-Moreno et al.[13] compared both pediatric (83 eyes, 10-year-old patients with mean SE of 0.3 D) and adult (75 eyes, 53-year-old patients with mean SE of 0.16 D) healthy patients, finding a mean SFCT of 312 and 302 μm, respectively. Park and Oh,[50] in a recent study with pediatric subjects, found a mean SFCT of 348.4 μm in the 48 eyes studied.

In the present study, the mean SFCT was found to be 301.89 μm. This figure is approximately 10 μm greater than that found by other authors using SD-OCT.[37–39,45–49] It is likely that the introduction of pediatric eyes into the study group resulted in a slight increase in the mean SFCT. Interestingly, these results match those of Ruiz-Moreno et al.,[13] who with the same device found almost the same CT in their patient group consisting of adults only. Swept-source OCT may result in a CT measurement slightly greater than that seen with SD-OCT. This may be explained by the higher quality of the images and by the fact that the measures were taken from the posterior edge of the RPE to the outer aspect of the lamina fusca, rather than the outer limit of the choroidal vessels.

Ruiz-Moreno et al.[13] with SS-OCT and Flores-Moreno et al.[48] with SD-OCT provide data about mean MCT. Ruiz-Moreno found it to be 275 μm in adults compared to 285 μm in pediatric subjects. Flores-Moreno obtained a result of 257 μm in healthy patients and 115 μm in highly myopic patients. We found that mean MCT was 258.69 μm, similar to these authors' results. Nevertheless, the present study is the first employing a subfoveal 8-mm line of the macula compared to the 6 mm studied by other authors. This was possible due to SS-OCT technology, which provides a more robust imaging of the temporal choroid, as this 2-mm increase was performed on the temporal sector. This may prove to be a clinically important measure, as it is in the temporal sector that greater variations of CT with age take place.

We found no statistically significant difference when comparing men to women. Subjects of both sexes showed almost identical choroidal profiles with a minimal difference in the temporal sector (Fig. 3), in which the females usually had slightly thinner choroids. Mean SFCT was 303.9 μm in men versus 296.4 μm in women. These slight, nonstatistically significant differences can be explained by the age differences of the two groups, 30.39 years for men and 37.48 years for women. Choroidal thickness was approximately 7 μm greater in men on average, but the men in this study were, on average, 7 years younger. According to the correlation formulas established by this database, CT in a sex- and age-matched group would likely have been almost identical.

A few studies have been previously performed in adults using high-penetration OCT[36,43,51] but without comparing different age groups. We analyzed CT comparing several ranges of age with a 20-year gap. The first two age groups spanned from age 0 to 10 and age 10 to 20 years. These ranges were selected because eye growth undergoes two phases, the first up to age 6 years, reaching emmetropization, and the second from 7 to 19 years, when global expansion of the eye takes place.[52] Park and Oh[50] (mean age of subjects 86.4 months, from 52 to 131 months) and Ruiz-Moreno et al.[13] studied CT in pediatric subjects, with only the latter comparing CT simultaneously with adults. The CT profile changed in every group (Figs. 4, 5, 6) and the choroid measured thinner as age increased, showing statistically significant differences. This decrease was found to be progressive until 40 years, at which

point the most significant variation took place, from 313.9 lm in the 21- to 40-year-old group to 264.6 lm in the 41- to 60-year-old group (49-lm difference). Interestingly, from 40 years on (41–60 vs. >60 years) the differences in CT were not found to be statistically significant, either mean MCT or SFCT. Variations when only one eye per patient (as in Ray and O'Day[53]) or both were taken into account were minimal, showing calculated decreases of 9.4 vs. 10 lm per decade in MCT and 8.5 vs. 8.87 lm per patient in SFCT.

One of the limitations of this study is the fact that the CT was manually determined. There is now an automated software commercially available, Topcon DRI OCT-1 software (version 9.01.003.02), for automated segmentation and thickness measurements in three-dimensional or radial scan mode; however, its accuracy in clinical practice has yet to be widely tested.

According to our results, the macular CT profile in a healthy population is similar between different age groups, with the choroid in healthy eyes getting thinner with age, particularly when adults older than 40 years are compared to children and younger adults. There were no differences due to sex. The greater CT variation due to age takes place in temporal sectors.

Acknowledgments

References

1. Coleman DJ, Lizzi FL. In vivo choroidal thickness measurement. Am J Ophthalmol. 1979;88:369–375.

2. Cheng H, Nair G, Walker TA, et al. Structural and functional MRI reveals multiple retinal layers. Proc Natl Acad Sci U S A. 2006;103:17525–17530.

3. Yannuzzi LA, Ober MD, Slakter JS, et al. Ophthalmic fundus imaging: today and beyond. Am J Ophthalmol. 2004;137:511–524.

4. Stanga PE, Lim JI, Hamilton P. Indocyanine green angiography in chorioretinal diseases: indications and interpretation: an evidence-based update. Ophthalmology. 2003;110:15–21.

5. Gabriele ML, Wollstein G, Ishikawa H, et al. Optical coherence tomography: history, current status, and laboratory work. Invest Ophthalmol Vis Sci. 2011;52:2425–2436.

6. Huang D, Swanson EA, Lin CP, et al. Optical coherence tomography. Science. 1991;254:1178–1181.

7. Spaide RF, Koizumi H, Pozzoni MC. Enhanced depth imaging spectral-domain optical coherence tomography. Am J Ophthalmol. 2008;146:496–500.

8. Huber R, Adler DC, Srinivasan VJ, Fujimoto JG. Fourier domain mode locking at 1050 nm for ultra-high-speed optical coherence tomography of the human retina at 236,000 axial scans per second. Opt Lett. 2007;32:2049–2051.

9. Lim H, de Boer JF, Park BH, Lee EC, Yelin R, Yun SH. Optical frequency domain imaging with a rapidly swept laser in the 815-870 nm range. Opt Express. 2006;14:5937–5944.

10. Unterhuber A, Povazay B, Hermann B, Sattmann H, Chavez-Pirson A, Drexler W. In vivo retinal optical coherence tomography at 1040 nm-enhanced penetration into the choroid. Opt Express. 2005;13:3252–3258.

11. Yasuno Y, Hong Y, Makita S, et al. In vivo high-contrast imaging of deep posterior eye by 1-micron swept source optical coherence tomography and scattering optical coherence angiography. Opt Express. 2007;15:6121–6139.

12. Copete S, Flores-Moreno I, Montero J, Duker JS, Ruiz-Moreno JM. Direct comparison of spectral-domain and swept-source OCT in the measurement of choroidal thickness in normal eyes [published online ahead of print November 28, 2013]. Br J Ophthalmol. doi:10.1136/bjophthalmol-2013-303904.

13. Ruiz-Moreno JM, Flores-Moreno I, Lugo F, Ruiz-Medrano J, Montero JA, Akiba M. Macular choroidal thickness in normal pediatric population measured by swept-source optical coherence tomography. Invest Ophthalmol Vis Sci. 2013;54:353–359.

14. Imamura Y, Fujiwara T, Margolis R, Spaide RF. Enhanced depth imaging optical coherence tomography of the choroid in central serous chorioretinopathy. Retina. 2009;29:1469–1473.

15. Maruko I, Iida T, Sugano Y, Ojima A, Sekiryu T. Subfoveal choroidal thickness in fellow eyes of patients with central serous chorioretinopathy. Retina. 2011;31:1603–1608.

16. Yannuzzi LA. Indocyanine green angiography: a perspective on use in the clinical setting. Am J Ophthalmol. 2011;151:745–751.

17. Chung SE, Kang SW, Lee JH, Kim YT. Choroidal thickness in polypoidal choroidal vasculopathy and exudative age-related macular degeneration. Ophthalmology. 2011;118:840–845.

18. Koizumi H, Yamagishi T, Yamazaki T, Kawasaki R, Kinoshita S. Subfoveal choroidal thickness in typical age-related macular degeneration and polypoidal choroidal vasculopathy. Graefes Arch Clin Exp Ophthalmol. 2011;249:1123–1128.

19. Manjunath V, Goren J, Fujimoto JG, Duker JS. Analysis of choroidal thickness in age-related macular degeneration using spectral-domain optical coherence tomography. Am J Ophthalmol. 2011;152:663–668.

20. Switzer DW Jr, Mendonca LS, Saito M, Zweifel SA, Spaide RF. Segregation of ophthalmoscopic characteristics according to choroidal thickness in patients with early age-related macular degeneration. Retina. 2012;32:1265–1271.

21. Ueta T, Obata R, Inoue Y, et al. Background comparison of typical age-related macular degeneration and polypoidal choroidal vasculopathy in Japanese patients. Ophthalmology. 2009;116:2400–2406.

22. Wood A, Binns A, Margrain T, et al. Retinal and choroidal thickness in early age-related macular degeneration. Am J Ophthalmol. 2011;152:1030–1038.

23. Chen W, Wang Z, Zhou X, Li B, Zhang H. Choroidal and photoreceptor layer thickness in myopic population. Eur J Ophthalmol. 2012;22:590–597.

24. Fujiwara T, Imamura Y, Margolis R, Slakter JS, Spaide RF. Enhanced depth imaging optical coherence tomography of the choroid in highly myopic eyes. Am J Ophthalmol. 2009;148:445–450.

25. Fureder W, Krauth MT, Sperr WR, et al. Evaluation of angiogenesis and vascular endothelial growth factor expression in the bone marrow of patients with aplastic anemia. Am J Pathol. 2006;168:123–130.

26. Ikuno Y, Tano Y. Retinal and choroid biometry in highly myopic eyes with spectral-domain optical coherence tomography. Invest Ophthalmol Vis Sci. 2009;50:3876–3880.

27. Wang NK, Lai CC, Chu HY, et al. Classification of early dry-type myopic maculopathy with macular choroidal thickness. Am J Ophthalmol. 2012;153:669–677.

28. Aoyagi R, Hayashi T, Masai A, et al. Subfoveal choroidal thickness in multiple evanescent white dot syndrome. Clin Exp Optom. 2012;95:212–217.

29. Channa R, Ibrahim M, Sepah Y, et al. Characterization of macular lesions in punctate inner choroidopathy with spectral domain optical coherence tomography. J Ophthalmic Inflamm Infect. 2012;2:113–120.

30. Fong AH, Li KK, Wong D. Choroidal evaluation using enhanced depth imaging spectral-domain optical coherence tomography in Vogt-Koyanagi-Harada disease. Retina. 2011; 31:502–509.

31. Nakai K, Gomi F, Ikuno Y, et al. Choroidal observations in Vogt-Koyanagi-Harada disease using high-penetration optical coherence tomography. Graefes Arch Clin Exp Ophthalmol. 2012; 250:1089–1095.

32. Say EA, Shah SU, Ferenczy S, Shields CL. Optical coherence tomography of retinal and choroidal tumors [published online ahead of print July 18, 2011]. J Ophthalmol. doi:10.1155/2011/385058.

33. Shields CL, Perez B, Materin MA, Mehta S, Shields JA. Optical coherence tomography of choroidal osteoma in 22 cases: evidence for photoreceptor atrophy over the decalcified portion of the tumor. Ophthalmology. 2007;114:e53–e58.

34. Ding X, Li J, Zeng J, et al. Choroidal thickness in healthy Chinese subjects. Invest Ophthalmol Vis Sci. 2011;52:9555–9560.

35. Ho J, Branchini L, Regatieri C, Krishnan C, Fujimoto JG, Duker JS. Analysis of normal peripapillary choroidal thickness via spectral domain optical coherence tomography. Ophthalmology. 2011;118:2001–2007.

36. Ikuno Y, Kawaguchi K, Nouchi T, Yasuno Y. Choroidal thickness in healthy Japanese subjects. Invest Ophthalmol Vis Sci. 2010;51:2173–2176.

37. Manjunath V, Taha M, Fujimoto JG, Duker JS. Choroidal thickness in normal eyes measured using Cirrus HD optical coherence tomography. Am J Ophthalmol. 2010;150:325–329.

38. Margolis R, Spaide RF. A pilot study of enhanced depth imaging optical coherence tomography of the choroid in normal eyes. Am J Ophthalmol. 2009;147:811–815.

39. Ouyang Y, Heussen FM, Mokwa N, et al. Spatial distribution of posterior pole choroidal thickness by spectral domain optical coherence tomography. Invest Ophthalmol Vis Sci. 2011;52: 7019–7026.

40. Brown JS, Flitcroft DI, Ying GS, et al. In vivo human choroidal thickness measurements: evidence for diurnal fluctuations. Invest Ophthalmol Vis Sci. 2009;50:5–12.

41. Tan CS, Ouyang Y, Ruiz H, Sadda SR. Diurnal variation of choroidal thickness in normal, healthy subjects measured by spectral domain optical coherence tomography. Invest Ophthalmol Vis Sci. 2012;53:261–266.

42. Usui S, Ikuno Y, Akiba M, et al. Circadian changes in subfoveal choroidal thickness and the relationship with circulatory factors in healthy subjects. Invest Ophthalmol Vis Sci. 2012; 53:2300–2307.

43. Ikuno Y, Maruko I, Yasuno Y, et al. Reproducibility of retinal and choroidal thickness measurements in enhanced depth imaging and high-penetration optical coherence tomography. Invest Ophthalmol Vis Sci. 2011;52:5536–5540.

44. Hirata M, Tsujikawa A, Matsumoto A, et al. Macular choroidal thickness and volume in normal subjects measured by swept-source optical coherence tomography. Invest Ophthalmol Vis Sci. 2011;52:4971–4978.

45. Wei WB, Xu L, Jonas JB, et al. Subfoveal choroidal thickness: the Beijing Eye Study. Ophthalmology. 2013;120:175–180.

46. Yamashita T, Yamashita T, Shirasawa M, Arimura N, Terasaki H, Sakamoto T. Repeatability and reproducibility of subfoveal choroidal thickness in normal eyes of Japanese using different SD-OCT devices. Invest Ophthalmol Vis Sci. 2012;53:1102–1107.

47. Shin JW, Shin YU, Cho HY, Lee BR. Measurement of choroidal thickness in normal eyes using 3D OCT-1000 spectral domain optical coherence tomography. Korean J Ophthalmol. 2012; 26:255–259.

48. Flores-Moreno I, Lugo F, Duker JS, Ruiz-Moreno JM. The relationship between axial length and choroidal thickness in eyes with high myopia. Am J Ophthalmol. 2013;155:314–319.

49. Xu J, Xu L, Du KF, et al. Subfoveal choroidal thickness in diabetes and diabetic retinopathy. Ophthalmology. 2013;120: 2023–2028.

50. Park KA, Oh SY. Choroidal thickness in healthy children. Retina. 2013;33:1971–1976.

51. Agawa T, Miura M, Ikuno Y, et al. Choroidal thickness measurement in healthy Japanese subjects by three-dimensional high-penetration optical coherence tomography. Graefes Arch Clin Exp Ophthalmol. 2011;249:1485–1492.

52. Ishii K, Iwata H, Oshika T. Quantitative evaluation of changes in eyeball shape in emmetropization and myopic changes based on elliptic fourier descriptors. Invest Ophthalmol Vis Sci. 2011;52:8585–8591.

53. Ray WA, O'Day DM. Statistical analysis of multi-eye data in ophthalmic research. Invest Ophthalmol Vis Sci. 1985;26: 1186–1188.

Investigative Ophthalmology & Visual Science

66

4.3 Morphologic Features of the Choroidoscleral Interface in a

Healthy Population Using Swept-Source Optical Coherence

Tomography

Morphologic Features of the Choroidoscleral Interface in a Healthy Population Using Swept-Source Optical Coherence Tomography

JORGE RUIZ-MEDRANO, IGNACIO FLORES-MORENO, JAVIER A. MONTERO, JAY S. DUKER, AND
JOSÉ M. RUIZ-MORENO

• OBJECTIVE: To analyze the morphologic features of the choroidoscleral interface in a healthy population using swept-source optical coherence tomography (SS OCT).

• DESIGN: Retrospective data analysis of a subgroup of eyes from a previous single-center, prospective, cross-sectional, noninterventional study.

• METHODS: A total of 276 healthy eyes from 154 subjects were evaluated using SS OCT. Inclusion criteria were best-corrected visual acuity between 20/20 and 20/25, spherical equivalent between ±3 diopters, and no systemic or ocular diseases. Two independent investigators analyzed the morphologic features of the choroidoscleral interface in a masked fashion, classifying the contour and shape as concave (bowl-shaped) or inflective (S-shaped contour with ‡1 inflection point).

• RESULTS: The presence of a temporal choroidoscleral interface inflection was identified in 12.8% of the eyes. The mean choroidal thickness was 372.1 ± 76.8 mm and the average distance from the inflection point to the fovea was 4427.3 ± 627.9 mm. Nine patients showed an inflective profile in both eyes. No changes in the retinal profile were found in any of these cases. The mean age of the patients with an inflective profile was 16 ± 19 years (range 4–82) vs 36 ± 25 years (range 3–95) in the group with a concave contour (P .001). The temporal choroidal thickness at 4000 and 5000 mm from the fovea was thicker in the group with a concave contour.

• CONCLUSIONS: Temporal choroidoscleral interface inflection or S-shaped profile of the choroidoscleral interface with focal thinning of the choroid can be considered a normal variation without clinical significance, especially in younger populations. (Am J Ophthalmol 2015;160(3):596–601. © 2015 by Elsevier Inc. All rights reserved.)

IN RECENT YEARS, STUDIES OF THE CHOROIDAL ANATomy in posterior segment disease using optical coherence tomography (OCT) have increased our knowledge of the role of choroidal changes in various con- ditions such as central serous chorioretinopathy,[1–4] age- related macular degeneration,[1,4–7] polypoidal choroidal vasculopathy,[1,4–7] myopic maculopathy,[8–10] posterior uveitis,[1,3,4,11,12] and choroidal tumors.[1,13,14] Spaide and associates[15] introduced a technique for improving choroidal imaging using spectral-domain OCT (SD OCT) devices called enhanced depth image (EDI) OCT. EDI OCT provides improved choroidal visualization in most eyes, permitting quantitative and reproducible determination of choroidal thickness. Longer-wavelength swept-source OCT (SS OCT)[16–19] is an innovative technology available for OCT imaging that further improves choroidal imaging compared to EDI SD OCT. Copete and associates,[20] Ruiz-Moreno and associates,[21] and our group[22] reported that reliable measurement of choroidal thickness is possible in 100% of eyes using an SS OCT device.

Age-related reduction of choroidal thickness in normal eyes,[23–28] choroidal thickness differences in adult and pediatric eyes,[21,22] and differences between right and left eye[29] are reported findings using this technique. However, knowledge of choroidal morphology is not complete yet. Adhi and associates[30] described significant alterations in choroidal morphologic features in eyes with advanced diabetic retinopathy (DR). These alterations included an irregular or a temporal choroidoscleral interface inflecting in most DR eyes. In addition, a recent paper reported a focal inferotemporal scleral bulge with choroidal thinning[31] in normal eyes modifying the normal contour and shape (bowl-shaped or concave when looking from the inside out) of the choroidoscleral interface.[30]

The aim of this study is to analyze the morphologic features of the choroidoscleral interface in a healthy population using SS OCT.

PATIENTS AND METHODS

THE DATA AND IMAGES OF A SPECIFIC POPULATION SUBgroup from a previously published prospective study were

analyzed.[22] This study followed the tenets of the Declaration of Helsinki and the original study was approved by the institutional review board of Vissum Alicante. Data were collected from December 2011 to January 2013. The subjects provided informed consent to participate in the research to study the thickness and morphology of the choroid in a healthy population. Participation was offered to subjects who were attending routine ocular examinations and voluntarily agreed to participate, provided they met the inclusion criteria, with no age limitations, and signed an informed consent. Inclusion criteria were best-corrected visual acuity (BCVA) between 20/20 and 20/25, spherical equivalent (SE) between 63 diopters (D), and no systemic or ocular diseases (other than cataract). Patients with prior history of any retinal condition in either eye were not included. All examinations were obtained in the afternoon (between 4 PM and 8 PM) to avoid diurnal variations.[32–34]

Two independent investigators performed an analysis of the morphologic features of the choroidoscleral interface in a masked fashion, classifying and labeling the contour and shape of the horizontal choroidoscleral interface as previously published.[30] Specifically, the choroidal morphology was defined as being concave (or bowl-shaped) or with temporal choroidoscleral interface inflecting (having an irregular or concave-convex-concave shape with ≥1 inflection point). If the contour was labeled as temporal choroidoscleral interface inflecting, choroidal thickness at the level of the inflection point was measured (as described below), as well as the distance to the fovea (Figure 1).

The mean choroidal thickness measurements in healthy eyes reported previously[22] were used as a reference to define focal thinning/thickening. According to Adhi and associates, eyes were considered to have focal thinning/thickening if choroidal thickness at the measured location was 50% less/more than that of the mean choroidal thickness of normal eyes at the corresponding location.[30] The procedure followed to analyze and measure choroidal thickness profile has been previously described.[22] The macular horizontal choroidal thickness profile (choroidal thickness measured using a horizontal line centered at the fovea, containing 1024 axial scans and with a length of 12 mm)[22] was created with an SS OCT system (Topcon Corporation, Tokyo, Japan), after the patients provided informed consent. A horizontal choroidal thickness profile of the macula was manually created by measuring the choroidal thickness from the posterior edge of retinal pigment epithelium (RPE) to the choroid/sclera junction under the fovea using the prototype software. Eight further determinations were performed every 1000 mm temporal (T1, T2, T3, T4, and T5) and nasal (N1, N2, and N3) to the fovea. The outer aspect of the lamina fusca, rather than the outer limit of the choroidal vessels, was the landmark used to determine the most distal aspect of the choroid and the inner edge of the sclera.
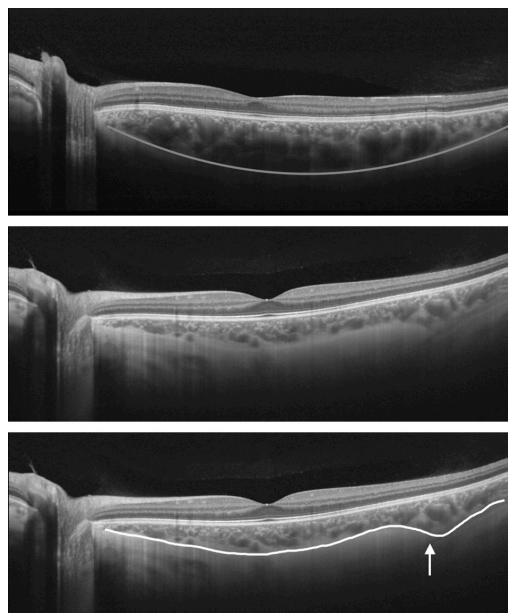

FIGURE 1. Choroidoscleral interface of healthy patients analyzed using swept-source optical coherence tomography. (Top) Bowl-shaped/concave choroid: The choroid grows steadily thinner toward nasal and temporal sectors. White line represents the bowl-shaped contour to the choroidoscleral interface. (Middle) Temporal choroidoscleral interface inflection: Evident choroidal thickening (inflection point) in relation to the 2 adjacent measured points at both sides of the inflection point, without any other relevant choroidal finding, in a 7-year-old boy. (Bottom) White line represents the temporal choroidoscleral interface; arrow pointing at choroidal inflection (bottom).

For this study, the reference mirror of SS OCT was placed at the deeper position of the retina so that the sensitivity was higher at the choroidal area in macular imaging. A 1-line scanning mode, which produces an OCT image containing 1024 axial scans with a scan length of 12 mm, was employed. Two observers determined choroidal thickness independently and in a masked fashion.

An experienced technician determined refractive errors and BCVA using an autorefractometer (Nidek, Gamagori, Japan) that was later checked by a certified optometrist.

Data obtained were statistically analyzed using a licensed version of SPSS 17.0 for Windows (SPSS, Chicago, Illinois, USA). The Kolmogorov-Smirnov test was applied for all data samples in order to check normality. Intergroup analysis was performed using the Student t test when samples were normally distributed or Mann-Whitney test when parametric statistics were not possible. The level of significance used was $P < .05$. The interobserver reproducibility was evaluated using intraclass correlation coefficient (ICC) for each variable measured (mean and 95% confidence

interval), coefficient of variation between graders, and Bland-Altman plots.

RESULTS

WE ANALYZED 276 EYES FROM 154 PATIENTS. NINETY-THREE patients (60.4%) were male and 61 (39.6%) were female. The presence of the concave or bowl-shaped contour of the horizontal choroidoscleral interface was found in 240 of the 276 eyes analyzed (87.2%). The presence of a temporal choroidoscleral interface inflection was identified in 36 out of 276 eyes (12.8%), 19 times in the left eye and 17 in the right eye. All the irregularities or concave-convex-concave shapes with ≥ 1 inflection point were found in the temporal aspect of the macular choroidal thickness profile. Only 1 inflection point was found in all eyes with a mean distance to the fovea of 4427.3 ⊝ 627.9 mm (range 2531–5492), and it was always located between 2000 and 5000 mm temporal the fovea, except in 6 eyes in which it was located more than 5000 mm away from it (Figure 2). Mean choroidal thickness at the site of the inflection point was 372.1 ⊝ 76.8 mm (range 168–538 mm). In 9 cases the temporal choroidoscleral interface inflection was bilateral (Figure 3). No changes in retinal profile were found in any of these cases.

Mean age of the patients with temporal choroidoscleral interface inflection was 16 ⊝ 19 years (range 4–82 years) vs 36 ⊝ 25 years (range 3–95 years) in the group with bowl-shaped contour (P ¼ .001; Student t test for unpaired data). Temporal choroidal thickness was also different between both groups. Mean choroidal thickness in the temporal choroidoscleral interface inflection group at the site of T4 was 317.6 ⊝ 80.2 mm (range 120–440 mm) vs 266.3 ⊝ 76.8 mm (range 105–504 mm) in the group with bowl-shaped contour (P ¼ .001; Mann-Whitney U test). Choroidal thickness in the temporal choroidoscleral interface inflection group was 286.0 ⊝ 71.7 mm (range 160–466 mm) at the site of T5, vs 252.5 ⊝ 77.2 mm (range 66–483 mm) in the bowl-shaped group (P ¼ .01; Mann-Whitney U test). In contrast, the difference of mean choroidal thickness at T1, T2, and T3 was not statistically different (P ¼ .26, P ¼ .39, and P ¼ .11, respectively; Mann-Whitney U test).

The prevalence of a temporal choroidoscleral interface inflection profile was 30 out of 120 (12.5%) in the group of patients aged 15 or younger, vs 6 out of 156 (3.8%) in the group of patients aged 16 or older (P < .01; x^2 test).

A high agreement in the measures taken by the 2 observers was found. The ICC values obtained for the variables evaluated were within the range 0.966–0.987. The Bland-Altman plots also confirmed high agreement between measures, using ⊝2 standard deviations as limits of reproducibility.
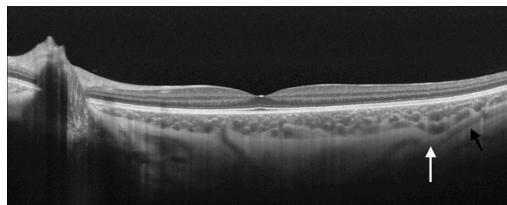

FIGURE 2. Choroidal inflection point in the temporal side of the right eye in a healthy 8-year-old girl analyzed with swept-source optical coherence tomography. An image was identified (white arrow) that could fit the superior edge of the insertion of the inferior oblique muscle in the sclera, together with a thin, hyporeflective line parallel to the choroidoscleral limit, which could match the intrascleral portion of the temporal long posterior ciliary artery (black arrow).
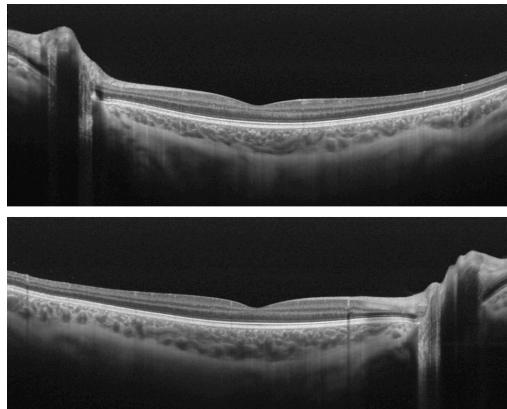
FIGURE 3. Bilateral temporal choroidoscleral interface inflection in a healthy 11-year-old boy analyzed with swept-source optical coherence tomography. (Top) Right eye; (Bottom) left eye.

DISCUSSION

THE HORIZONTAL MACULAR CHOROIDAL THICKNESS PROfile in healthy people has been described by our group[22] and by other authors.[21,23–28] The choroid normally is thickest in the subfoveal region, decreasing slowly and progressively toward the temporal aspect and more steeply toward the optic nerve,[22,35,36] with a bowl-shaped contour.[30]

Adhi and associates described significant alterations in choroidal morphologic features in the majority of eyes with DR. They found an irregular temporal choroidoscleral interface inflection point in 8 of 9 eyes with nonproliferative DR (89%), 9 of 10 eyes with proliferative DR (90%), and 13 of 14 eyes with diabetic macular edema (93%) compared with 0 of 24 in controls.[30] The presence of an

irregular temporal choroidoscleral interface inflection contour with focal thinning of the choroid has been detected in some diseases (diabetic retinopathy and age-related macular degeneration).[30,37,38]

Dolz-Marco and associates[31] reported a bilateral case of focal inferotemporal scleral bulge with a concave choroidal thinning surrounded by normal choroidal tissue. The authors hypothesized that this finding could be related to the inferior oblique muscle leading to inward compression of the choroid, not being able to study the scleral wall, as it was not entirely visible.[31]

No anomalies in the fundus examination were found that could justify this thickening in our series of patients with temporal choroidoscleral interface inflection. SS OCT analysis did not detect any alteration in the choroid of these patients other than 1 inflection point (Figures 1–3). On the other hand, an image that could represent the superior edge of the insertion of the inferior oblique muscle in the sclera was identified (Figure 2), together with a thin, hyporeflective line parallel to the sclera/choroid limit that could match the intrascleral portion of the temporal long posterior ciliary artery (Figures 2 and 4).

The reason why retinal vessels seem to be hyperreflective in OCT images while choroidal vessels look hyporeflective is related to the velocity of blood cells through them. The blood flow velocity inside choroidal vessels is much higher than that of retinal vessels. OCT imaging is based on interferometry, where an interference fringe is detected to construct the intensity of the signal. The fast speed of the blood cells makes the interference fringe vanish; thus no signal is observed inside the choroidal vessels. On the other hand, blood cell speed is relatively slow in the case of retinal vascular structures, which contributes to the interference signal as a hyperreflective signal.

Reported studies on the anatomy of the posterior aspect of the globe and the vascular and muscular structures and its relation to the sclera show that the anterior and superior limit of the posterior insertion of the inferior oblique muscle coincides with the horizontal line/meridian, within 5.7 mm of the fovea.[39]

The mean distance from the inflection point to the fovea was 4427 mm in our series and always located temporal to the fovea. The presence of the inflection point is probably related to the insertion of the inferior oblique muscle, which is believed to be 5.7 mm from the fovea. The traction applied to the sclera by the tendon might cause a
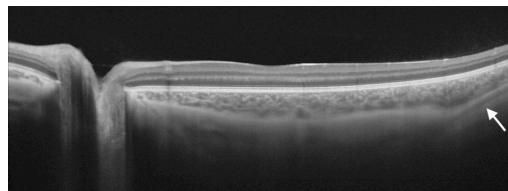
FIGURE 4. Swept-source optical coherence tomography performed inferior to the fovea of a young patient. Temporal long posterior ciliary artery can be seen at the level of the choroidoscleral inflection point. A thin, hyporeflective line parallel to the choroidoscleral limit that could match the intrascleral portion of the temporal long posterior ciliary artery can be identified (arrow).

separation of the scleral wall, leading to its deformation and a thickening of the choroid. This theory is supported by Figures 2 and 4, and is compatible with the tractional theory. Based on the anatomic descriptions of this region,[39] the parallel, hyporeflective line at this level could correspond to the intrascleral portion of the temporal long posterior ciliary artery (Figures 2 and 4).

The fact that this finding is more frequent in younger healthy people, especially those under age 15, could be explained by the reduced scleral stiffness in younger age,[40] which could facilitate the deformation induced by the traction of the inferior oblique muscle tendon.

The limitations of our study are the manual determination of the choroidal thickness and the fact that it only shows the horizontal choroidal thickness profile. Automatic software is now commercially available: Topcon DRI OCT-1 software (Ver. 9.01.003.02) for automated segmentation and thickness measurements in 3-dimensional or radial scan mode. However, its accuracy in clinical practice is yet to be widely tested.

In conclusion, this temporal choroidoscleral interface inflection with focal thinning of the choroid can be considered a normal variation without clinical significance, especially among young people. Further studies of the whole macular profile, including the complete insertion of the inferior oblique muscle, and with a larger number of patients will be necessary in order to establish the final characteristics of these variations and their incidence in a healthy population.

REFERENCES

1. Stanga PE, Lim JI, Hamilton P. Indocyanine green angiography in chorioretinal diseases: indications and interpretation: an evidence-based update. Ophthalmology 2003;110(1): 15–21.

2. Imamura Y, Fujiwara T, Margolis R, Spaide RF. Enhanced depth imaging optical coherence tomography of the choroid in central serous chorioretinopathy. Retina 2009;29(10): 1469–1473.

3. Maruko I, Iida T, Sugano Y, Ojima A, Sekiryu T. Subfoveal choroidal thickness in fellow eyes of patients with central serous chorioretinopathy. Retina 2011;31(8):1603–1608.

4. Yannuzzi LA. Indocyanine green angiography: a perspective on use in the clinical setting. Am J Ophthalmol 2011;151(5): 745–751.

5. Chung SE, Kang SW, Lee JH, Kim YT. Choroidal thickness in polypoidal choroidal vasculopathy and exudative age-related macular degeneration. Ophthalmology 2011;118(5): 840–845.

6. Koizumi H, Yamagishi T, Yamazaki T, Kawasaki R, Kinoshita S. Subfoveal choroidal thickness in typical age-related macular degeneration and polypoidal choroidal vasculopathy. Graefes Arch Clin Exp Ophthalmol 2011; 249(8):1123–1128.

7. Ueta T, Obata R, Inoue Y, et al. Background comparison of typical age-related macular degeneration and polypoidal choroidal vasculopathy in Japanese patients. Ophthalmology 2009;116(12):2400–2406.

8. Chen W, Wang Z, Zhou X, Li B, Zhang H. Choroidal and photoreceptor layer thickness in myopic population. Eur J Ophthalmol 2012;22(4):590–597.

9. Fujiwara T, Imamura Y, Margolis R, Slakter JS, Spaide RF. Enhanced depth imaging optical coherence tomography of the choroid in highly myopic eyes. Am J Ophthalmol 2009; 148(3):445–450.

10. Fureder W, Krauth MT, Sperr WR, et al. Evaluation of angiogenesis and vascular endothelial growth factor expression in the bone marrow of patients with aplastic anemia. Am J Pathol 2006;168(1):123–130.

11. Aoyagi R, Hayashi T, Masai A, et al. Subfoveal choroidal thickness in multiple evanescent white dot syndrome. Clin Exp Optom 2012;95(2):212–217.

12. Channa R, Ibrahim M, Sepah Y, et al. Characterization of macular lesions in punctate inner choroidopathy with spectral domain optical coherence tomography. J Ophthalmic Inflamm Infect 2012;2(3):113–120.

13. Say EA, Shah SU, Ferenczy S, Shields CL. Optical coherence tomography of retinal and choroidal tumors. J Ophthalmol 2011; http://dx.doi.org/10.1155/2011/385058.

14. Shields CL, Perez B, Materin MA, Mehta S, Shields JA. Optical coherence tomography of choroidal osteoma in 22 cases: evidence for photoreceptor atrophy over the decalcified portion of the tumor. Ophthalmology 2007;114(12):e53–58.

15. Spaide RF, Koizumi H, Pozzoni MC. Enhanced depth imaging spectral-domain optical coherence tomography. Am J Ophthalmol 2008;146(4):496–500.

16. Huber R, Adler DC, Srinivasan VJ, Fujimoto JG. Fourier domain mode locking at 1050 nm for ultra-high-speed optical coherence tomography of the human retina at 236,000 axial scans per second. Opt Lett 2007;32(14): 2049–2051.

17. Lim H, de Boer JF, Park BH, Lee EC, Yelin R, Yun SH. Optical frequency domain imaging with a rapidly swept laser in the 815-870 nm range. Opt Express 2006;14(13):5937–5944.

18. Unterhuber A, Povazay B, Hermann B, Sattmann H, Chavez-Pirson A, Drexler W. In vivo retinal optical coherence tomography at 1040 nm-enhanced penetration into the choroid. Opt Express 2005;13(9):3252–3258.

19. Yasuno Y, Hong Y, Makita S, et al. In vivo high-contrast imaging of deep posterior eye by 1-micron swept source optical coherence tomography and scattering optical coherence angiography. Opt Express 2007;15(10):6121–6139.

20. Copete S, Flores-Moreno I, Montero J, Duker JS, Ruiz-Moreno JM. Direct comparison of spectral-domain and swept-source OCT in the measurement of choroidal thickness in normal eyes. Br J Ophthalmol 2014;98(3):334–338.

21. Ruiz-Moreno JM, Flores-Moreno I, Lugo F, Ruiz-Medrano J, Montero JA, Akiba M. Macular choroidal thickness in normal pediatric population measured by swept-source optical coherence tomography. Invest Ophthalmol Vis Sci 2013;54(1):353–359.

22. Ruiz-Medrano J, Flores-Moreno I, Peña-García P, Montero JA, Duker JS, Ruiz-Moreno JM. Macular choroidal thickness profile in a healthy population measured by Swept-Source Optical Coherence Tomography. Invest Ophthalmol Vis Sci 2014;55(6):3532–3542.

23. Ding X, Li J, Zeng J, et al. Choroidal thickness in healthy Chinese subjects. Invest Ophthalmol Vis Sci 2011;52(13):9555–9560.

24. Ho J, Branchini L, Regatieri C, Krishnan C, Fujimoto JG, Duker JS. Analysis of normal peripapillary choroidal thickness via spectral domain optical coherence tomography. Ophthalmology 2011;118(10):2001–2007.

25. Ikuno Y, Kawaguchi K, Nouchi T, Yasuno Y. Choroidal thickness in healthy Japanese subjects. Invest Ophthalmol Vis Sci 2010;51(4):2173–2176.

26. Manjunath V, Taha M, Fujimoto JG, Duker JS. Choroidal thickness in normal eyes measured using Cirrus HD optical coherence tomography. Am J Ophthalmol 2010;150(3):325–329.

27. Margolis R, Spaide RF. A pilot study of enhanced depth imaging optical coherence tomography of the choroid in normal eyes. Am J Ophthalmol 2009;147(5):811–815.

28. Ouyang Y, Heussen FM, Mokwa N, et al. Spatial distribution of posterior pole choroidal thickness by spectral domain optical coherence tomography. Invest Ophthalmol Vis Sci 2011;52(9):7019–7026.

29. Ruiz-Medrano J, Flores-Moreno I, Peña-García P, Montero JA, Duker JS, Ruiz-Moreno JM. Asymmetry in macular choroidal thickness profile between both eyes in a healthy population. Retina 2015; http://dx.doi.org/10.1097/ IAE.0000000000000590.

30. Adhi M, Brewer E, Waheed NK, Duker JS. Analysis of morphological features and vascular layers of choroid in diabetic retinopathy using spectral-domain optical coherence tomography. JAMA Ophthalmol 2013;131(10):1267–1274.

31. Dolz-Marco R, Gallego-Pinazo R, López-Gálvez MI, Díaz-Llopis M, Shields CL. Focal inferotemporal scleral bulge with choroidal thinning: a new observation on high-penetration optical coherence tomography. Retina 2015;35(3):600–602.

32. Brown JS, Flitcroft DI, Ying GS, et al. In vivo human choroidal thickness measurements: evidence for diurnal fluctuations. Invest Ophthalmol Vis Sci 2009;50(1):5–12.

33. Tan CS, Ouyang Y, Ruiz H, Sadda SR. Diurnal variation of choroidal thickness in normal, healthy subjects measured by spectral domain optical coherence tomography. Invest Ophthalmol Vis Sci 2012;53(1):261–266.

34. Usui S, Ikuno Y, Akiba M, et al. Circadian changes in subfoveal choroidal thickness and the relationship with circulatory factors in healthy subjects. Invest Ophthalmol Vis Sci 2012; 53(4):2300–2307.

35. Ikuno Y, Maruko I, Yasuno Y, et al. Reproducibility of retinal and choroidal thickness measurements in enhanced depth imaging and high-penetration optical coherence tomography. Invest Ophthalmol Vis Sci 2011;52(8): 5536–5540.

36. Chen FK, Yeoh J, Rahman W, Patel PJ, Tufail A, Da Cruz L. Topographic variation and interocular symmetry of macular choroidal thickness using enhanced depth imaging optical coherence tomography. Invest Ophthalmol Vis Sci 2012; 53(2):975–985.

37. Regatieri CV, Branchini L, Carmody J, Fujimoto JG, Duker JS. Choroidal thickness in patients with diabetic retinopathy analyzed by spectral-domain optical coherence tomography. Retina 2012;32(3):563–568.

38. Manjunath V, Goren J, Fujimoto JG, Duker JS. Analysis of choroidal thickness in age-related macular degeneration using spectral-domain optical coherence tomography. Am J Ophthalmol 2011;152(4):663–668.

39. Siam AL, El-Mamoun TA, Ali MH. A restudy of the surgical anatomy of the posterior aspect of the globe: an essential topography for exact macular buckling. Retina 2011;31(7): 1405–1411.

40. Pallikaris IG, Kymionis GD, Ginis HS, Kounis GA, Tsilimbaris MK. Ocular rigidity in living human eyes. Invest Ophthalmol Vis Sci 2005;46(2):409–414.

Biosketch

Jorge Ruiz-Medrano, MD, is an Ophthalmology resident at Clínico San Carlos University Hospital in Madrid, Spain. He received his MD from Universidad Autónoma de Madrid Medical College in June 2011. His research interests include advanced retinal and choroidal image analysis and he is currently working on a PhD on the study of the choroid using Swept-Source optical coherence tomography.

4.4 Asymmetry in Macular Choroidal Thickness Profile

between both eyes in a healthy population measured by

Swept-Source Optical Coherence Tomography

ASYMMETRY IN MACULAR CHOROIDAL THICKNESS PROFILE BETWEEN BOTH EYES IN A HEALTHY POPULATION MEASURED BY SWEPT-SOURCE OPTICAL COHERENCE TOMOGRAPHY

JORGE RUIZ-MEDRANO, MD,* IGNACIO FLORES-MORENO, MD, PhD,† PABLO PEÑA-GARCÍA, MSc,†
JAVIER A. MONTERO, MD, PhD,‡ JAY S. DUKER, MD,§ JOSÉ M. RUIZ-MORENO, MD, PhD†¶

Purpose: To determine the difference in macular choroidal thickness (CT) profile between eyes in healthy individuals using swept-source optical coherence tomography.

Design: Cross-sectional noninterventional study.

Participants: One hundred and forty eyes from 70 healthy patients with spherical equivalent between ±3 D and with difference #0.25 D between eyes were scanned using a swept-source optical coherence tomography (Topcon Corporation).

Methods: Cross-sectional noninterventional study. One hundred and forty eyes from 70 healthy patients with spherical equivalent between ±3 D and with difference #0.25 D between eyes were scanned using a swept-source optical coherence tomography (Topcon Corporation). A horizontal CT profile of the macula was created in both eyes by manually measuring the subfoveal CT from the posterior edge of retinal pigment epithelium (RPE) to the choroid/sclera junction. Three determinations were performed at successive points 1,000 mm nasal to the fovea and 5 more temporal to the fovea. The differences in CT between both eyes were analyzed.

Results: Mean age was 25.4 ± 19.9 years (from 4 to 75). The mean spherical equivalent was 0.18 ± 1.37 D (from ⁻3 to +3). Mean macular nasal CT was thicker in the right eye (RE) than in the left eye (LE) (228.11 ± 69.23 mm vs. 212.27 ± 62.71 mm; P = 0.0002; Student's t-test paired data). Mean subfoveal CT and mean temporal CT was not statistically significantly different between the eyes. No statistically significant differences were observed comparing spherical equivalent in the RE compared with the LE. Both men and women showed a thicker mean nasal choroid in the RE versus the left (men, 226.97 ± 61.56 mm vs. 209.87 ± 60.31 mm; women, 229.63 ± 79.39 mm vs. 215.47 ± 66.68 mm, P = 0.003 and P = 0.03, respectively; Student's t-test paired data). At each nasal determination, CT in the RE was statistically significantly thicker than the LE (N1: 283.72 ± 81.10 mm vs. 269.76 ± 75.81 mm [P = 0.001]; in N2: 230.45 ± 73.47 mm vs. 211.33 ± 66.92 mm [P = 0.0002]; and in N3: 170.16 ± 61.00 mm vs. 155.72 ± 53.87 mm [P = 0.008], respectively).

Conclusion: To the best of our knowledge, this is the first report suggesting thicker macular nasal choroid in the RE compared with the LE. In contrast, subfoveal CT and temporal CT were not found to be different between eyes.

The choroid and its involvement in a variety of ocular pathologies has been the subject of intensive study during the past few years. The choroid plays a role in or is affected by pathologies, such as central serous chorioretinopathy,[1–4] age-related macular degeneration,[1,5–10] posterior segment tumors,[1,11–13] myopic maculopathy,[14–17] posterior uveitis[1,6,18–22] and polypoidal choroidal vasculopathy.[1,7,8] It may also have influence in glaucoma,[23–26] and even in neurologic pathologies, such as migraine[27] and Alzheimer disease.[28] Advances in optical coherence tomography (OCT) in recent years allows deep high-resolution imaging of the posterior eye layers "in vivo."[1] Optical coherence tomography's brief acquisition time[29,30] makes the examination easier for patients who are less cooperative, such as children, the elderly, and those with poor vision.[17,31]

2067

Recently, with the improvements in spectral domain optical coherence tomography provided by enhanced-depth imaging[32] and swept-source optical coherence tomography (SS-OCT) technology,[33–36] which is able to image deeper into the choroid, the choroidal thickness (CT) profiles of healthy populations have been studied.[31,37–39]

The aim of this study is to determine whether there are differences in horizontal macular CT profile between the two eyes in a large population of healthy individuals using SS-OCT.

Patients and Methods

This is a cross-sectional noninterventional study, performed at Castilla La Mancha University Spain. This study followed the tenets of the Declaration of Helsinki. The institutional review board approved this study. All examinations were obtained in the afternoon to avoid diurnal variations.[40–42]

Choroidal thickness was manually measured in 140 eyes from 70 patients with no known ocular or systemic disease. Their macular area was studied with an SS-OCT system (Topcon Corporation, Tokyo, Japan), after they provided informed consent. Inclusion criteria were best-corrected visual acuity of 20/20, spherical equivalent (SE) between ±3 diopters (D), with difference ≠0.25 D between eyes and no systemic diseases. Eyes with any history of mild retinal diseases were not included.

The SS-OCT device used to image the full-thickness choroid and sclera[43] uses a tunable laser as a light source operated at 100,000 Hz, A-scan repetition rate in the 1-mm wavelength region. The device can perform image averaging of up to 96 B-scans at each location. For the macular imaging performed in this study, the reference mirror was placed at the deeper

position of the retina so that the sensitivity was higher in the choroid. A one-line scanning mode, which produces an OCT image containing 1,024 axial scans with a scan length of 12 mm was used. This sampling space in object space corresponds to 11.7 mm/pixel. Lateral resolution was set to be 20 mm with 24-mm axial eye length, whereas axial resolution was 8 mm in retina.[44] Lateral and axial resolution were independent.

Acquisition time for the scan protocol was 1 second. Both eyes were scanned consecutively. A horizontal CT profile of the macula was manually created measuring CT from the posterior edge of RPE to the choroid/sclera junction under the fovea, in a line perpendicular to the retinal surface. The outer aspect of the lamina fusca/inner border of the sclera rather than the outer limit of the choroidal vessels was determined as the outer limit of the choroid.[38,45]

Five determinations were performed every 1,000 mm temporal (T1, T2, T3, T4 and T5) and 3 more nasal (N1, N2 and N3) to the fovea (Figure 1).

From the *Ophthalmology Unit, Clínico San Carlos University Hospital, Madrid, Spain; †Department of Ophthalmology, Castilla La Mancha University, Albacete, Spain; ‡Ophthalmology Unit, Pío del Río Hortega University Hospital, Valladolid, Spain; §New England Eye Center, Tufts Medical Center, Boston, Massachusetts; and ¶Instituto Europeo de la Retina, Baviera, Spain.

Reprint requests: Jorge Ruiz-Medrano, MD, Ophthalmology Unit, Clínico San Carlos University Hospital, Madrid, Spain; e-mail: jorge.ruizmedrano@gmail.com

Fig. 1. Example of choroidal thickness measures at SFCT and N3, N2, and N1 in two eyes of one patient (top RE and bottom LE), from the posterior edge of RPE to the choroid/sclera junction.

Eyes with SE beyond ±3 D and with difference ‑0.25 D between eyes were excluded. An experienced technician determined refractive errors and best-corrected visual acuity using an auto-refractometer (Nidek, Gamagohri, Japan) that was later checked by a certified optometrist.

The differences in mean CT and CT at each independent location between both eyes were analyzed. Two observers determined CT independently and in a masked fashion.

Statistical Analysis

For the statistical treatment of the data, the program used was version 17.0 of SPSS for Windows (SPSS, Chicago, IL). The interobserver reproducibility was evaluated using intraclass correlation coefficient for each variable measured (mean and 95% confidence interval [CI]), coefficient of variation between graders and Bland–Altman plots. The mean of the measures obtained by the two observers was the data used for the rest of calculations. Kolmogorov–Smirnov test was applied for all data samples to check normality. Comparison between groups was performed using the Student's t-test when samples were normally distributed or Mann–Whitney test when parametric statistics were not possible. The level of significance used was always the same (P ˏ 0.05). The homogeneity of variances was checked using the Levene's test. Bivariate correlations were evaluated using Spearman correlation coefficients. For the development of predictive models, linear regression was used. Mean macular nasal CT was determined by the arithmetic mean of the values obtained at N3, N2, and N1, whereas the mean macular temporal CT was calculated by the mean of T1, T2, T3, T4, and T5.

Results

Forty patients (57.1%) were male (80 eyes) and 30 patients (42.9%) were female (60 eyes). Mean age was 25.4 ± 19.9 years (from 4 to 75). Mean SE was 0.18 ± 1.37 D (from ‑3 to +3). Mean macular nasal horizontal CT was statistically thicker in the right eye (RE) 228.11 ± 69.23 mm, range 105.33 to 391.33 mm (95% CI: 211.61–244.62) on average, than in the left eye (LE) 212.27 ± 62.71 mm, range 84.17 to 356.83 mm (95% CI: 197.32–227.22) (P = 0.0002; Student's t-test paired data) (Figure 2). Mean subfoveal CT (SFCT) was 315.86 ± 76.78 mm (95% CI: 297.42–334.41) in the RE versus 308.41 ± 75.51 mm (95% CI: 290.99–325.83) in the LE (P = 0.138, Student's t-test paired data) and mean macular temporal CT was 292.02 ± 63.68 mm (95% CI: 276.62–307.31) in the
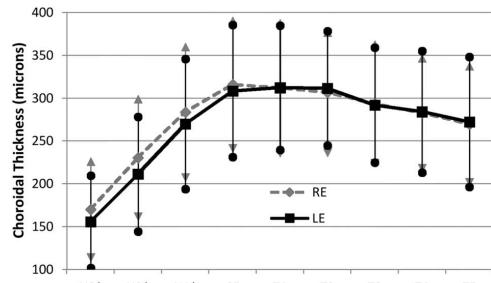
Fig. 2. Mean horizontal choroidal thickness (mm) profile.

RE versus 294.15 ± 54.69 mm (95% CI: 280.58–307.72) in the LE (P = 0.602; Student's t-test paired data). No statistically significant differences were observed comparing SE between the REs (0.18 ± 1.33 D; 95% CI: ‑0.14 to 0.50) versus the LEs (0.19 ± 1.37 D; 95% CI: −0.13 to 0.51) (P = 0.517; Wilcoxon's test). With respect to sex, there were no statistically significant differences between eyes for SFCT or mean temporal CT (Table 1).

The cohort of males in this population studied had a mean age of 19 years (range, 4 to 74 years). When analyzing mean nasal CT by sex, men manifested a nasal choroid thicker in the RE, 226.97 ± 61.56 mm (95 CI: 207.29–246.66) versus 209.87 ± 60.31 mm in the LE (95% CI: 190.58–229.16) (P = 0.003, Student's t-test paired data). In the female cohort group, the mean age was 32.8 ± 18.3 years (from 8 to 75) statistically significantly older than men (P ˏ 0.05). The mean nasal CT of 229.63 ± 79.39 mm in the RE (95% CI: 199.99–259.28) versus 215.47 ± 66.68 mm in the LE (95% CI: 190.57–240.368) (P = 0.03; Student's t-test paired data).

Studying the CT at each individual location in the nasal sector, CT in the RE at N1 was 283.72 ± 81.10 mm (95% CI: 264.39–303.069) versus 269.76 ± 75.81 mm in the LE (95% CI: 251.68–287.83) (P = 0.001, Student's t-test paired data); at N2, RE CT was 230.45 ± 73.47 mm (95% CI: 212.93–247.97) versus 211.33 ± 66.92 mm in the LE (95% CI: 195.37–227.29) (P = 0.0002, Student's t-test paired data); and at N3, RE CT was 170.16 ± 61.00 mm (95% CI: 155.62–184.71) versus 155.72 ± 53.87 mm in the LE (95% CI: 142.88–168.57) (P = 0.008, Student's t-test paired data).

The choroid was thicker in the RE at every nasal location for both sexes except for women at N1, where differences were not statistically significant (P = 0.259; Table 2).

The correlation of nasal CT between RE and LE at each location (N3, N2, and N1) was r = 0.853, 0.842 and 0.822, respectively (P ˏ 0.001; Spearman

78

Table 1. Choroidal Thickness (mm) at SF, Mean Temporal, T1, T2, T3, T4, and T5 by Eye

	RE	LE	P*
SFCT (95% CI)	315.86 ± 76.78 (297.42–334.41)	308.41 ± 75.51 (290.99–325.83)	0.138
Mean TCT (95% CI)	292.02 ± 63.68 (276.62–307.31)	294.15 ± 54.69 (280.58–307.72)	0.602
T1 (95% CI)	311.75 ± 78.14 (292.96–330.51)	312.12 ± 68.42 (295.68–328.55)	0.883
T2 (95% CI)	306.57 ± 73.05 (286.02–321.12)	311.46 ± 63.42 (296.23–312.39)	0.188
T3 (95% CI)	293.42 ± 71.96 (276.14–310.71)	291.99 ± 61.01 (277.34–306.65)	0.961
T4 (95% CI)	282.46 ± 68.21 (266.08–298.85)	284.04 ± 67.24 (267.89–300.20)	0.626
T5 (95% CI)	269.71 ± 72.66 (251.39–287.04)	272.20 ± 75.76 (255.68–291.81)	0.585

*Student's t-test paired data.

TCT, temporal choroidal thickness.

correlation test). The correlation between the mean nasal CT of RE and LE is shown by this equation:

$$\text{Mean nasal CT RE } (mm) = 23.437 + 0.964$$
$$\cdot \text{ mean nasal CT LE } (mm):$$
$$r^2 = 0.763:$$

A high agreement in the measures taken by the 2 observers was found as can be seen in Table 3. The intraclass correlation coefficient values obtained for the variables evaluated were within the range 0.976 to 0.988. The Bland–Altman plots (Figure 3) also confirmed high agreement between measures.

Discussion

Several studies have been published about CT in healthy populations. Ding et al analyze the CT in 210 healthy volunteers (420 eyes) with no ophthalmic disease history using enhanced-depth imaging spectral domain optical coherence tomography at multiple locations: SFCT and 1 mm and 3 mm temporal, nasal, superior, and inferior to the fovea. However, the authors did not analyze any differences between the eyes.[46]

Ikuno et al[47] studied CT and its profile with an SS-OCT device in 86 eyes of 43 healthy Japanese subjects as well as the correlation with axial length, refractive error and age, but they also published no data concerning any differences between right and LEs.

In contrast, Chen et al[48] reported the factors influencing topographical and interocular variations in CT in a 50 healthy adult population using enhanced-depth imaging spectral domain optical coherence tomography. They measured SFCT and also performed CT measurements at 4 paramacular loci (3 mm superior, inferior, temporal, and nasal to the foveal center).

They analyzed the relationship between interocular differences in CT. The differences in CT between RE and LE were 1.0 mm at SFCT, 13.6 mm at nasal and −2.9 mm at temporal location, which was not statistically significant different. Of note, there was a trend toward a thicker nasal CT (14 mm) in REs.

When comparing these data with the series reported in this article, at the same locations (SCFT, N3 CT and T3 CT), we observed that the difference comparing RE and LE was 7.45 mm in mean SFCT, 1.43 mm at T3, and 14.44 mm at N3. The differences between mean nasal CT (P = 0.0002), mean nasal CT in men (P = 0.003) and in women (P = 0.03), and mean CT at each nasal location (P = 0.001, 0.002 and 0.08,

Table 2. Choroidal Thickness (mm) at N1, N2, and N3 by Eye and Sex

	RE	LE	P*
N1			
Men (95% CI)	284.08 ± 68.49 (262.17–305.98)	265.51 ± 68.89 (243.48–287.54)	0.006
Women (95% CI)	283.25 ± 96.63 (247.17–319.33)	275.42 ± 85.06 (243.65–307.18)	0.259
Total group (95% CI)	283.72 ± 81.09 (111.00–475.00)	269.76 ± 75.81 (251.68–287.83)	0.008
N2			
Men (95% CI)	228.98 ± 64.97 (208.19–249.75)	208.73 ± 65.64 (187.73–229.72)	0.001
Women (95% CI)	232.42 ± 84.62 (200.82–264.02)	214.80 ± 69.58 (188.82–240.78)	0.026
Total group (95% CI)	230.45 ± 73.48 (212.93–247.97)	211.33 ± 66.93 (195.37–227.29)	,0.001
N3			
Men (95% CI)	167.86 ± 58.71 (149.09–186.64)	155.38 ± 53.62 (138.23–172.52)	0.007
Women (95% CI)	173.23 ± 64.81 (149.03–197.44)	156.18 ± 55.12 (135.60–176.77)	0.016
Total group (95% CI)	170.16 ± 61.00 (155.62–184.71)	155.72 ± 53.87 (142.88–168.57)	0.001

*Student's t-test paired data.

Table 3. Intraclass Coefficient and Coefficients of Variation of Each Observer at Each Measurement Point

	ICC	95% CI	CV Observer 1	CV Observer 2
N3	0.976	0.962–0.985	0.349	0.355
N2	0.979	0.967–0.987	0.316	0.330
N1	0.988	0.982–0.993	0.282	0.292
SF	0.985	0.975–0.990	0.251	0.254
T1	0.982	0.972–0.989	0.236	0.236
T2	0.976	0.962–0.985	0.213	0.228
T3	0.977	0.964–0.986	0.226	0.233
T4	0.979	0.967–0.987	0.254	0.247
T5	0.976	0.962–0.985	0.284	0.272

CV, coefficient of variation; ICC, intraclass correlation coefficient.

respectively) were statistically significant. The choroid was thicker in the RE at every nasal location for both sexes except for women at N1 (P = 0.259; Table 2).

The correlation of the CT obtained by Chen et al between eyes was strongest for SFCT (r = 0.90; P ⌐ 0.001, Spearman correlation test), for nasal locations was r = 0.83 (P ⌐ 0.001, Spearman correlation test), and weakest for temporal locations (r = 0.49; P ⌐ 0.001, Spearman correlation test).[40] In our patients, the study of correlation for mean CT at SF, N3, and T3 was similar (r = 0.860, 0.853 and 0.754, respectively, P ⌐ 0.001; Spearman correlation test).

The CT profile described in their article[48] is very similar to the CT profile obtained in our work comparing REs to LEs (Figure 2).

It is difficult to explain the strong and consistent evidence that REs have a thicker nasal choroid than LEs in a healthy young population. One possibility is a differential in blood flow between the two eyes due to lack of anatomic symmetry at the aortic arch. Such asymmetry has been suggested to explain the differences in incidence/prevalence of vascular pathologies between REs and left eyes with respect to metastatic bacterial endophthalmitis[49] and retinal artery occlusion.[49–53]

Choroidal circulation is generated from short posterior ciliary arteries that penetrate through the sclera around of optical nerve in a variable number between 10 and 20; so the nasal choroid studied in our cases (choroid between fovea and optical nerve) is directly supplied from these short posterior ciliary arteries. Furthermore, short posterior ciliary arteries are branches of the ophthalmic artery, which is a branch of the internal carotid artery, which is a branch of the common carotid artery.[53]

The difference generated by the fact that the origin of the right common carotid artery lays in the brachiocephalic trunk instead of emerging directly from the aorta (as the left common carotid artery) is
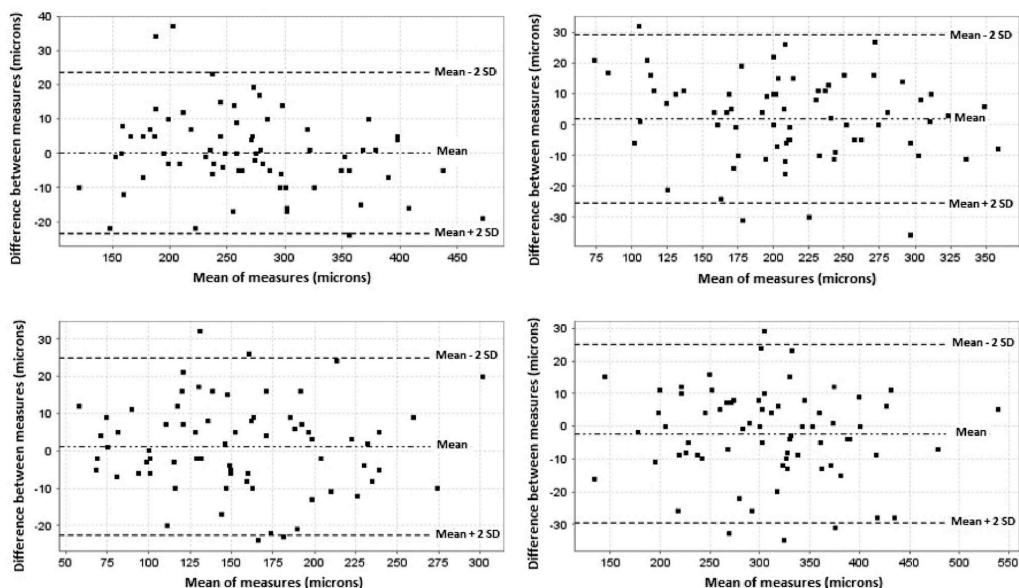

Fig. 3. Bland–Altman plots for interobserver correlation in measurement location from N3 to SFCT. N1 (top left), N2 (top right), N3 (bottom left), and SF (bottom right).

presumably responsible of a more proximal and direct blood flow to the right carotid.[49]

Given that most of the choroidal structure is vascular tissue (the mean vessel density in outer choroid is 87%[54]), a supposed higher blood flow in the right versus left short posterior ciliary arteries may explain why the nasal choroid is thicker in RE, as stated in our study, and as described previously by Chen et al.[48]

In this study, as in previous articles,[31] we used SE instead of axial length determinations since the procedure is less invasive and previous indications from the literature show that refraction, which is more convenient to obtain, provides equivalent modeling capability as axial length.[55]

The limitations of this article are the relatively small number of eyes (140, 70 per group), study of the thickness limited to a line beneath the fovea, the use of SE instead of axial length, the fact that no correction was made for other variables, such as central corneal thickness, intraocular pressure, systemic medication, and blood pressure, and the impossibility to determine whether the vessels of the nasal choroid are wider in the RE than in the left. This is due to the fact the resolution provided by the current technology does not allow a proper and accurate analysis of choroidal vessel thickness, and there is no way to make sure you are analyzing the largest diameter of a vessel because of the irregularity of choroidal vascularization. However, selecting patients with similar SE between eyes, the wide span of ages (from 4 to 75 years) and the high level of statistical significance would support the findings of a thicker choroid nasal to the fovea in the RE versus LE. New studies with larger number of patients and with methods to measure choroidal blood flow (directly or indirectly) will be necessary to verify our results.

Key words: choroidal thickness, choroidal thickness asymmetry, nasal choroidal thickness, healthy population, SS-OCT.

References

1. Stanga PE, Lim JI, Hamilton P. Indocyanine green angiography in chorioretinal diseases: indications and interpretation: an evidence-based update. Ophthalmology 2003;110:15−21.
2. Oh JH, Oh J, Togloom A, et al. Biometric characteristics of eyes with central serous chorioretinopathy. Invest Ophthalmol Vis Sci 2014;55:1502−1508.
3. Razavi S, Souied EH, Cavallero E, et al. Assessment of choroidal topographic changes by swept source optical coherence tomography after photodynamic therapy for central serous chorioretinopathy. Am J Ophthalmol 2014;157:851−860.
4. Imamura Y, Fujiwara T, Margolis R, Spaide RF. Enhanced depth imaging optical coherence tomography of the choroid in central serous chorioretinopathy. Retina 2009;29: 1469−1473.
5. Mrejen S, Spaide RF. The relationship between pseudodrusen and choroidal thickness. Retina 2014;34:1560−1566.
6. Yannuzzi LA. Indocyanine green angiography: a perspective on use in the clinical setting. Am J Ophthalmol 2011;151:745−751.
7. Chung SE, Kang SW, Lee JH, Kim YT. Choroidal thickness in polypoidal choroidal vasculopathy and exudative age-related macular degeneration. Ophthalmology 2011;118:840−845.
8. Koizumi H, Yamagishi T, Yamazaki T, et al. Subfoveal choroidal thickness in typical age-related macular degeneration and polypoidal choroidal vasculopathy. Graefes Arch Clin Exp Ophthalmol 2011;249:1123−1128.
9. Sizmaz S, Kucukerdonmez C, Kal A, et al. Retinal and choroidal thickness changes after single anti-VEGF injection in neovascular age-related macular degeneration: ranibizumab vs bevacizumab. Eur J Ophthalmol 2014;24:904−910.
10. Jia Y, Bailey ST, Wilson DJ, et al. Quantitative optical coherence tomography angiography of choroidal Neovascularization in age-related macular degeneration. Ophthalmology 2014; 121:1435−1444.
11. Shields CL, Manalac J, Das C, et al. Choroidal melanoma: clinical features, classification, and top 10 pseudomelanomas. Curr Opin Ophthalmol 2014;25:177−185.
12. Al-Dahmash SA, Shields CL, Kaliki S, et al. Enhanced depth imaging optical coherence tomography of choroidal metastasis in 14 eyes. Retina 2014;34:1588−1593.
13. Shields CL, Perez B, Materin MA, et al. Optical coherence tomography of choroidal osteoma in 22 cases: evidence for photoreceptor atrophy over the decalcified portion of the tumor. Ophthalmology 2007;114:53−58.
14. Flores-Moreno I, Lugo F, Duker JS, Ruiz-Moreno JM. The relationship between axial length and choroidal thickness in eyes with high myopia. Am J Ophthalmol 2013;155:314−319.
15. Chen W, Wang Z, Zhou X, et al. Choroidal and photoreceptor layer thickness in myopic population. Eur J Ophthalmol 2012; 22:590−597.
16. Fujiwara T, Imamura Y, Margolis R, et al. Enhanced depth imaging optical coherence tomography of the choroid in highly myopic eyes. Am J Ophthalmol 2009;148:445−450.
17. Read SA, Collins MJ, Vincent SJ, Alonso-Caneiro D. Choroidal thickness in myopic and nonmyopic children assessed with enhanced depth imaging optical coherence tomography. Invest Ophthalmol Vis Sci 2013;54:7578−7586.
18. Kim M, Kim H, Kwon HJ, et al. Choroidal thickness in Behcet's uveitis: an enhanced depth imaging-optical coherence tomography and its association with angiographic changes. Invest Ophthalmol Vis Sci 2013;54:6033−6039.
19. Zhang X, Zuo C, Li M, et al. Spectral-domain optical coherence tomographic findings at each stage of punctate inner choroidopathy. Ophthalmology 2013;120:2678−2683.
20. Aoyagi R, Hayashi T, Masai A, et al. Subfoveal choroidal thickness in multiple evanescent white dot syndrome. Clin Exp Optom 2012;95:212−217.
21. Channa R, Ibrahim M, Sepah Y, et al. Characterization of macular lesions in punctate inner choroidopathy with spectral domain optical coherence tomography. J Ophthalmic Inflamm Infect 2012;2:113−120.
22. Fong AH, Li KK, Wong D. Choroidal evaluation using enhanced depth imaging spectral-domain optical coherence tomography in Vogt-Koyanagi-Harada disease. Retina 2011; 31:502−509.
23. Park HY, Lee NY, Shin HY, Park CK. Analysis of macular and peripapillary choroidal thickness in glaucoma patients by enhanced depth imaging optical coherence tomography. J Glaucoma 2014;23:225−231.

24. Chen S, Wang W, Gao X, et al. Changes in choroidal thickness after trabeculectomy in primary angle closure glaucoma. Invest Ophthalmol Vis Sci 2014;55:2608–2613.

25. Suh W, Cho HK, Kee C. Evaluation of peripapillary choroidal thickness in unilateral normal-tension glaucoma. Jpn J Ophthalmol 2014;58:62–67.

26. Saeedi O, Pillar A, Jefferys J, et al. Change in choroidal thickness and axial length with change in intraocular pressure after trabeculectomy. Br J Ophthalmol 2014;98:976–979.

27. Dadaci Z, Doganay F, Oncel Acir N, et al. Enhanced depth imaging optical coherence tomography of the choroid in migraine patients: implications for the association of migraine and glaucoma. Br J Ophthalmol 2014;98:972–975.

28. Gharbiya M, Trebbastoni A, Parisi F, et al. Choroidal thinning as a new finding in Alzheimer's disease: evidence from enhanced depth imaging spectral domain optical coherence tomography. J Alzheimers Dis 2014;40:907–917.

29. Gabriele ML, Wollstein G, Ishikawa H, et al. Optical coherence tomography: history, current status, and laboratory work. Invest Ophthalmol Vis Sci 2011;51:2425–2436.

30. Huang D, Swanson EA, Lin CP, et al. Optical coherence tomography. Science 1991;254:1178–1181.

31. Ruiz-Moreno JM, Flores-Moreno I, Lugo F, et al. Macular choroidal thickness in normal pediatric population measured by swept-source optical coherence tomography. Invest Ophthalmol Vis Sci 2013;54:353–359.

32. Spaide RF, Koizumi H, Pozzoni MC. Enhanced depth imaging spectral-domain optical coherence tomography. Am J Ophthalmol 2008;146:496–500.

33. Huber R, Adler DC, Srinivasan VJ, Fujimoto JG. Fourier domain mode locking at 1050 nm for ultra-high-speed optical coherence tomography of the human retina at 236,000 axial scans per second. Opt Lett 2007;32:2049–2051.

34. Lim H, de Boer JF, Park BH, et al. Optical frequency domain imaging with a rapidly swept laser in the 815-870 nm range. Opt Express 2006;14:5937–5944.

35. Unterhuber A, Povazay B, Hermann B, et al. In vivo retinal optical coherence tomography at 1040 nm-enhanced penetration into the choroid. Opt Express 2005;13:3251–3258.

36. Yasuno Y, Hong Y, Makita S, et al. In vivo high-contrast imaging of deep posterior eye by 1-micron swept source optical coherence tomography and scattering optical coherence angiography. Opt Express 2007;15:6121–6139.

37. Copete S, Flores-Moreno I, Montero J, et al. Direct comparison of spectral-domain and swept-source OCT in the measurement of choroidal thickness in normal eyes. Br J Ophthalmol 2014;98:334–338.

38. Ruiz-Medrano J, Flores-Moreno I, Peña-García P, et al. Macular choroidal thickness profile in a healthy population measured by swept-source optical coherence tomography. Invest Ophthalmol Vis Sci 2014;55:3532–3542.

39. Yiu G, Pecen P, Sarin N, et al. Characterization of the choroid-scleral junction and suprachoroidal layer in healthy individuals on enhanced-depth imaging optical coherence tomography. JAMA Ophthalmol 2014;132:174–181.

40. Branchini LA, Adhi M, Regatieri CV, et al. Analysis of choroidal morphologic features and vasculature in healthy eyes using spectral-domain optical coherence tomography. Ophthalmology 2013;120:1901–1908.

41. Brown JS, Flitcroft DI, Ying GS, et al. In vivo human choroidal thickness measurements: evidence for diurnal fluctuations. Invest Ophthalmol Vis Sci 2009;50:5–12.

42. Tan CS, Ouyang Y, Ruiz H, Sadda SR. Diurnal variation of choroidal thickness in normal, healthy subjects measured by spectral domain optical coherence tomography. Invest Ophthalmol Vis Sci 2012;53:261–266.

43. Usui S, Ikuno Y, Akiba M, et al. Circadian changes in sub-foveal choroidal thickness and the relationship with circulatory factors in healthy subjects. Invest Ophthalmol Vis Sci 2012;53:2300–2307.

44. Ikuno Y, Maruko I, Yasuno Y, et al. Reproducibility of retinal and choroidal thickness measurements in enhanced depth imaging and high-penetration optical coherence tomography. Invest Ophthalmol Vis Sci 2011;51:5536–5540.

45. Hirata M, Tsujikawa A, Matsumoto A, et al. Macular choroidal thickness and volume in normal subjects measured by swept-source optical coherence tomography. Invest Ophthalmol Vis Sci 2011;51:4971–4978.

46. Ding X, Li J, Zeng J, et al. Choroidal thickness in healthy Chinese subjects. Invest Ophthalmol Vis Sci 2011;51:9555–9560.

47. Ikuno Y, Kawaguchi K, Nouchi T, Yasuno Y. Choroidal thickness in healthy Japanese subjects. Invest Ophthalmol Vis Sci 2010;51:2173–2176.

48. Chen FK, Yeoh J, Rahman W, et al. Topographic variation and interocular symmetry of macular choroidal thickness using enhanced depth imaging optical coherence tomography. Invest Ophthalmol Vis Sci 2012;53:975–985.

49. Greenwald MJ, Lisa G, Wohl LG, Sell CH. Metastatic bacterial endophthalmitis: a contemporary reappraisal. Surv Ophthalmol 1986;31:81–101.

50. Hayreh SS, Zimmerman MB. Amaurosis fugax in ocular vascular occlusive disorders: prevalence and pathogeneses. Retina 2014;34:115–122.

51. Leavitt JA, Larson TA, Hodge DO, Gullerud RE. The incidence of central retinal artery occlusion in Olmsted County, Minnesota. Am J Ophthalmol 2011;151:820–823.

52. Hayreh SS, Podhajsky PA, Zimmerman MB. Retinal artery occlusion: associated systemic and ophthalmic abnormalities. Ophthalmology 2009;116:1928–1936.

53. Harris A, Kagemann PL, Cioffi GA. Assessment of human ocular Hemodynamics. Surv Ophthalmol 1998;42:509–533.

54. Shorab M, Wu K, Fawzi AA. A pilot study of morphometric analysis of choroidal vasculature in vivo, using en face optical coherence tomopraphy. PLoS One 2012;7:e48631.

55. Nishida Y, Fujiwara T, Imamura Y, et al. Choroidal thickness and visual acuity in highly myopic eyes. Retina 2012;32:1229–1236.

4.5 Analysis of age-related Choroidal Layers thinning in

Healthy Eyes Using Swept-Source Optical Coherence

Tomography

ANALYSIS OF AGE-RELATED CHOROIDAL LAYERS THINNING IN HEALTHY EYES USING SWEPT-SOURCE OPTICAL COHERENCE TOMOGRAPHY

JORGE RUIZ-MEDRANO, MD,* IGNACIO FLORES-MORENO, MD, PhD,*† PABLO PEÑA-GARCÍA, MSc,†
JAVIER A. MONTERO, MD, PhD,‡ JULIÁN GARCÍA-FEIJÓO, MD, PhD,* JAY S. DUKER, MD,§
JOSÉ M. RUIZ-MORENO, MD, PhD†¶

Purpose: To study the changes in the choroidal layers thickness with age in a healthy population using swept-source optical coherence tomography.

Methods: Retrospective data analysis of a subgroup of eyes from a previous single-center, prospective, cross-sectional, noninterventional study. One hundred and sixty-nine healthy eyes were evaluated using swept-source optical coherence tomography. Inclusion criteria were best-corrected visual acuity between 20/20 and 20/25, spherical equivalent between ±3 diopters, and no systemic or ocular diseases. Two independent investigators determined the macular horizontal choroidal thickness (CT) and the Haller's layer thickness across a 9 mm line centered at the fovea. Subjects were divided into five age groups.

Results: Mean subfoveal choroidal thickness was 305.76 ± 80.59 μm (95% confidence interval: 294.85–319.33). Mean subfoveal thickness for Haller's layer was 215.47 ± 67.70 μm (95% confidence interval: 207.30–227.86) and mean subfoveal thickness for choriocapillaris plus Sattler's layer was 87.31 ± 40.40 μm (95% confidence interval: 83.38–95.65). No significant differences were found due to gender. Choroidal thickness profile was similar between groups with choroidal thickness and Haller's layer thickness decreasing with age ($P = 0.002$).

Conclusion: Choroidal and Haller's layer thickness profiles are similar between different age groups. Age-related choroidal thinning is mostly at the expense of Haller's layer.

RETINA 0:1–9, 2016

The choroid is a highly vascular, pigmented tissue located between the retina and the sclera, responsible for the oxygenation and nourishment of the outer retina.[1] Its study has been updated during the past few years due to breakthroughs in imaging technology. Previous testing such as fluorescein angiography and indocyanine green angiography provide valuable information about the choroid but are not able to do quantification or cross-sectional images.[2-4] B scan ultrasonography and Doppler technology permit such cross-sectional imaging but with resolution that does not allow study of the individual layers. It was not until the development of the optical coherence tomography (OCT) that the "in vivo" study of the choroid was possible in a reproducible, quantifiable, and reliable fashion.[5] The choroid's posterior location and the light dispersion induced by the retinal pigment epithelium made it initially difficult to study the choroid in its full thickness through OCT. Enhanced-depth imaging OCT[6] and more recently longer-wavelength, deep-penetration swept-source OCT (SS-OCT) provide high-resolution images of the choroid and the choroidoscleral interface contour and shape.[7-11]

1

The choroid plays a role in the development and progression of a wide variety of ocular diseases such as age-related macular degeneration,[12–14] central serous chorioretinopathy,[15,16] uveitis,[17,18] and high myopia[19] among others. Age-related thinning has been documented,[20–28] as well as variations in the choriodoscleral profile[29] and asymmetry between both eyes in healthy population.[30]

The choroid consists of three layers: the choriocapillaris, a medium-sized vessel layer (Sattler's layer), and a large-sized vessel layer (Haller's layer). The "in vivo" anatomy of the healthy choroid has to be established to define its alterations.

Spaide stated that choroidal thinning is a manifestation of a loss of visible vessels and small-vessel disease (in patients with higher prevalence of glaucoma or age-related macular degeneration than similarly aged controls) that other authors call senile choroidal sclerosis with the findings of vascular sheathing and obliteration of choroidal channels.[31] Histopathological findings show profound atrophy of the choroid with loss of small and medium vessels.[20,31]

This vascular sclerosis may even provide a potential explanation of the high prevalence of glaucoma in Spaide's sample, with vascular sclerosis leading to a reduced blood supply to the prelaminar portion of the optic nerve referred as senile sclerotic glaucoma.[20] Choriocapillaris loss has also been related to the production of vascular endothelial growth factor due to the presence of a deprived retinal pigment epithelium and outer retina, which may receive less oxygen and metabolites than needed.[32]

The purpose of this paper is to study the possible age-related thickness variations of different choroidal layers in the macular area.

Patients and Methods

The data and images of a specific population subgroup from a previously published prospective study were analyzed.[22,29,30] This study followed the tenets of the Declaration of Helsinki and the original study was approved by the institutional review board of Vissum Alicante. Data were collected from December 2011 to January 2013. Participation was offered to subjects, attending routine ocular examinations, who voluntarily agreed to participate, provided they met the inclusion criteria, with no limit of age and signed an informed consent. Inclusion criteria were best corrected visual acuity between 20/20 and 20/25, spherical equivalent between ±3 diopters (D) and no systemic or ocular diseases (other than cataract).
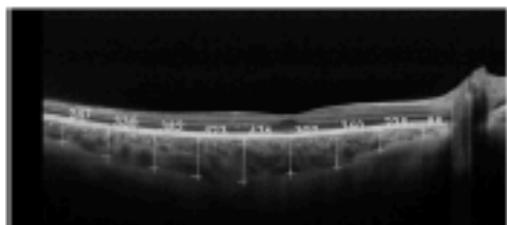
Fig. 1. SS-OCT image of an example of choroidal thickness measures in all different nine locations, from the posterior edge of retinal pigment epithelium to the choroid/sclera junction; from N3 position (right) to T5 position (left).

Patients with prior history of any retinal pathology in either eye were not included. All examinations were obtained in the afternoon to avoid diurnal variations (between 16:00 and 20:00 hours).[33]

The macular area of all patients was studied with a SS-OCT system (Topcon Corp, Tokyo, Japan). The SS-OCT device used to image the full-thickness choroid and sclera is equipped with a tunable laser as a light source operated at 100,000 Hz A-scan repetition rate in the 1-μm wavelength region. A one-line scanning mode, which produces an OCT image that contains 1,024 axial scans with a scan length of 12 mm was used (averaging up to 96 B-scans). This sampling space in object space corresponds to 11.7 μm/pixel. Lateral resolution is set to be 20 μm with 24 mm axial eye length, whereas axial resolution is 8 μm in retina. Lateral and axial resolution is independent.
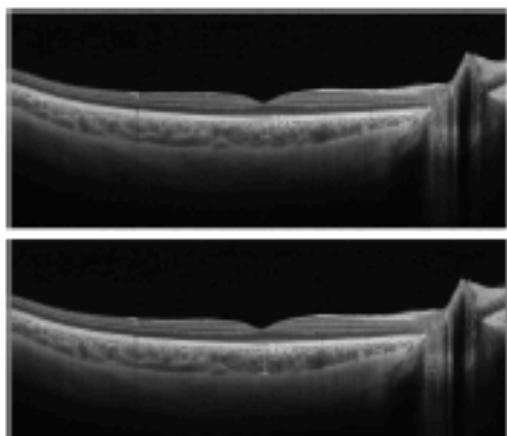
Fig. 2. SS-OCT image of large choroidal vessel measuring 100 μm or more within the closest proximity to the location of the subfoveal CT measurement point (top). The distance from their innermost edge to the choroid/sclera junction was calculated to obtain the Haller's layer thickness (bottom). The measurements of this layer were subtracted from the total CT at all nine measurement locations to obtain the choriocapillaris plus the Sattler's layer thicknesses.

Table 1. General Population

Mean CT (mean ± SD), 95% CI	278.24 ± 63.87 (269.00–288.82)
Mean HT (mean ± SD), 95% CI	191.93 ± 52.41 (185.47–201.73)
Mean ST (mean ± SD), 95% CI	83.72 ± 28.82 (80.83–89.78)
Mean SFCT (mean ± SD), 95% CI	305.76 ± 80.59 (294.85–319.33)
Mean HSFT (mean ± SD), 95% CI	215.47 ± 67.70 (207.30–227.86)
Mean SSFT (mean ± SD), 95% CI	87.31 ± 40.40 (83.38–95.65)

Measurements in micrometers.
CI, confidence interval; CT, choroidal thickness; HSFT, Haller subfoveal thickness; HT, Haller thickness; SD, standard deviation; SFCT, subfoveal choroidal thickness; SSFT, Sattler subfoveal thickness; ST, Sattler thickness.

Acquisition time was 1 second that permitted high quality images even in subjects as young as 3 years old. A horizontal CT profile of the macula was manually created measuring CT (from the posterior edge of retinal pigment epithelium to the choroid/sclera junction) under the fovea using the prototype software. The outer aspect of the lamina fusca, rather than the outer limit of the choroidal vessels, was the landmark used to determine the most distal aspect of the choroid.[22] Five further determinations were performed every 1,000 μm temporal (T1, T2, T3, T4, and T5) and 3 more nasal (N1, N2, and N3) to the fovea (Figure 1). Mean macular CT value was the average value of all nine determinations.

Following the methods proposed by Branchini et al[34] for choroidal vasculature analysis, large choroidal vessels measuring 100 μm or more, and within the closest proximity to the locations of the CT measurement points were identified and the distance from their innermost edge to the choroid/sclera junction was calculated to obtain the Haller's layer thickness (large choroidal vessels) (Figure 2). The measurements of this layer were subtracted from the total CT at the same nine locations to obtain the choriocapillaris plus the Sattler's layer (medium choroidal vessels) thicknesses. As stated by these authors, current OCT devices do not have enough resolution to differentiate between these 2 layers yet, so they were analyzed together.[34] Those locations in which the choroid was 100 μm or thinner were not taken into account for statistical analysis.

To analyze the possible evolution of the CT, the study group was divided into 5 sub-groups[22] according to age distribution: 0 years to 10 years (n = 40), 11 years to 20 years (n = 25), 21 years to 40 years (n = 27), 41 years to 60 years (n = 38), and older than 60 years (n = 39). If both eyes of the same patient met the inclusion criteria, the eye with the highest image quality was used. An experienced technician determined refractive errors and best corrected visual acuity using an auto-refractometer (Nidek, Gamagori, Japan) that was later checked by a certified optometrist. Two independent observers determined the clear delineation of both choroidal limits (retinal pigment epithelium and choroido-scleral junction) and measured the thickness of the choroid and its layers. Results were expressed in mean ± standard deviation (SD).

Statistical Analysis

Data obtained were statistically analyzed using a licensed version of SPSS 17.0 for Windows (SPSS, Chicago, IL). The inter-observer reproducibility was evaluated using intraclass correlation coefficient (ICC) for each variable measured (mean and 95% confidence interval), coefficient of variation between graders, and Bland Altman plots.

The average value of the two observers' determinations was used for the rest of calculations. Kolmogorov–Smirnov test was applied for all data samples to check normality. Comparison between groups was performed using the Student t test when samples were normally distributed or Mann–Whitney test when parametric statistics were not possible. The level of significance used was $P < 0.05$. The homogeneity of variances was checked using the Levene test. For the comparison of several independent samples the Analysis of Variance (ANOVA) or Kruskal–Wallis test were used depending on whether normality could be assumed.

Results

CT was manually measured in 169 eyes from 169 patients. Mean age was 33.5 ± 24.9 years (range 3–
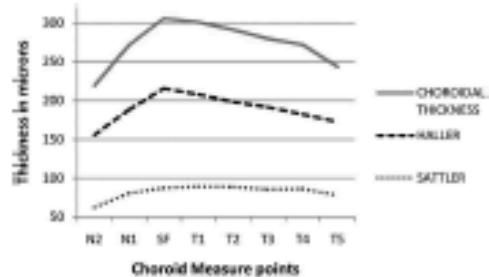
Fig. 3. Choroidal, Haller's and choriocapillaris plus Sattler's layer thickness profiles of our sample (measurements in micrometers).
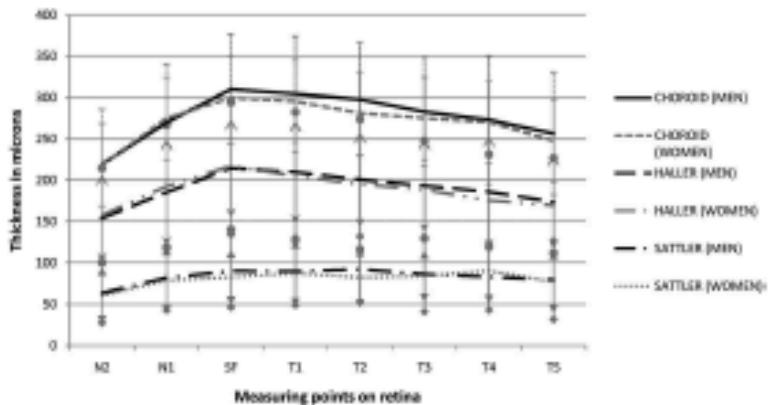
Fig. 4. Choroidal, Haller's and choriocapillaris plus Sattler's layer thickness in men compared with women (measurements in micrometers).

95). Mean spherical equivalent was +0.10 ± 1.36 D (+3 to −3). Mean subfoveal CT was 305.76 ± 80.59 μm (95% confidence interval: 294.85–319.33). Mean subfoveal thickness for Haller's layer was 215.47 ± 67.70 μm (95% confidence interval: 207.30–227.86) and mean subfoveal thickness for choriocapillaris plus Sattler's layer was 87.31 ± 40.40 μm (95% confidence interval: 83.38–95.65).

CT was less than 100 μm thick in 31 eyes at N3, 7 at N2 and 1 at N1. These cases were not taken into account to avoid any possible errors, and due to the large number of eyes that did not reach 100 μm at N3, this point was not taken into account for the statistical analysis in any of the patients. Mean macular horizontal CT was 278.24 ± 63.87 μm (95% confidence interval: 269.00–288.82). Mean macular horizontal Haller's layer thickness was 191.93 ± 52.41 μm (95% confidence interval: 185.47–201.73) and mean macular horizontal choriocapillaris plus Sattler's layer thickness was 83.72 ± 28.82 μm (95% confidence interval: 80.83–89.78) (Table 1). The horizontal choroidal layers' profiles can be seen in Figure 3.

No statistically significant differences in choroidal, Haller, or choriocapillaris plus Sattler's layers thickness were found in men compared with women (Figure 2). Both sexes showed similar profiles for all three measurements (Figure 4).

Mean subfoveal choroidal thickness of the different age study groups established decreased progressively when comparing the younger group with the group aged older than 60 years (P = 0.029; Kruskal–Wallis test). Mean subfoveal Haller's thickness was 233.39 ± 49.47 μm in the 0 year to 10 years group, 235.51 ± 77.49 μm in the 11 years to 20 years group, and then progressively decreased to reach 190.32 ± 77.01 μm in the older than 60 years group (P = 0.063; Kruskal–Wallis test). Mean subfoveal choriocapillaris plus Sattler's thickness did not show this trend towards a progressive thinning with age (P = 0.444; Kruskal–Wallis test) (Table 3).

Mean macular horizontal CT of the different age groups showed a statistically significant progressive reduction from the 0-year to 10years old group to the older than 60 years old group (P < 0.001; Kruskal–Wallis test). Mean horizontal Haller's layer thickness

Table 2. Men vs. Women

	Men (N = 103)	Women (N = 66)	Comparison (Student *t* Test), *P*
Age	34.24 ± 25.62 (4 to 85)	37.76 ± 23.47 (3 to 95)	0.383
Spherical equivalent, D	0.15 ± 1.34 (−3.00 to 3.00)	0.17 ± 1.34 (−3.00 to 3.00)	0.998
Mean choroidal thickness, 95% CI	282.04 ± 58.19 (144.38 to 394.63) [269.65, 292.99]	273.13 ± 72.03 (143.31 to 442.13) [257.22, 293.20]	0.357
Mean Haller thickness, 95% CI	193.19 ± 48.59 (103.63 to 295.50) [184.39, 203.87]	190.39 ± 58.18 (105.69 to 337.86) [178.25, 207.32]	0.571
Mean Sattler thickness, 95% CI	85.18 ± 30.28 (40.75 to 185.44) [81.11, 93.26]	81.70 ± 26.40 (37.44 to 153.19) [75.83, 89.02]	0.390

CI, confidence interval.
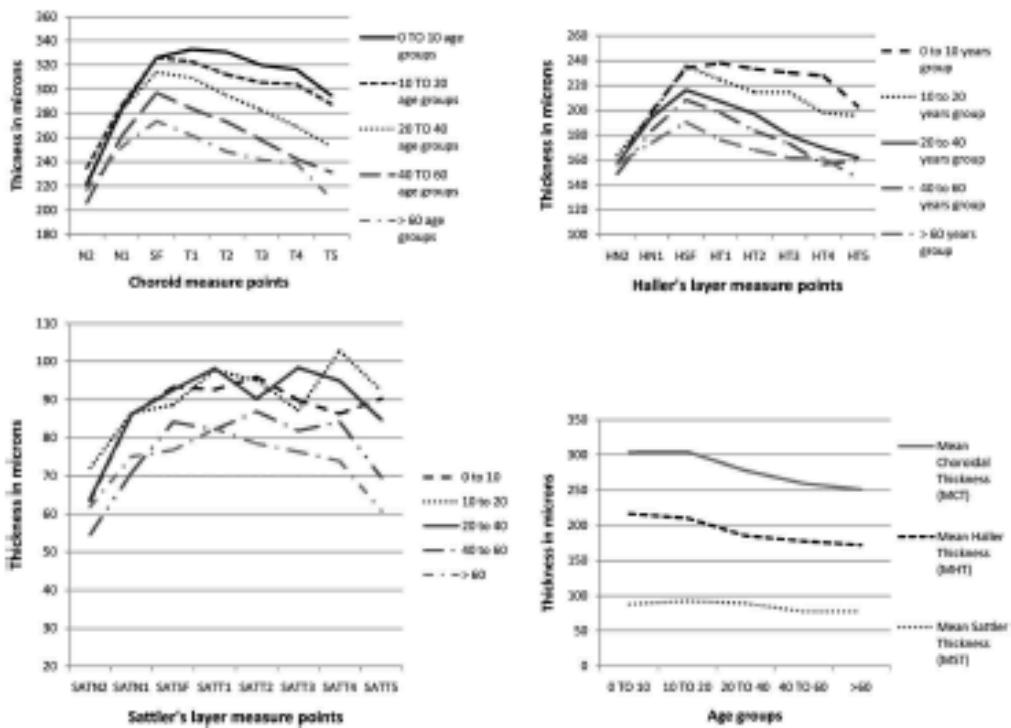
Fig. 5. Choroidal thickness profile in different age groups (top left), Haller's layer thickness profile in different age groups (top right), Sattler plus choriocapillaris layer profile in different age groups (bottom left) and mean thickness of choroid, Haller's, and Sattler's layers by age (bottom right) (measurements in micrometers).

also decreased in a similar way from the younger group to the older than 60 years old group ($P = 0.002$; Kruskal–Wallis test). Mean horizontal choriocapillaris plus Sattler's layer thickness did not show this trend towards a progressive thinning either from the 0 year to 10 years old group or the older than60 years old group ($P = 0.109$; Kruskal–Wallis test) (Table 2).

CT profile was similar among the different age groups with both CT and Haller's layer thickness decreasing with age ($P = 0.002$) (Figure 5). Choriocapillaris plus Sattler's layer thickness showed an age-dependent reduction trend as well, but the difference was not statistically significant ($P = 0.109$). The choroid and Haller's layer are thinnest in the most nasal aspect, they grow to reach their thickest levels at subfoveal locations and then they steadily decrease towards the temporal sector. On the other hand, the choriocapillaris plus Sattler's layer was thinnest in the nasal side reaching its thickest point under the fovea; however, its thickness remained stable during the first 4,000 μm towards the temporal sectors and then slightly decreased at 5,000 μm from the fovea (Figure 5).

Correlation Analysis and Linear Regression Models

The thickness reduction of the choroid, Haller's, and Sattler's layers correlated with age. This correlation was stronger for the whole choroidal thickness and Haller's layers and weaker for the choriocapillaris plus Sattler's layer (Table 2). Multiple regression analysis models predicted are as follows:

1. Macular choroidal thickness (μm) = 295.187 − 0.931 × Age (years) $r^2 = 0.130$, $P < 0.001$
2. Haller's layer thickness (μm) = 207.029 − 0.694 × Age (years) $r^2 = 0.149$, $P < 0.001$
3. Sattler's layer thickness (μm) = 88.159 − 0.237 × Age (years) $r^2 = 0.035$, $P = 0.005$

Mean CT was reduced by 0.93 μm per year. Mean Haller's layer thickness was responsible for 0.69 μm, whereas Sattler's layer was accountable for 0.24 μm per year, suggesting that Haller's layer thinning was responsible for almost 75% of CT reduction with age.

Table 3. Age-related choroidal thickness variations

	Age Groups, Years					Comparison Kruskal–Wallis Test, P
	0 to <10	10 to <20	20 to <40	40 to <60	≥60	
Mean SFT (mean ± SD), 95% CI	325.99 ± 55.71 (303.72–345.36)	325.83 ± 91.73 (290.02–364.74)	313.86 ± 81.10 (284.61–348.77)	295.90 ± 79.16 (270.85–322.89)	273.46 ± 88.32 (248.13–305.39)	0.029
Mean HSFT (mean ± SD), 95% CI	233.39 ± 49.47 (218.22–249.86)	235.51 ± 77.49 (204.19–268.17)	216.12 ± 63.51 (192.49–242.74)	208.13 ± 65.69 (189.27–232.45)	190.32 ± 77.01 (170.33–220.26)	0.068
Mean SSFT (mean ± SD), 95% CI	93.29 ± 34.15 (82.58–104.42)	88.65 ± 41.07 (73.75–107.65)	92.57 ± 54.88 (77.37–120.78)	84.12 ± 36.87 (73.89–98.13)	81.21 ± 37.54 (69.29–93.63)	0.444
Mean CT (mean ± SD), 95% CI	304.04 ± 46.70 (289.16–319.04)	304.39 ± 69.07 (274.44–334.17)	277.93 ± 65.00 (254.92–306.35)	259.50 ± 62.16 (238.01–279.46)	250.86 ± 64.09 (231.40–275.43)	<0.001
Mean HT (mean ± SD), 95% CI	216.45 ± 39.44 (203.24–228.46)	210.05 ± 54.21 (187.17–234.06)	185.29 ± 50.86 (168.94–209.18)	177.65 ± 47.64 (163.58–195.35)	171.83 ± 59.92 (154.85–196.03)	0.002
Mean ST (mean ± SD), 95% CI	87.79 ± 25.38 (80.14–96.37)	92.36 ± 30.86 (80.35–107.04)	90.14 ± 37.03 (76.93–106.22)	77.57 ± 27.84 (68.99–88.56)	77.49 ± 22.04 (70.09–85.85)	0.100

Measurements in micrometers.
CI, confidence interval; CT, choroidal thickness; HSFT, Haller subfoveal thickness; HT, Haller thickness; SD, standard deviation; SFT, subfoveal choroidal thickness; SSFT, Sattler subfoveal choroidal thickness; ST, Sattler thickness.

If we take into account older than 40 years old patients only, Multiple regression analysis models predicted are as follows:

1. Macular choroidal thickness $(\mu m) = 310.13 - 1.00 \times$ Age (years) $r^2 = 0.12$, $P = 0.023$

This predicts a reduction of 1.00 micron per year.

Gender had no influence in mean CT or that of any of its layers. The influence of spherical equivalent on mean CT was not analyzed in this study as patients had to fit within the ±3D limit established as inclusion criteria.

Intraclass correlation coefficient in CT for the 2 independent observers varied between 0.961 and 0.978 for CT and between 0.706 and 0.787 for Haller's layer thickness (Table 3). There were no statistically significant differences between variation coefficients obtained by each observer ($P > 0.05$; Wilcoxon test).

Discussion

The choroid has been proven to become thinner with age.[20] In a previous study our research group evaluated the choroid of healthy individuals across a wide age span (3–95 years old) finding that macular CT profile in healthy population was similar among the different age groups, and that healthy choroid showed a trend to become thinner with age, particularly comparing adults older than 40 years with children and younger adults. These differences were not attributable to gender and greater age-related CT variations appeared in the temporal sectors.[22] Analyzing our results, it can be stated that the choroid has a wide extent of normal thickness, with less than 5% of healthy population presenting CT thicker than 320 μm and no differences in CT between sexes.

SS-OCT (1,040 nm) was chosen to perform this study due to its reported precision and accuracy, permitting determination of full choroidal thickness in up to 100% of the eyes in previous papers.[11,21] Other devices were not so reliable while determining the limit between the sclera and the choroid.[24,25,36] CT was successfully determined in 100% of the eyes in this study. Esmaeelpour et al used a spectral domain optical coherence tomography (840 nm) with a raster protocol image consisting of 512 A-scans and 512 B-scans across a 36° × 36° field to automatically analyze the choroidal layers of 45 healthy eyes with a mean age of 44 years (ranging from 23 to 84 years old), although using a different method.[37] Mean CT through the areas analyzed was 228 μm and the thickness of the Haller's layer and Sattler's layer + choriocapillaris were 141 μm and 87 μm, respectively.[37]

Adhi et al[22] studied 24 eyes of 24 patients with a mean age of 64 years. CT measurements were manually performed using the caliper provided by the spectral domain optical coherence tomography device and the choroid-sclera limit was well delimited in 79% of the eyes. The imaging protocol used consisted of one-line rasters centered at the fovea. Subfoveal CT was 276 μm, subfoveal Haller's layer thickness was 224 μm, and subfoveal Sattler's layer + choriocapillaris was 52 μm.[27]

Using the same method, Branchini et al[34] analyzed the choroidal layers of 42 eyes of 42 patients with a mean age of 52 years, locating the choroid-sclera limit in 92% of them. They manually measured CT and its layers at the subfoveal location using 2 more measurement points 750 μm away from the fovea in both the nasal and the temporal sectors. They found the subfoveal CT of their sample to be of 256 μm. Haller's layer and Sattler's layer + choriocapillaris thickness were 204 and 53 μm, respectively.[34]

In the present study, 169 eyes of 169 patients were analyzed using a SS-OCT device, being the largest sample analyzing choroidal layers to the best of our knowledge. The mean age was lower that other studies at 33.5 years old, whereas visualization of the choroidoscleral interface was possible in all of the eyes. Our figures for subfoveal CT, Haller's layer, and Sattler's layer + choriocapillaris (305.8, 208.6 and 87.3 μm respectively) are larger than those presented by other authors.[27,34,37] A similar finding was observed when in a previous paper our group compared CT measurements with other series using spectral domain optical coherence tomography devices, with a difference of roughly 10 μm.[19,22,24,35-38] This difference and the fact that the mean age of our sample is considerably younger than that of other series could explain the different results.

To evaluate the choroid and its layers across the macula we added 8 more measure points to the subfoveal location (3 nasally and 5 more temporally, although N3 was not taken into account as described before). The mean values for CT, Haller's layer, and Sattler's layers + choriocapillaris thickness were 260.81, 180.2, and 78.2 μm respectively. CT profile showed a similar morphology across different age groups with both CT and Haller's layer thickness decreasing significantly with age ($P < 0.001$). Choriocapillaris plus Sattler's layer thickness showed an age-dependent reduction trend, but was not statistically significant ($P = 0.124$). Our linear regression models led to a predicted loss of 0.93 μm per year in CT, 0.69 of those were due to the thinning of Haller's layer, which explained 75% of the age-related thinning of the choroid. No differences due to gender were found in CT, or any of its layers in any age group. Our study

Table 4. Correlation analysis

	ICC (Choroid)	ICC (Haller)
N3	0.967 (0.956–0.976)	0.755 (0.682–0.813)
N2	0.978 (0.970–0.984)	0.760 (0.688–0.817)
N1	0.972 (0.962–0.979)	0.753 (0.679–0.811)
SF	0.977 (0.970–0.983)	0.787 (0.722–0.838)
T1	0.977 (0.969–0.983)	0.765 (0.694–0.821)
T2	0.978 (0.970–0.984)	0.733 (0.655–0.796)
T3	0.972 (0.962–0.979)	0.749 (0.675–0.809)
T4	0.964 (0.952–0.973)	0.754 (0.681–0.813)
T5	0.961 (0.948–0.971)	0.706 (0.622–0.775)

Mean and 95% CI.
ICC, Intraclass correlation coefficient.

shows that most of the age-related thinning of the choroid of normal eyes is due to the reduction of large vessels. These findings in healthy eyes disagree with histopathological findings in eyes with marked senile sclerosis that show atrophy of small and medium vessels mostly.[20,31]

Spaide[20] stated that age-related loss of choroidal thickness was directly related to the loss of visible vessels, implying that it is a manifestation of small-vessel disease affecting the choroid. These data are not comparable with ours, as Spaide[20] only included eyes with CT under 125 μm. Sarks'[31] paper describes only 2 cases with choroidal sclerosis whose retinoscopy showed well-demarcated areas of choroidal sclerosis that are probably in relation with atrophic age-related macular degeneration, whereas our study analyzes healthy patients. This age-related choroidal thinning could be a key factor to establish the role of the choroid in retinal pathology.

The limitations of this study are the facts that it is retrospective, the choriocapillaris could not be differentiated from Sattler's layer due to the limitations in imaging technology and that despite the high intraclass correlation coefficient (Table 4), the measures for all layers were manually determined.

According to our results, CT and Haller's layer grow progressively thinner as patients grow older and their profiles are similar between different groups of age. Age-related choroidal thinning seems to be mostly at the expense of Haller's layer. There were no differences due to gender.

Acknowledgments

J. Ruiz-Medrano and I. Flores-Moreno; Conceptualization of the manuscript and review and synthesis of the literature: J. Ruiz-Medrano and J. M. Ruiz-Moreno; Analysis and interpretation of data: J. Ruiz-Medrano, I. Flores-Moreno, J. A. Montero, and J. M. Ruiz-Moreno; Critical review and revision of the manuscript: J. Ruiz-Medrano, I. Flores-Moreno, J. A. Montero, J. S. Duker, J. García-Feijoo, and J. M. Ruiz-Moreno; Drafting of the manuscript: J. Ruiz-Medrano; Final approval of the version to be published: J. Ruiz-Medrano, I. Flores-Moreno, J. A. Montero, J. S. Duker, J. García-Feijóo, and J. M. Ruiz-Moreno; Providing language help: J. S. Duker, J. García-Feijóo, and J. A. Montero.

Detail has been removed from this case description/these case descriptions to ensure anonymity. The editors and reviewers have seen the detailed information available and are satisfied that the information backs up the case the authors are making.

References

1. Guyer DR, Schachat AP, Green WR. The choroid: structural considerations. In: Ryan SJ, ed. Retina. 4th ed. Philadelphia, PA: Elsevier Mosby; 2006:33–34.
2. Spaide RF, Yannuzzi LA, Slakter JS, et al. Indocyanine green videoangiography of idiopathic polypoidal choroidal vasculopathy. Retina 1995;15:100–110.
3. Yannuzzi LA, Ober MD, Slakter JS, et al. Ophthalmic fundus imaging: today and beyond. Am J Ophthalmol 2004;137:511–524.
4. Stanga PE, Lim JI, Hamilton P. Indocyanine green angiography in chorioretinal diseases: indications and interpretation: an evidence-based update. Ophthalmology 2003;110:15–21.
5. Huang D, Swanson EA, Lin CP, et al. Optical coherence tomography. Science 1991;254:1178–1181.
6. Spaide RF, Koizumi H, Pozzoni MC. Enhanced depth imaging spectral-domain optical coherence tomography. Am J Ophthalmol 2008;146:496–500.
7. Huber R, Adler DC, Srinivasan VJ, Fujimoto JG. Fourier domain mode locking at 1050 nm for ultra-high-speed optical coherence tomography of the human retina at 236,000 axial scans per second. Opt Lett 2007;32:2049–2051.
8. Lim H, de Boer JF, Park BH, et al. Optical frequency domain imaging with a rapidly swept laser in the 815–870 nm range. Opt Express 2006;14:5937–5944.
9. Unterhuber A, Povazay B, Hermann B, et al. In vivo retinal optical coherence tomography at 1040 nm-enhanced penetration into the choroid. Opt Express 2005;13:3252–3258.
10. Yasuno Y, Hong Y, Makita S, et al. In vivo high-contrast imaging of deep posterior eye by 1-micron swept source optical coherence tomography and scattering optical coherence angiography. Opt Express 2007;15:6121–6139.
11. Copete S, Flores-Moreno I, Montero J, et al. Direct comparison of spectral-domain and swept-source OCT in the measurement of choroidal thickness in normal eyes. Br J Ophthalmol 2014;98:334–338.
12. Chung SE, Kang SW, Lee JH, Kim YT. Choroidal thickness in polypoidal choroidal vasculopathy and exudative age-related macular degeneration. Ophthalmology 2011;118:840–845.
13. Koizumi H, Yamagishi T, Yamazaki T, et al. Subfoveal choroidal thickness in typical age-related macular degeneration and polypoidal choroidal vasculopathy. Graefes Arch Clin Exp Ophthalmol 2011;249:1123–1128.
14. Ueta T, Obata R, Inoue Y, et al. Background comparison of typical age-related macular degeneration and polypoidal choroidal vasculopathy in Japanese patients. Ophthalmology 2009;116:2400–2406.
15. Imamura Y, Fujiwara T, Margolis R, Spaide RF. Enhanced depth imaging optical coherence tomography of the choroid in central serous chorioretinopathy. Retina 2009;29:1469–1473.
16. Maruko I, Iida T, Sugano Y, et al. Subfoveal choroidal thickness in fellow eyes of patients with central serous chorioretinopathy. Retina 2011;31:1603–1608.
17. Aoyagi R, Hayashi T, Masai A, et al. Subfoveal choroidal thickness in multiple evanescent white dot syndrome. Clin Exp Optom 2012;95:212–217.
18. Channa R, Ibrahim M, Sepah Y, et al. Characterization of macular lesions in punctate inner choroidopathy with spectral domain optical coherence tomography. J Ophthalmic Inflamm Infect 2012;2:113–120.
19. Flores-Moreno I, Lugo F, Duker JS, Ruiz-Moreno JM. The relationship between axial length and choroidal thickness in eyes with high myopia. Am J Ophthalmol 2013;155:314–319.
20. Spaide RF. Age-related choroidal atrophy. Am J Ophthalmol 2009;147:801–810.
21. Ruiz-Moreno JM, Flores-Moreno I, Lugo F, et al. Macular choroidal thickness in normal pediatric population measured by swept-source optical coherence tomography. Invest Ophthalmol Vis Sci 2013;54:353–359.
22. Ruiz-Medrano J, Flores-Moreno I, Peña-García P, et al. Macular choroidal thickness profile in a healthy population measured by swept-source optical coherence tomography. Invest Ophthalmol Vis Sci 2014;55:3532–3542.
23. Ding X, Li J, Zeng J, et al. Choroidal thickness in healthy Chinese subjects. Invest Ophthalmol Vis Sci 2011;52:9555–9560.
24. Manjunath V, Taha M, Fujimoto JG, Duker JS. Choroidal thickness in normal eyes measured using cirrus HD optical coherence tomography. Am J Ophthalmol 2010;150:325–329.
25. Margolis R, Spaide RF. A pilot study of enhanced depth imaging optical coherence tomography of the choroid in normal eyes. Am J Ophthalmol 2009;147:811–815.
26. Ouyang Y, Heussen FM, Mokwa N, et al. Spatial distribution of posterior pole choroidal thickness by spectral domain optical coherence tomography. Invest Ophthalmol Vis Sci 2011;52:7019–7026.
27. Adhi M, Brewer E, Waheed NK, Duker JS. Analysis of morphological features and vascular layers of choroid in diabetic retinopathy using spectral-domain optical coherence tomography. JAMA Ophthalmol 2013;131:1267–1274.
28. Dolz-Marco R, Gallego-Pinazo R, López-Gálvez MI, et al. Focal inferotemporal scleral bulge with choroidal thinning: a new observation on high-penetration optical coherence tomography. Retina 2015;35:600–602.
29. Ruiz-Medrano J, Flores-Moreno I, Montero JA, et al. Morphological features of the choroidoscleral interface in a healthy population using swept-source optical coherence tomography. Am J Ophthalmol 2015;160:596–601.
30. Ruiz-Medrano J, Flores-Moreno I, Peña-García P, et al. Asymmetry in macular choroidal thickness profile between both eyes in a healthy population. Retina 2015;35:2067–2073.
31. Sarks SH. Senile choroidal sclerosis. Br J Ophthalmol 1973;57:98–109.

32. Grossniklaus HE, Green WR. Choroidal neovascularization. Am J Ophthalmol 2004;137:496–503.

33. Brown JS, Flitcroft DI, Ying GS, et al. In vivo human choroidal thickness measurements: evidence for diurnal fluctuations. Invest Ophthalmol Vis Sci 2009;50:5–12.

34. Branchini LA, Adhi M, Regatieri CV, et al. Analysis of choroidal morphologic features and vasculature in healthy eyes using spectral-domain optical coherence tomography. Ophthalmology 2013;120:1901–1908.

35. Wei WB, Xu L, Jonas JB, et al. Subfoveal choroidal thickness: the Beijing Eye Study. Ophthalmology 2013;120:175–180.

36. Yamashita T, Yamashita T, Shirasawa M, et al. Repeatability and reproducibility of subfoveal choroidal thickness in normal eyes of Japanese using different SD-OCT devices. Invest Ophthalmol Vis Sci 2012;53:1102–1107.

37. Esmaeelpour M, Kajic V, Zabihian B, et al. Choroidal Haller's and Sattler's layer thickness measurement using 3-dimensional 1060-nm optical coherence tomography. PLoS One 2014;9: e99690.

38. Xu J, Xu L, Du KF, et al. Subfoveal choroidal thickness in diabetes and diabetic retinopathy. Ophthalmology 2013;120: 2023–2028.

4.6 Age-related changes in choroidal vascular density of

healthy subjects based on image binarization of Swept-Source

Optical Coherence Tomography

Jan 10, 2017

RE: Retina-216-1129R1, entitled "Age-related changes in choroidal vascular density of healthy subjects based on image binarization of Swept-Source Optical Coherence Tomography"

Dear Dr. Ruiz-Medrano,

I am pleased to inform you that your manuscript has been accepted for publication in RETINA The Journal of Retinal and Vitreous Diseases. Your manuscript will be forwarded immediately to the production staff for copy editing. It will be placed in an upcoming issue as soon as possible.

OPEN ACCESS
If you indicated in the revision stage that you would like your submission, if accepted, to be made open access, please go directly to step 2. If you have not yet indicated that you would like your accepted article to be open access, please follow the steps below to complete the process:
1. Notify the journal office via email that you would like this article to be available open access. Please send your Email to retina@retinajournal.com. Please include your article title and manuscript number.
2. A License to Publish (LTP) form must be completed for your submission to be made available open access. Please download the form from http://links.lww.com/LWW-ES/A49, sign it, and Email the completed form to the journal office.
3. **Within 48 hours of receiving this e-mail:** Go to http://wolterskluwer.qconnect.com to pay for open access. If you have not previously used this site to place an order, you will need to register for an account (your login will be different from your Editorial Manager login). When placing your order, you will be asked for the following information. Please enter exactly as shown:
a. Article Title - Age-related changes in choroidal vascular density of healthy subjects based on image binarization of Swept-Source Optical Coherence Tomography
b. Manuscript Number - Retina-216-1129R1

Thank you for submitting your manuscript to us for review and allowing us to publish it for you in RETINA.

With Kind Regards,

Alexander J. Brucker, M.D.
Editor in Chief
RETINA The Journal of Retinal and Vitreous Diseases

Title: Age-related changes in choroidal vascular density of healthy subjects based on image binarization of Swept-Source Optical Coherence Tomography.

Short title: Normal subjects choroid vascular density.

Jorge Ruiz-Medrano1, José M Ruiz-Moreno2, 3, Abhilash Goud4, Kiran Kumar Vupparaboina5, Soumya Jana5, Jay Chhablani4.

1 Jules Gonin Eye Hospital. Fondation Asile des Aveugles. Lausanne. SWITZERLAND.

2 Department of Ophthalmology, Castilla La Mancha University. Albacete. SPAIN.

3 Vissum Corporation. SPAIN.

4 Smt. Kanuri Santhamma Retina Vitreous Centre. L V Prasad Eye Institute Hyderabad. INDIA.

5 Department of Electrical Engineering, Indian Institute of Technology Hyderabad, Telangana, INDIA.

Key words: Swept-Source optical coherence tomography, SS-OCT, choroidal vascular density, choroidal thickness, vascular area, stromal area.

Word count: 2720

Summary statement:

Choroidal vascular density in healthy patients based on image binarization of Swept-Source Optical Coherence Tomography.

Jorge Ruiz-Medrano, José M Ruiz-Moreno, Abhilash Goud, Kiran Kumar Vupparaboina, Soumya Jana, Jay Chhablani.

Based on the analysis of choroidal stroma and vessel area using a new automated segmentation and binarization software based on validated algorithms across a wide span of ages (3 to 85), the luminal area and the percentage of vascular/total area decrease with increasing age while stromal area remains stable.

Abstract

Objective: To analyze the vascular density of the choroid in a healthy population using swept-source optical coherence tomography (SS-OCT).

Methods: Cross-sectional, non-interventional study. Inclusion criteria: Best Corrected Visual Acuity (BCVA) between 20/20 to 20/25, spherical equivalent (SE) between ± 3 diopters (D), no systemic or ocular diseases and ages ranging from 3 to 85 years old. 136 eyes from 136 subjects were analyzed, 86 eyes (63.2%) were from male and 50 eyes (36.8%) from female subjects. The eyes were divided into different age groups to analyse the possible age-related changes. Twelve mm horizontal, fovea-centered B-scans were used. Choroidal stroma and vessel area analysis involved automated segmentation and binarization using validated algorithms.

Results: Mean age was 33.1 ± 24.5 years. Mean choroidal area was 0.5554 ± 0.1377 mm2. Mean stromal area was 0.2524 ± 0.0762 mm2, and mean vascular region area was 0.3029 ± 0.0893 mm2. The percentage of choroidal vascularity (vascular area/total area) was 54.40 ± 8.35 %. Choroid area, vascular region and percentage of choroidal vascular density were statistically higher in the <18-year-old group vs. >18-year-old group ($p < 0.001$). Stromal region was not different ($p = 0.46$). In the same way, choroid area, vascular region and percentage of choroidal vascular density between the five age groups was statistically different ($p < 0.001$), showing larger figures in the 0-10 years old group; but not stromal region ($p = 0.71$). There were no gender-related differences.

Conclusions: The luminal area and the percentage of vascular/total area decrease with increasing age while stromal area remains stable.

Introduction

Since Spaide et al introduced enhanced depth imaging (EDI) technique which improved choroidal imaging using spectral domain Optical Coherence Tomography (SD-OCT) devices, our knowledge of the role of choroidal changes in various conditions such as central serous chorioretinopathy[1-4], age-related macular degeneration[1, 4-10], polypoidal choroidal vasculopathy[1, 4-6, 9], myopic maculopathy[11-15], posterior uveitis[1, 3, 4, 16-19] and choroidal tumors[1, 20, 21]. Swept-source longer-wavelength[23-26] is a technology for OCT (SS-OCT) imaging that permits further improvement in choroidal study. Copete et al[27] and Ruiz-Moreno et al[28, 29] reported that reliable measurement of choroidal thickness (CT) is possible in 100% of eyes using an SS-OCT device.

Age-related reduction of CT in normal eyes[30-35], CT differences in adult and paediatric eyes[28, 29] and differences between right and left eye[36] have been reported using this technique. However, knowledge of choroidal morphology is not complete yet. Adhi et al[37] described significant alterations in choroidal morphological features in eyes with advanced diabetic retinopathy. In addition, a recent paper reported a focal inferotemporal scleral bulge with choroidal thinning in normal eyes modifying the normal contour and shape (convex or bowl-shaped) of the choroidoscleral interface.[38]

Sonoda et al, using a binarization technique to analyse the luminal and stromal areas separately, show that both these areas decreased with increasing age and axial length. They affirm that the method should be of great help in analysing the choroid, and the normative data collected should provide basic information about the normal choroid.[39] Agrawal et al introduced a novel OCT term: Choroidal vascularity index (CVI), to assess vascularity of the subfoveal choroid. They showed that on a single cross sectional EDI-OCT image, two-thirds (~66%) of the subfoveal choroid is vascular in healthy eyes.[40]

The aim of this paper is to analyse the vascular density of the choroid in a healthy population using SS-OCT and compare the differences in choroidal vascularity with increasing age.

Subjects and Methods

This was a cross-sectional, non-interventional study. It followed the tenets of the Declaration of Helsinki. All examinations were obtained in the afternoon to avoid diurnal variations (16:00-20:00).[41-43] Inclusion criteria were: Best Corrected Visual Acuity (BCVA) between 20/20 to 20/25, spherical equivalent (SE) between ± 3 diopters (D), no systemic or ocular diseases (other than cataract). Eyes with any history of any retinal diseases in the fellow eye were not included. Eyes with spherical equivalent (SE) beyond ±3 D were excluded. Only the left eye was used for the study (image quality allowed for a proper binarization in 136 out of 141 eyes). The data and images of a specific population subgroup from a previously published prospective study were analyzed.[38] The original study was approved by the institutional review board of Vissum Alicante. Data were collected from December 2011 to January 2013. The subjects provided informed consent to participate in the research to study the thickness and morphology of the choroid in a healthy population. Participation was offered to subjects who were attending routine ocular

examinations and voluntarily agreed to participate, provided they met the inclusion criteria, with no age limitations, and signed an informed consent.38

Image analysis: four parameters were calculated: choroid area, vascular and stromal area and percentage of choroidal vascularity (vascular area/total area). Choroidal stroma and vessel area analysis involved (i) automated binarization of an OCT B-scan and (ii) automated segmentation of the binarized choroid layer using previously validated algorithm.44 We used the central 9 mm from the 12 mm b scans obtained. The automated binarization involved (a) preprocessing, (b) exponential and non-linear enhancement, and (c) thresholding. OCT images were de-noised using the BM3D (block matching and 3D filtering) technique. Subsequently, adaptive histogram equalization considering 8x8 blocks was performed to increase the image contrast to better visualize various structures, especially choroidal vessels. Thresholding was based on Otsu's thresholding algorithm.45 Next, exponential enhancement (exponentiation factor=6, empirically obtained) was performed on raw OCT images to increase the dynamic range of pixel intensities. This was followed by non-linear enhancement where each row of the resulting image was multiplied by the square of its row number, which ensures the uniform distribution of pixel intensities among stroma and vessel regions. Finally, thresholding, based on a histogram, was employed to obtain the binarized OCT B-scan.

At this point, we defined choroid's inner and outer boundaries to segment the binarized choroid layer. Choroidal segmentation was obtained using a recent method proposed by our group,46 which reported reproducibility of 98-99%. The choroid was localized in two steps, by first identifying the choroid inner boundary (CIB) and then the choroid outer boundary (COB) from the de-noised images. The CIB was found by locating the RPE inner boundary based on the comparative brightness of the RPE, and then using a gradient-based Canny edge operator (threshold 0.4, standard deviation 2) for delineation. Then, the COB was defined by structural similarity (SSIM) index, comparing a scleral window to the neighbourhood of every pixel in the potential COB area. Subsequently, the detected CIB and COB were used in segmenting the choroid layer from the previously obtained binarized images. Finally, the binarized choroid layer was used to quantify the stromal area, vessel area and percentage choroidal vascularity (Figures 1 and 2).

The data were correlated with mean choroidal thickness (CT), subfoveal CT (SFCT), age, SE and gender. A horizontal CT profile of the macula was manually created measuring CT (from the posterior edge of RPE to the choroid/sclera junction) under the fovea (SFCT) using the prototype software. The outer aspect of the lamina fusca, rather than the outer limit of the choroidal vessels, was the landmark used to determine the most distal aspect of the choroid. Five further determinations were performed every 1000 μm temporal (T1, T2, T3, T4 and T5) and three more nasal (N1, N2 and N3) to the fovea (Figure 3).

An experienced technician determined refractive errors and BCVA using an auto-refractometer (Nidek, Gamagohri, Japan) that was later checked by a certified optometrist.

To study the possible age-related evolution of vascular density the study group was divided into 2 sub-groups according to age distribution: Subjects aged 18 or younger (59 eyes) and subjects older than 18 (77 eyes). Mean age was 33.1±24.5 years (from

3 to 85). The sample was further divided into 5 groups (0-10, 11-20, 21-40, 41-60 and more than 60 years old) to analyse the possible age-related changes like in previous papers.29

Mean SE was 0.11±1.38 D (from +3 to -3). 136 left eyes from 136 subjects were analysed, 86 eyes (63.2%) were from male and 50 eyes (36.8%) from female subjects (Table 1).

For this study, the reference mirror of SS-OCT was placed at the deeper position of the retina so that the sensitivity was higher at the choroid area in macular imaging. A one-line scanning mode, which produces an OCT image that contains 1024 axial scans with a scan length of 12 mm, was employed. Two observers determined CT independently and in a masked fashion.

Data obtained were statistically treated using a licensed version of SPSS 17.0 for Windows (SPSS, Chicago, IL). Kolmogorov-Smirnov test was applied for all data samples in order to check normality. Inter groups analysis was performed using the Student t test when samples were normally distributed or Mann-Whitney test when parametric statistics were not possible. The level of significance used was $P<0.05$. For study correlation Pearson correlation test was used.

Results

Mean SFCT was 305.77±78.29 mμ (range 144.50 to 539.50) and mean CT was 261.66±61.66 mμ (range 134.6 to 455.28). Mean choroidal area was 0.5554±0.1377 mm2 (range 1.0057 to 0.2738). Mean stromal area was 0.2524±0.0762 mm2 (range 0.1074 to 0.4601), and mean vascular region area was 0.3029±0.0893 mm2 (range 0.1104 to 0.5537). The percentage of choroidal vascularity (vascular area/total area) of the choroid area studied was 54.40±8.35 % (range 33.34 to 77.04, Table 1).

Choroid area, vascular region and percentage of choroidal vascular density were statistically higher in the <18-year-old group vs. >18-year-old group (p<0.001 for all three comparisons; Student t test). Stromal region was not different (p=0.46 Student t test), (Table 2). In the same way, there were statistically significant differences when comparing choroid area, vascular region and percentage of choroidal vascular density between all five age groups (p<0.001 for all three comparisons; ANOVA test), being higher in the 0-10-year-old group; but not for stromal region (p=0.71; ANOVA test) (Table 3). There were no differences between men and women.

A negative statistical significant correlation between choroid area, vascular region and percentage of choroidal vascular density were found for age (r=-0.396, p=0.000; r=-0.664, p=0.000 and r=-.653, p=0.000 respectively, Pearson correlation) but not for stromal area (r=0.063, p=0.46; Pearson correlation). No significant correlations were found between the four parameters studied, gender and SE. Mean CT and mean SFCT were significant correlated with choroid area (r=0.872, p=0.000 and r=0.802, p=0.000; Pearson correlation).

The coefficients of variation (the ratio of the standard deviation [σ] to the mean [μ]) were: choroidal area 26%, stromal region 30%, vascular region 31%, percentage of vascularity 15%, CT 24% and SFCT 26%.

Discussion

It is necessary to increase our knowledge on age-related variations of the choroidal structure in normal eyes so certain findings in everyday patients can be correctly interpreted. CT, its variations and the modifications of each of its layers have been already studied. 29,46 It would be interesting to understand the changes in stroma or vascular region separately to further explore the pathogenesis of its various diseases.

Histologically, the choroid is composed of blood vessels and stroma (pigment cells, smooth muscles, neurons, vascular walls, and connective tissue).47 Using SD-OCT and even SS-OCT, which provides higher penetrance and resolution, it is not possible to differentiate between both these structures. Sonoda et al used a binarization technique to differentiate vascular/luminal areas from stromal areas of the choroid.48 Even though certainty that dark areas represent vascular structures and clearer areas represent stroma is not complete, this has been empirically accepted.49,50

On the other hand, it is known that the amount of eNOS is reduced and the vascular tone decreases with increasing age, which leads to a decrease of circulating blood volume.51,52 Thus, this should also be expected at the level of the choroid, with decreasing vascular areas. This may also be a consequence of a reduction of the number of choroidal vessels with age, as oxidative stress is known to damage endothelial cells.

A histologic study showed that the volume of the cellular and interstitial components of the choroid decrease with increasing age.53 More recently, some groups performed a detailed biochemical analysis of the choroid and reported that the CT decreased with increasing age, accompanied by significant decreases in a serine protease inhibitor, fibrillar collagen, and the amount of celular components.54,55 These findings would speak against the findings of no age-related reduction of stromal areas found in this series. Nevertheless, the possibility of inducting changes during sample management should be taken into account, so more studies are necessary to confirm this discrepancy.

Sonoda et al 39 studied the proportion of luminal and stromal areas of normal choroids in the OCT images obtained by EDI-OCT, in a prospective study. They reported that the luminal area, the stromal area and the ratio of luminal/stromal area also decreased significantly with increasing age, showing that the area of the vascular lumen decreased more than the stromal area with increasing age. They also found that the age was significantly and negatively correlated with the total choroid area, luminal area, stromal area and the luminal to stromal ratio. However, interpretation of these data is difficult in their study as they used subjects with different ages and SE (from -6 to +3.5D), and both these two are key factors influencing CT. The SE range of our series was of ±3D, with no significant correlation with any of the 4 parameters studied. There was no significant difference in SE between different age groups either. Furthermore, they did not evaluate children.

Agrawal et al 40 stated that CVI may potentially be used to assess vascular status of the choroid, after analysing 345 healthy eyes (55% females) from 45 to 85 years old, with EDI-OCT and the binarization technique proposed by Snoda et al.39,48 CT was automatically measured and only right eyes were used. The area of

the choroid studied was 1.5 mm wide in the subfoveolar position and CVI was calculated as the proportion of luminal area to total choroid area, being similar to our percentage of vascularity. They concluded that CVI is less variable than SFCT and that it is less influenced by other factors, especially by age. They proposed CVI as a more stable index that could be useful to analyse variations in the choroid when compared to the more classic CT. In their series SFCT was the only factor associated with CVI, whereas stromal area did not have a significant association with SFCT. Clinically, measuring the proportion of vascularity of the eye would provide more information compared to CT measurements alone.40

Our study group was younger than in previous reports (33.1±24.5 vs. 55.9±18.8 vs. 61.5±8.7 years respectively) and with a broader age-span towards younger subjects (from 3 to 85 vs. 22 to 90 vs. 45 to 85 respectively), which could influence our results. Our SE was 0.11±1.38 D (from +3 to -3) vs. -1.23±2.3 D (-6 to 3.5) in Sonoda's study. Mean SFCT was 305.77±78.29 µm vs. 241.34±97.11 in Agrawal's study. This difference could be justified by our younger sample.29

Mean choroid area measured it is not comparable between the three studies given the different B-scan lengths used in each study: 9 mm in our study vs. 7.5 or 1.5 mm in the others; and the same happens with stromal and vascular areas.

Agrawal's CVI is a very similar concept to our percentage of vascularity, being of 65.61±2.3% vs. 54.40±8.35% in our sample. In Sonoda's study stromal and, more significantly vascular area, are correlated with age. However, our main input in relation to previous studies is that stromal area and age are not correlated.

OCT angiography and en-face SS-OCT have been used to perform quantitative and qualitative studies of choroidal vascularity.56-59 Nevertheless, our results about choroidal vascular density cannot be compared with the results obtained using OCT angiography or en-face SS-OCT given that only subfoveal axial scans were used to carry our study.

Our study has several limitations though. Our study results are limited to normal healthy eyes, therefore cannot be applicable to pathologic eyes. We report results of single fovea-centered, horizontal 12 mm scans, so as the running directions of the choroidal blood vessels are known to be irregular further studies using differently oriented scans would be necessary to prove our results. However, our results could differ if we consider a volume scan over the macular region. Similarly, our results are unable to report focal changes in macular region. There could be another concern about measurements of dark and white regions as vessel or stroma, however, thresholding for binarization is performed using standard technique.45

In conclusion, using binarization techniques luminal and stromal areas can be separately analysed and show that the area of the choroid, the luminal area and the percentage vascular/total area decrease with increasing age while stromal area remains stable. Our results should provide basic information about age-related changes in normal choroid. Application of this information could be very useful while using choroid as biomarker for various vision restorative therapies.

References.

1.   Stanga PE, Lim JI, Hamilton P. Indocyanine green angiography in chorioretinal diseases: indications and interpretation: an evidence-based update. Ophthalmology 2003;110:15-21.
2.   Imamura Y, Fujiwara T, Margolis R, Spaide RF. Enhanced depth imaging optical coherence tomography of the choroid in central serous chorioretinopathy. Retina 2009;29:1469-73.
3.   Maruko I, Iida T, Sugano Y, Ojima A, Sekiryu T. Subfoveal choroidal thickness in fellow eyes of patients with central serous chorioretinopathy. Retina 2011;31:1603-8.
4.   Yannuzzi LA. Indocyanine green angiography: a perspective on use in the clinical setting. Am J Ophthalmol 2011;151:745-51.
5.   Chung SE, Kang SW, Lee JH, Kim YT. Choroidal thickness in polypoidal choroidal vasculopathy and exudative age-related macular degeneration. Ophthalmology 2011;118:840-5.
6.   Koizumi H, Yamagishi T, Yamazaki T, Kawasaki R, Kinoshita S. Subfoveal choroidal thickness in typical age-related macular degeneration and polypoidal choroidal vasculopathy. Graefes Arch Clin Exp Ophthalmol 2011;249:1123-8.
7.   Manjunath V, Goren J, Fujimoto JG, Duker JS. Analysis of choroidal thickness in age-related macular degeneration using spectral-domain optical coherence tomography. Am J Ophthalmol 2011;152:663-8.
8.   Switzer DW, Jr., Mendonca LS, Saito M, Zweifel SA, Spaide RF. Segregation of Ophthalmoscopic Characteristics According to Choroidal Thickness in Patients with Early Age-Related Macular Degeneration. Retina 2012;32:1265-71.
9.   Ueta T, Obata R, Inoue Y, et al. Background comparison of typical age-related macular degeneration and polypoidal choroidal vasculopathy in Japanese patients. Ophthalmology 2009;116:2400-6.
10.   Wood A, Binns A, Margrain T, et al. Retinal and choroidal thickness in early age-related macular degeneration. Am J Ophthalmol 2011;152:1030-1038.
11.   Chen W, Wang Z, Zhou X, Li B, Zhang H. Choroidal and photoreceptor layer thickness in myopic population. Eur J Ophthalmol 2012;22:590-7.
12.   Fujiwara T, Imamura Y, Margolis R, Slakter JS, Spaide RF. Enhanced depth imaging optical coherence tomography of the choroid in highly myopic eyes. Am J Ophthalmol 2009;148:445-50.
13.   Fureder W, Krauth MT, Sperr WR, et al. Evaluation of angiogenesis and vascular endothelial growth factor expression in the bone marrow of patients with aplastic anemia. Am J Pathol 2006;168:123-30.
14.   Ikuno Y, Tano Y. Retinal and choroidal biometry in highly myopic eyes with spectral-domain optical coherence tomography. Invest Ophthalmol Vis Sci 2009;50:3876-80.
15.   Wang NK, Lai CC, Chu HY, et al. Classification of early dry-type myopic maculopathy with macular choroidal thickness. Am J Ophthalmol 2012;153:669-77.
16.   Aoyagi R, Hayashi T, Masai A, et al. Subfoveal choroidal thickness in multiple evanescent white dot syndrome. Clin Exp Optom 2012;95:212-7.

17.   Channa R, Ibrahim M, Sepah Y, et al. Characterization of macular lesions in punctate inner choroidopathy with spectral domain optical coherence tomography. J Ophthalmic Inflamm Infect 2012;2:113-20.

18.   Fong AH, Li KK, Wong D. Choroidal evaluation using enhanced depth imaging spectral-domain optical coherence tomography in Vogt-Koyanagi-Harada disease. Retina 2011;31:502-9.

19.   Nakai K, Gomi F, Ikuno Y, et al. Choroidal observations in Vogt-Koyanagi-Harada disease using high-penetration optical coherence tomography. Graefes Arch Clin Exp Ophthalmol 2012;250:1089-95.

20.   Say EA, Shah SU, Ferenczy S, Shields CL. Optical coherence tomography of retinal and choroidal tumors. J Ophthalmol 2012;2012:385058.

21.   Shields CL, Perez B, Materin MA, Mehta S, Shields JA. Optical coherence tomography of choroidal osteoma in 22 cases: evidence for photoreceptor atrophy over the decalcified portion of the tumor. Ophthalmology 2007;114:e53-8.

22.   Spaide RF, Koizumi H, Pozzoni MC. Enhanced depth imaging spectral-domain optical coherence tomography. Am J Ophthalmol 2008;146:496-500.

23.   Huber R, Adler DC, Srinivasan VJ, Fujimoto JG. Fourier domain mode locking at 1050 nm for ultra-high-speed optical coherence tomography of the human retina at 236,000 axial scans per second. Opt Lett 2007;32:2049–2051.

24.   Lim H, de Boer JF, Park BH, Lee EC, Yelin R, Yun SH. Optical frequency domain imaging with a rapidly swept laser in the 815-870 nm range. Opt Express 2006;14:5937–5944.

25.   Unterhuber A, Povazay B, Hermann B, Sattmann H, Chavez-Pirson A, Drexler W. In vivo retinal optical coherence tomography at 1040 nm-enhanced penetration into the choroid. Opt Express 2005;13:3252–3258.

26.   Yasuno Y, Hong Y, Makita S, et al. In vivo high-contrast imaging of deep posterior eye by 1-micron swept source optical coherence tomography and scattering optical coherence angiography. Opt Express 2007;15:6121–6139.

27.   Copete S, Flores-Moreno I, Montero J, Duker JS, Ruiz-Moreno JM. Direct Comparison of Spectral-Domain and Swept-Source OCT in The Measurement of Choroidal Thickness in Normal Eyes. Br J Ophthalmol 2014;98:334-8.

28.   Ruiz-Moreno JM, Flores-Moreno I, Lugo F, Ruiz-Medrano J, Montero JA, Akiba M. Macular choroidal thickness in normal pediatric population measured by swept-source optical coherence tomography. Invest Ophthalmol Vis Sci 2013;54:353-9.

29.   Ruiz-Medrano J, Flores-Moreno I, Peña-García P, Montero JA, Duker JS, Ruiz-Moreno JM. Macular choroidal thickness profile in a healthy population measured by Swept-Source Optical Coherence Tomography. Invest Ophthalmol Vis Sci 2014;55:3532-42.

30.   Ding X, Li J, Zeng J, et al. Choroidal thickness in healthy Chinese subjects. Invest Ophthalmol Vis Sci 2011;52:9555-60.

31.   Ho J, Branchini L, Regatieri C, Krishnan C, Fujimoto JG, Duker JS. Analysis of normal peripapillary choroidal thickness via spectral domain optical coherence tomography. Ophthalmology 2011;118:2001-7.

32.   Ikuno Y, Kawaguchi K, Nouchi T, Yasuno Y. Choroidal thickness in healthy Japanese subjects. Invest Ophthalmol Vis Sci 2010;51:2173-6.

33.	Manjunath V, Taha M, Fujimoto JG, Duker JS. Choroidal thickness in normal eyes measured using Cirrus HD optical coherence tomography. Am J Ophthalmol 2010;150:325-329.

34.	Margolis R, Spaide RF. A pilot study of enhanced depth imaging optical coherence tomography of the choroid in normal eyes. Am J Ophthalmol 2009;147:811-5.

35.	Ouyang Y, Heussen FM, Mokwa N, et al. Spatial distribution of posterior pole choroidal thickness by spectral domain optical coherence tomography. Invest Ophthalmol Vis Sci 2011;52:7019-26.

36.	Ruiz-Medrano J, Flores-Moreno I, Peña-García P, Montero JA, Duker JS, Ruiz-Moreno JM. Asymmetry in macular choroidal thickness profile between both eyes in a healthy population. Retina 2015;35:2067-73.

37.	Adhi M, Brewer E, Waheed NK, Duker JS. Analysis of morphological features and vascular layers of choroid in diabetic retinopathy using spectral-domain optical coherence tomography. JAMA Ophthalmol 2013;131:1267–1274

38.	Ruiz-Medrano J, Flores-Moreno I, Montero JA, Duker JS, Ruiz-Moreno JM. Morphological features of the choroidoscleral interface in a healthy population using Swept-source Optical Coherence Tomography. Am J Ophthalmol 2015;160:596-601.

39.	Sonoda S, Sakamoto T, Yamashita T, et al. Luminal and Stromal Areas of Choroid Determined by Binarization Method of Optical Coherence Tomographic Images. Am J Ophthalmol 2015;159:1123–1131.

40.	Agrawal R, Gupta P, Tan KA, Cheung CM, Wong TY, Cheng CY. Choroidal vascularity index as a measure of vascular status of the choroid: Measurements in healthy eyes from a population-based study. Sci Rep 2016;6:2109.

41.	Brown JS, Flitcroft DI, Ying GS, et al. In vivo human choroidal thickness measurements: evidence for diurnal fluctuations. Invest Ophthalmol Vis Sci 2009;50:5-12.

42.	Tan CS, Ouyang Y, Ruiz H, Sadda SR. Diurnal variation of choroidal thickness in normal, healthy subjects measured by spectral domain optical coherence tomography. Invest Ophthalmol Vis Sci 2012;53:261-6.

43.	Usui S, Ikuno Y, Akiba M, Maruko I, Sekiryu T, Nishida K, Iida T. Circadian changes in subfoveal choroidal thickness and the relationship with circulatory factors in healthy subjects. Invest Ophthalmol Vis Sci 2012;53:2300-7.

44.	Vupparaboina KK, Nizampatnam S, Chhablani J, Richhariya A, Jana S. Automated estimation of choroidal thickness distribution and volume based on OCT images of posterior visual section. Comput Med Imaging Graph. 2015;46:315-27.

45.	Otsu N. A threshold selection method from gray-level histograms. Automatica 1975;11:23-27.

46.	Ruiz-Medrano J, Flores-Moreno I, Peña-Garcia I et al. Analysis of age-related Choroidal Layers thinning in Healthy Eyes Using Swept-Source Optical Coherence Tomography. Retina (forthcoming).

47.	Kur J, Newman EA, Chan-Ling T. Cellular and physiological mechanisms underlying blood flow regulation in the retina and choroid in health and disease. Prog Retin Eye Res 2012;31:377–406.

48.   Sonoda S, Sakamoto T, Yamashita T, et al. Choroidal structure in normal eyes and after photodynamic therapy determined by binarization of optical coherence tomographic images. Invest Ophthalmol Vis Sci 2014;55:3893–3899.

49.   Castro-Correia J. Understanding the choroid. Int Ophthalmol 1995;19:135–147.

50.   Branchini LA, Adhi M, Regatieri CV, et al. Analysis of choroidal morphologic features and vasculature in healthy eyes using spectral-domain optical coherence tomography. Ophthalmology 2013;120:1901–1908.

51.   Toda N. Age-related changes in endothelial function and blood flow regulation. Pharmacol Ther 2012;133:159–176.

52.   Stenmark KR, Yeager ME, El Kasmi KC, et al. The adventitia: essential regulator of vascular wall structure and function. Annu Rev Physiol 2013;75:23–47.

53.   Friedman E, Smith TR, Kuwabara T. Senile choroidal vascular patterns and drusen. Arch Ophthalmol 1963;69:220–230.

54.   Sohn EH, Khanna A, Tucker BA, Abramoff MD, Stone EM, Mullins RF. Structural and biochemical analyses of choroidal thickness in human donor eyes. Invest Ophthalmol Vis Sci 2014;55:1352–1360.

55.   Kumar A, Zhao L, Fariss RN, McMenamin PG, Wong WT. Vascular associations and dynamic process motility in perivascular myeloid cells of the mouse choroid: implications for function and senescent change. Invest Ophthalmol Vis Sci 2014;55:1787–1796.

56.   Sohrab M, Wu K, Fawzi AA. A pilot study of morphometric analysis of choroidal vasculature in vivo, using en face optical coherence tomography. PLoS One 2012;7:e48631.

57.   Cole ED, Novais EA, Louzada RN, et al. Visualization of Changes in the Choriocapillaris, Choroidal Vessels, and Retinal Morphology After Focal Laser Photocoagulation Using OCT Angiography. Invest Ophthalmol Vis Sci 2016;57:OCT356-61.

58.   Wakatsuki Y, Shinojima A, Kawamura A, Yuzawa M. Correlation of Aging and Segmental Choroidal Thickness Measurement using Swept Source Optical Coherence Tomography in Healthy Eyes. PLoS One 2015;10:e0144156.

59.   Ferrara D, Waheed NK, Duker JS. Investigating the choriocapillaris and choroidal vasculature with new optical coherence tomography technologies. Prog Retin Eye Res 2016;52:130-55.

Figure legends

Figure 1: Swept source Optical coherence tomographic images of choroid converted to binarization images of two healthy eyes. The B-scan image (a) is converted to a binary image using software. Choroid limits are delineated (b). The luminal area and the stromal area can be seen. The binarized image and the margin of the traced area are merged, which shows that the traced areas coincide with the dark areas of the choroidal areas of the SS-OCT image (c).

Figure 2: Swept source Optical coherence tomographic images of choroid converted to binarization images of two healthy eyes. The B-scan image (a) is converted to a binary image using software. Choroid limits are delineated (b). The luminal area and

the stromal area can be seen. The binarized image and the margin of the traced area are merged, which shows that the traced areas coincide with the dark areas of the choroidal areas of the SS-OCT image (c).

Figure 3: SS-OCT image of an example of choroidal thickness measures in all different nine locations, from the posterior edge of RPE to the choroid/sclera junction; from N3 position to T5 position.

Table legends
Table 1: Sample demographics. Age: years. SE: spherical equivalent (diopetrs). BCVA: Best Corrected Visual Acuity (decimal). SFCT: SubFoveal Choroidal Thickness (mµ). MCT: Mean Choroidal Thickness (µm). Choroidal area, Stromal region, Vascular region: mm2. *%

Table 2: Choroid area, vascular region, stromal region and percentage of choroidal vascular density in the <18-year-old group vs. >18-year-old group.

Table 3: Choroid area, vascular region, stromal region and percentage of choroidal vascular density comparison between all five age groups.

Figure 1
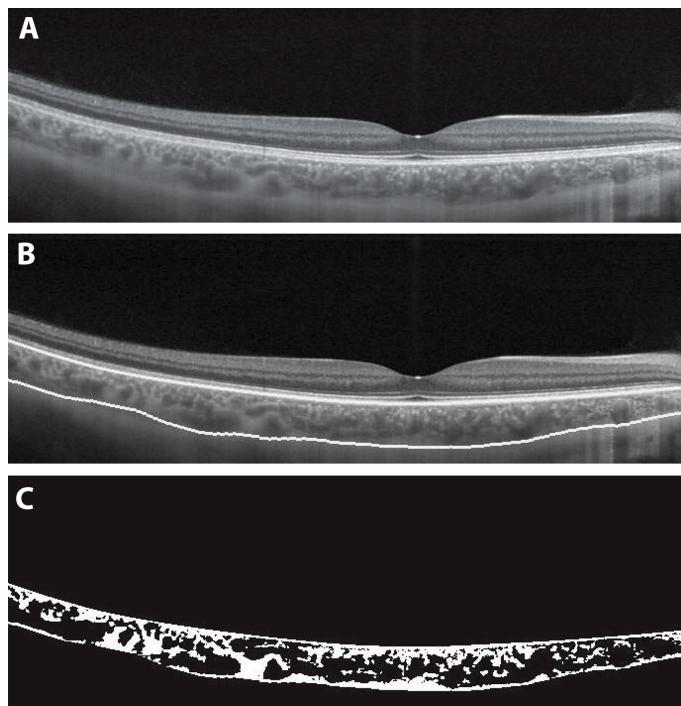
Figure 2
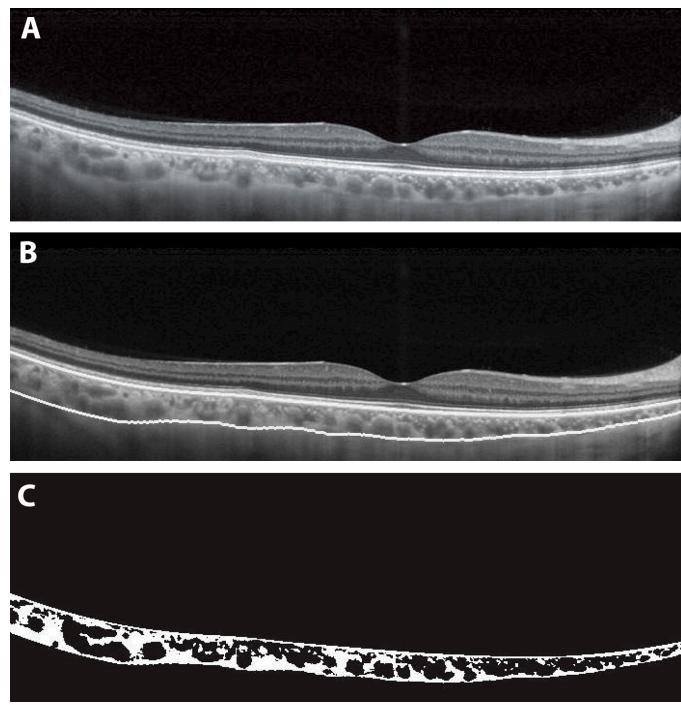
Figure 3
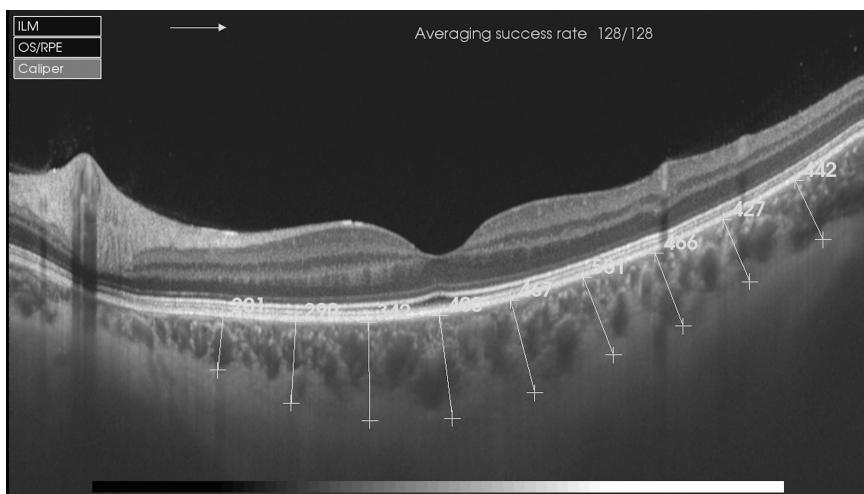
Table 1

	n	Mean	Standard deviation	Minimum	Maximum
Age	136	33.11	24.53	3	85
SE	134	0.11	1.38	-3	3
BCVA	135	0.97	0.06	0.8	1
SFCT	136	305.77	78.29	144.50	539.50
MCT	136	261.66	61.66	134.67	455.28
Choroidal Area	136	0.5554	0.1377	0.2738	1.0057
Stromal Region	136	0.2524	0.0762	0.1074	0.4601
Vascular Region	136	0.3029	0.0893	0.1104	0.5537
Percentage of vascularity*	136	54.40	8.33	33.34	77.04

Age: years. SE: spherical equivalent (diopetrs). BCVA: Best Corrected Visual Acuity (decimal). SFCT: SubFoveal Choroidal Thickness (mµ). MCT: Mean Choroidal Thickness (µm). Choroidal area, Stromal region, Vascular region: mm^2. *%

Table 2.

	≤18 years	>18 years	P[*]
N	59	77	
Choroidal Area	0.6149± 0.1202	0.5098± 0.1334	<0.001
Stromal Region	0.2480± 0.0727	0.2558± 0.0791	0.55
Vascular Region	0.3668± 0673	0.2540± 0715	<0.001
Percentage of vascularity**	60.16± 6.51	49.98± 6.79	<0.001

Mean ± standard deviation
mm^2
[*]Student t test
[**]%

Table 3.

	0-10 years	11-20 years	21-40 years	41-60 years	>60 years	P[*]
N	38	22	26	20	30	
Choroidal Area	0.6246± 0.1000	0.5919± 0.1500	0.5470± 0.1533	0.4764± 0.0920	0.5010± 0.1369	<0.001
Stromal Region	0.2473± 0.0568	0.2478± 0.948	0.2540± 0.0769	0.2405± 0.0645	0.2690± 0.0935	0.712
Vascular Region	0.3772± 0.0641	0.3441± 0.0711	0.2930± 0.0848	0.2358± 0.0484	0.2320± 0.0598	<0.001
Percentage of vascularity**	60.56± 5.80	59.25± 7.60	53.67± 5.30	49.76± 7.09	46.76± 6.32	<0.001

Mean ± standard deviation
mm^2
[*]ANOVA test
[**]%

110

5. DISCUSIÓN

5. DISCUSIÓN

La investigación de la coroides ha sido tradicionalmente difícil. La AVI permite la visualización de los vasos coroideos,[27,59] y los avances más recientes en tecnología OCT han añadido información de la anatomía de coroides en forma de cortes trasversales.[72] La mejora de las imágenes de capas más profundas proporcionada por el SD-OCT ha permitido el estudio de la coroides en todo su espesor, incrementando nuestro conocimiento sobre la fisiopatología y la etiología de multitud de enfermedades oculares.[45,57,58,60–63,66–69,73]

Prototipos de SS-OCT con mayor longitud de onda (1050-1060 nm) se han utilizado en los últimos años mejorando la calidad de las imágenes obtenidas. Programas más rápidos y con mayor definición pueden ayudar a superar el efecto barrera del EPR y las alteraciones inducidas por el movimiento.[74,75]

Las publicaciones sobre grosor coroideo establecen un adelgazamiento progresivo de la coroides con la edad.[41,74,76–79] Margolis describió un adelgazamiento de 1,56 μm por año de vida.[41] Por otra parte, Agawa[75] y Li[80] reportaron que la correlación entre el grosor coroideo y la edad no existía en ojos con longitudes axiales por debajo de los 25 mm. El efecto de la edad en el grosor coroideo de la población pediátrica no había sido estudiado con anterioridad.

En nuestra serie de pacientes, el OCT Swept-Source permitió la visualización de la coroides hasta la esclerótica en todos los casos con imágenes de buena calidad, permitiendo la correcta medida del grosor coroideo. El grosor coroideo medio subfoveal fue muy parecido entre los dos grupos (312.9±65.3 μm en el grupo de estudio vs. 305.6±102.6 μm en el grupo control) (P=0.19). El grosor coroideo macular

medio fue ligeramente diferente (285.2±56.7 μm en el grupo de estudio vs. 275.2±92.7 μm en el grupo control) (P=0.08). El grosor coroideo subfoveal y nasal fue similar en los dos grupos; sin embargo, el grosor coroideo temporal fue mayor en el grupo de estudio en la población pediátrica alcanzando la significación estadística en los puntos de medida T2 y T3 (P=0.014 y P=0.002 respectivamente), quedándose cerca de la misma también en T1 (P=0,059). Estos datos sugieren que el grosor coroideo temporal parece reducirse con la edad, llegando a ser menor que el grosor subfoveal en el adulto. Este hallazgo se ve reforzado por la correlación negativa estadísticamente significativa que existe entre el grosor coroideo y la edad para todo el grupo en los puntos de medida T1, T2 y T3.

Los resultados de grosor coroideo en nuestro grupo control son similares a los reportados previamente en la literatura científica. La edad media de nuestro grupo control fue de 53,2±15,6 años, similar a la publicada en otras series, haciendo las muestras comparables entre ellas.[41,76,77] De todas formas, también existen publicaciones con poblaciones de estudio más jóvenes que nuestro grupo control;[74,75,79,80] esta información debe de considerarse con precaución dada la fuerte correlación hallada entre la edad y el grosor coroideo en los adultos.[41]

El grosor coroideo medio subfoveal de nuestro grupo control (312,9±65,3 μm) es mayor que el hallado por otros autores: Margolis describe un grosor subfoveal medio de 287±76 μm,[41] Manjunath[77] 272±81 μm y Ouyang 297±82 μm.[79] El grosor coroideo subfoveal fue mayor en otras series publicadas: Ikuno 354±111μm;[74] Agawa 348±73 μm;[75] Branchini 337-347 μm;[72] Li 342±118 μm.[80] La

edad media de los pacientes de estos estudios es menor que la edad media de los pacientes de nuestro grupo control.

Ikuno determinó el grosor coroideo macular (en lugar del subfoveolar) usando dos aparatos diferentes.[45] Según sus datos, el grosor coroideo medio es 292,7 μm (utilizando un SS-OCT clásico) y de 283,7 μm (con EDI-OCT), en una población 37,6 años vs. 275,2 μm en una muestra de 53,2 años en nuestra serie. Branchini determinó el grosor coroideo en un grupo de pacientes de 35,2 años de edad utilizando tres plataformas diferentes. El grosor coroideo en posición N1 fue de 313,3 μm con un OCT RTVue, 319,8 μm con Spectralis y 320,4 μm con Cirrus; en nuestro grupo control fue de 290 μm en N1. Branchini encontró un grosor 335,9 μm con RTVue, 346,8 μm con Spectralis y 339,3 μm con Cirrus en posición T1; en esa posición el grosor fue de 299 μm en nuestro grupo control. Según Ikuno,[74] el grosor coroideo medio fue de 227 μm a 3 mm nasal a la fóvea y 337 μm a 3 mm temporal a la fóvea en un grupo de pacientes de 39,4 años. En la serie de Margolis[41] el grosor coroideo fue de 203 μm 2 mm nasal a la fóvea y 268 μm 2 mm temporal a la fóvea en una población que promediaba los 50,4 años de edad. En nuestra serie el grosor coroideo fue de 205 μm en N3 (2,25 mm nasal a la fóvea) y 281 μm en T3 (2,25 mm temporal a la fóvea).Sin embrago, la mayoría de estas determinaciones son muy similares dada la corrección por edad de 1,56 μm por año que establece Margolis.

No se pudieron comparar estos datos con nuestro grupo de estudio dado que este tipo de medidas en pacientes pediátricos no habían sido publicadas hasta el momento. Sin embargo, en nuestra serie no hemos encontrado diferencias entre niños y adultos a excepción de la coroides temporal a la fóvea. La edad a la que la

114

coroides comienza a adelgazarse como algún autor ha sugerido aún está por determinar. Estaría en probable relación con las alteraciones y modificaciones vasculares propias de la edad. Hallamos una correlación estadísticamente significativa entre el grosor coroideo y la edad, el grosor coroideo y el equivalente esférico (EE) y el grosor coroideo subfoveal y el EE en el grupo de estudio.

El perfil topográfico de grosor coroideo del grupo control en nuestra serie es más grueso en posición subfoveal, seguido por el sector temporal y nasal en este orden. Este perfil es similar al descrito previamente en otras series. Pero el perfil del grupo estudio fue diferente (mayor en el sector temporal con 320, 322 y 324 μm, seguido por el subfoveal con 312 μm y por el nasal con 281, 239 y 195 μm).

Las diferentes plataformas de OCT utilizadas para las investigaciones que aparecen en la literatura proporcionan diferentes niveles de calidad de imagen, permitiendo una visualización más o menos adecuada de la línea que separa la coroides de la esclerótica. En nuestra muestra todos los pacientes fueron examinados con un SS-OCT, mostrando de forma clara el límite posterior de la coroides. Los porcentajes sobre la proporción de coroides que fueron capaces de ser medidas correctamente en los diferentes estudios publicados ha sido de 74%[77] a 90%[76] de los ojos examinados por un Cirrus HD-OCT y de 95.8% de los ojos examinados por un Heildeberg EDI-OCT. Dos artículos que comparan diferentes OCT aportan una capacidad de medida de 96.,4% y 90.,7% respectivamente.[72,81] La elevada correlación intraclase entre los tres observadores independientes (de 0,91 a 0,98) remarca la precisión de medida que proporciona el SS-OCT.

El adelgazamiento progresivo de la coroides con la edad es un factor clave

para establecer el papel que juega la coroides en la patología retiniana. Aunque Ikuno[74] llevó a cabo un estudio similar en el que describió el grosor de la coroides en sujetos japoneses sanos, no incluyó pacientes de un rango de edad amplio. Además, la pérdida de grosor coroideo subfoveal que puede deducirse de nuestro estudio es de 0,852 μm al año, lejos de las 4,32 μm por año predichas por otros estudios anteriores, alcanzando pues diferentes conclusiones.

La primera de nuestras publicaciones representó la serie más grande publicada hasta la fecha sobre las mediciones del grosor coroideo con tecnología SS-OCT. Se eligió esta plataforma para llevar a cabo el estudio ya que sus características permiten un estudio de la coroides con más precisión que la anteriormente publicada en otros estudios que utilizaron otros modelos de OCT desde un punto de vista teórico. Esta precisión ha sido demostrada en artículos publicados por Copete[47] o Ruiz-Moreno,[46] utilizando este mismo prototipo. El grosor de la coroides pudo ser determinado en el 100% de los pacientes de sus respectivos estudios. En nuestro caso, usando el SS-OCT la coroides pudo medirse con éxito en el 100% de los ojos estudiados. Wei[82] midió con éxito el 93,2% de 3.468 ojos (el estudio más grande publicado hasta la fecha) utilizando un OCT de Heidelberg Spectralis con la modalidad EDI. La elección de Manjunah[77] fue el Cirrus HD-OCT sin tecnología EDI, y fue capaz de medir la coroides en sólo el 74% de los ojos. Yamashita[81] y Shin[83] utilizaron un Topcon SD-OCT y fueron capaces de medir correctamente un 63,3 % y un 90,7% de los ojos respectivamente. Copete[47] comparó la capacidad del SD-OCT y el SS-OCT obteniendo buenas imágenes en el 70,4 y el 100% respectivamente.

Margolis[41] estudió un grupo de 54 ojos con un EE medio de -1,3 dioptrías (D) hallando un grosor coroideo subfoveal medio 287 μm, similar a los resultados de Flores-Moreno[64] y a los de Manjunath[77] que publicó grosores de 272 μm en 34 ojos de una muestra de 51,1 años de edad. Xu[84] comparó diabéticos frente a no diabéticos, hallando un grosor coroideo subfoveal de 266 μm en el grupo control (1.795 sujetos).

Como se ha comentado con anterioridad, la coroides también se ha estudiado en la población pediátrica con tecnología SS-OCT.[46] Park[85] en un estudio más reciente con pacientes pediátricos encontró un grosor coroideo subfoveal medio de 348,4 μm en los 48 ojos que evaluó.

En este estudio el grosor coroideo subfoveal medio fue de 301,89 μm. Este dato es entorno a 10 μm mayor que el encontrado por otros autores que utilizaron tecnología SD-OCT. Es lógico pensar que la introducción de pacientes en edad pediátrica en nuestra muestra pueda haber llevado a este ligero incremento. De manera interesante, estos resultados coinciden con los encontrados por nuestro grupo, que usando el mismo OCT hallaron prácticamente el mismo grosor en su grupo de pacientes adultos. El SS-OCT puede dar lugar a unas medidas ligeramente superiores a las proporcionadas por los SD-OCT. Esto puede ser explicado por una mayor calidad de las imágenes y por el hecho de que nuestras medidas fueron tomadas desde límite más posterior del EPR hasta el límite más externo de la lámina fusca, en lugar de hasta el límite externo de los vasos coroideos.

Ruiz-Moreno con un SS-OCT y Flores-Moreno con un SD-OCT proporcionaron datos sobre grosores coroideos maculares medios. Ruiz-Moreno obtuvo un grosor de

275 μm en los adultos que estudió frente a las 285 μm que obtuvo en los pacientes pediátricos. Flores-Moreno obtuvo grosores de 257 μm en los pacientes de su grupo control, frente a 115 μm en los altos miopes estudiados. Nosotros hallamos un grosor coroideo macular medio de 258,69 μm, similar a los resultados proporcionados por estos autores. Sin embargo, nuestro estudio fue el primero en analizar grosores a lo largo de un corte de 8 mm de la mácula, centrado en la fóvea de los pacientes, por los 6 mm estudiados con anterioridad por otros autores. Esto fue gracias a que el SS-OCT proporciona imágenes de gran calidad también en el sector más temporal, que es precisamente donde se produjo este incremento de 2 mm de la zona estudiada. Esto podría ser clínicamente relevante dado que es en este sector temporal donde se producen las variaciones más significativas en términos de grosor.

No se encontraron diferencias estadísticamente significativas entre hombres y mujeres. Los sujetos de ambos sexos mostraron perfiles prácticamente idénticos con diferencias mínimas en el sector más temporal, en el que las mujeres mostraron tener una coroides ligeramente más delgada. El grosor subfoveal medio fue 303,9 μm en hombres vs. 296,4 μm en mujeres. Esta pequeña diferencia no significativa, se explica con facilidad dada la diferencia de edad entre ambos grupos (30,39 años en el caso de los hombres y 37,48 en las mujeres). El grosor fue cercano a 7 μm mayor de media en el caso de los hombres, pero en esta muestra eran 7 años más jóvenes. Si hacemos caso a las fórmulas de correlación que se obtienen de nuestra base de datos, el grosor coroideo en un grupo pareado por edad y sexo hubiera sido prácticamente idéntico.

Hay estudio previos que utilizan OCT de alta penetración para el estudio del grosor coroideo en adultos, pero no llevaron a cabo comparaciones entre diferentes grupos de edad. En el presente estudio se compararon las diferencias de grosor entre diferentes grupos de edad, a intervalos de 20 años. Sin embargo, los dos grupos más jóvenes se formaron a intervalos de 10 años (0-10 y 10-20 años) dado que el crecimiento ocular ocurre teóricamente en dos fases: la primera hasta los 6 años de edad, alcanzando la emetropización; y la segunda de los 7 a los 19 años, momento en el que tiene lugar la expansión global de los tejidos oculares.[86] El perfil de grosor coroideo fue diferente en cada grupo y la coroides se adelgazó progresivamente en cada grupo de edad, mostrando diferencias estadísticamente significativas entre los diferentes grupos. Esta reducción fue claramente progresiva hasta los 40 años, momento en el que tuvo lugar la reducción más llamativa, pasando de las 313,9 μm en el grupo de 21 a 40 años de edad a las 264,6 μm en el grupo de 41 a 60 años (49 μm de diferencia). De manera interesante, a partir de los 40 años (41-60 vs. >60) las diferencias de grosor coroideo no fueron estadísticamente significativas en lo que respecta al grosor macular medio ni al grosor subfoveal medio. Si tenemos en cuenta las diferencias halladas al considerar un solo ojo por paciente (como recomienda en su artículo Ray[87]) o ambos, éstas fueron mínimas. Se obtuvieron predicciones de reducción del grosor coroideo de 9,4 vs. 10 μm por década de vida en grosor macular medio; y de 8,5 vs. 8,87 μm por década en grosor coroideo subfoveal.

Sabemos pues que la coroides es más gruesa en localización subfoveal y que este grosor se reduce de manera progresiva hacia el sector temporal, reduciéndose

de una manera más acusada hacia el nervio óptico,[88,89] con un contorno o un perfil de forma cóncava.[90]

Adhi describió alteraciones significativas en las características morfológicas de la coroides de la mayoría de los ojos de pacientes con retinopatía diabética que estudió. Hallaron que la interfaz esclero-coroidea presentaba una forma irregular, con un punto de inflexión en 8 de los 9 ojos estudiados con retinopatía diabética no proliferativa (89%), en 9 de los 10 ojos estudiados con retinopatía diabética proliferativa (90%) y en 13 de 14 ojos (93%) con edema macular diabético. Por el contrario, no hallaron esta alteración en ninguno de los 24 controles que se emplearon para su estudio.[90] La presencia de un perfil esclero-coroideo irregular con un punto de inflexión y un adelgazamiento focal de la coroides se ha descrito en algunas enfermedades como la retinopatía diabética y la DMAE.[73,90,91]

Dolz-Marco reportó un caso de protrusión focal inferotemporal de la esclerótica con un adelgazamiento cóncavo de la coroides, rodeado de coroides normal.[92] Los autores plantearon la hipótesis de que este hallazgo podría estar en relación con la inserción del músculo oblicuo inferior, que podría dar lugar a una compresión de la coroides, sin ser capaces de pronunciarse sobre la situación de la esclerótica, al no ser completamente visible.

En nuestra serie de pacientes no se halló ninguna anomalía en el fondo de ojo que pudiera justificar este engrosamiento focal en los pacientes que presentaban la inflexión esclero-coroidea. El análisis con SS-OCT no detectó ninguna alteración de la coroides en estos pacientes, aparte de la inflexión. Por otro lado se identificó una imagen que podría representar el borde superior de la inserción del músculo oblicuo

inferior en la esclerótica, junto con un fina línea hiper-reflectiva, paralela a la esclerótica que podría corresponder la porción intraescleral de una arteria ciliar posterior larga.

La razón por la cual los vasos de la retina aparecen como hiper-reflectivos en las imágenes de OCT mientras que los vasos coroideos aparecen hipo-reflectivos está en relación con la velocidad de las células sanguíneas que los recorren. La velocidad del flujo sanguíneo en los vasos de la coroides es mucho mayor que en los vasos de la retina. La elevada velocidad de los eritrocitos en la coroides hace que la señal de interferencia desaparezca, resultando en una señal nula en el interior de sus vasos. Por el contrario, la velocidad de los mismos es mucho menor en la circulación retiniana, lo que lleva a que la señal de interferencia produzca una imagen hiper-reflectiva.

Los estudios publicados sobre la anatomía de la parte más posterior del globo ocular, los músculos y sus vasos indican que el límite superior de la inserción del músculo oblicuo inferior, coincide con el meridiano horizontal del ojo a unos 5,7 mm de la fóvea. [93]

La distancia media del punto de inflexión a la fóvea fue de 4.427 μm en nuestra muestra y situado siempre en el sector temporal de la mácula. La presencia de este punto de inflexión está probablemente en relación con la inserción del músculo oblicuo inferior, que como se ha comentado con anterioridad se halla a unos 5,7 mm de la fóvea. La tracción ejercida sobre la esclerótica por el tendón de este músculo puede ser la responsable de una separación de la pared de la esclerótica y el consiguiente engrosamiento coroideo. Basándose en las

descripciones anatómicas de la región, la línea paralela, hipo-reflectiva a este nivel puede corresponder con el segmento intraescleral de una arteria ciliar posterior larga temporal.

El hecho de que este hallazgo sea más frecuente entre los pacientes más jóvenes, especialmente entre los menores de 15 años, se puede explicar por la menor rigidez de la esclerótica entre la población más joven,[94] lo que podría facilitar la deformación inducida por la tracción muscular inducida por el tendón del músculo oblicuo inferior.

Son varios los estudios publicados sobre el grosor coroideo en poblaciones sanas. Ding estudió el grosor coroideo de 210 voluntarios sanos (420 ojos) sin enfermedades oftalmológicas utilizando un EDI-OCT y en múltiples localizaciones de la mácula: En posición subfoveal y a 1 y 3 mm en dirección superior, inferior nasal y temporal a la fóvea. Sin embargo, los autores no estudiaron la existencia de diferencias entre los ojos.[78] Ikuno estudió el grosor y el perfil de la coroides de 86 ojos de 43 pacientes sanos con un SS-OCT, así como la correlación entre el mismo con la longitud axial, el error refractivo y la edad, pero no analizó las diferencias existentes entre ojos derechos e izquierdos.[74]

Por el contrario, Chen[89] describió la variación inter-ocular en lo que respecta al grosor coroideo en una población de 50 adultos sanos usando tecnología EDI-OCT. Midió el grosor subfoveal y realizó medidas en 4 localizaciones paramaculares: 3 mm superior, inferior, nasal y temporal. Las diferencias encontradas fueron de 1 μm en localización subfoveal, 13,6 μm nasal a la fóvea y -2,9 μm temporal a la misma (diferencias no estadísticamente significativas). Lo que parece claro es que muestran

una tendencia hacia un mayor grosor del sector nasal de la mácula en ojos derechos (14 μm).

Al comparar estos resultados con los obtenidos en el presente estudio en las mismas localizaciones (subfoveal, N3 y T3), se observa una diferencia entre ojos derechos e izquierdos de 7,45 μm en grosor subfoveal medio, 1,43 μm en T3 y 14,44 μm en N3. Las diferencias entre grosor coroideo nasal medio (p=0,0002), grosor coroideo nasal medio en hombres (p=0,003) y en mujeres (p=0,03), y el grosor coroideo medio en cada punto de medida nasal a la fóvea (p=0,001; 0,002 and 0,08 respectivamente) fueron estadísticamente significativas. La coroides resultó ser más gruesa en los ojos derechos en cada punto de medida nasal para ambos sexos, a excepción de las mujeres en N1 (p=0,259).

La correlación entre el grosor coroideo inter-ocular obtenido por Chen fue más fuerte para el grosor coroideo subfoveal (r=0,90; p<0,001, test de correlación de Spearman), mientras que para los puntos nasales fue de r=0,83 (p<0,001). Para los puntos de medida temporales fue más débil (r=0,49; p<0,001). En la presente serie el estudio de correlación para el grosor coroideo medio en posición subfoveal, N3 y T3 fue similar (r=0,860; 0,853 y 0,754 respectivamente, p<0,001; test de correlación de Spearman). El perfil de grosor coroideo descrito en su artículo es muy similar al perfil descrito en el presente trabajo comparando ojos derechos e izquierdos.

Es difícil explicar la evidencia fuerte y consistente que existe sobre un mayor grosor coroideo en ojos derechos en el sector nasal de la mácula en la población sana. Una posible explicación podría ser un distinto flujo sanguíneo entre ambos ojos dada la falta de simetría del arco aórtico. Dicha asimetría ha sido usada como la

hipótesis que podría explicar las diferencias de incidencia y prevalencia de determinadas patologías vasculares entre ojos derechos e izquierdos, como es el caso de la endoftalmitis bacteriana metastásica[95] y las oclusiones arteriales retinianas.[96-99]

La circulación coroidea tiene su origen en las arterias ciliares posteriores cortas, que penetran la esclerótica alrededor del nervio óptico en un número que varía entre 10 y 20; la mitad nasal de la coroides macular estudiada en este trabajo está pues directamente suministrada por estas arterias ciliares posteriores cortas. Éstas son ramas derivadas de la arteria oftálmica, que es una rama de la carótida interna, que a su vez es rama de la arteria carótida común.[99]

La diferencia generada por el hecho de que el origen de la arteria carótida común derecha yace en el tronco braquiocefálico, mientras que la carótida común izquierda sale directamente de la aorta, es posiblemente la responsable de un flujo más directo en la mitad derecha de este árbol vascular.[95]

Dado que la mayor parte de la estructura coroidea está formada por tejido vascular (la densidad vascular media de la coroides externa ronda el 87%),[100] un teórico flujo sanguíneo más elevado en el ojo derecho con relación al ojo izquierdo a través de las arterias ciliares posteriores podría explicar por qué la coroides nasal es más gruesa en los ojos derechos como se afirma en este estudio y como fue sugerido previamente por Chen.[89]

En este estudio, así como en trabajos precedentes se utilizó el EE en lugar de la longitud axial dado que el procedimiento es menos invasivo y más rápido, ya que anteriores indicaciones en la literatura demuestran que la refracción, más fácil de

obtener, posee la misma capacidad para generar los modelos necesario que la longitud axial.[101]

La coroides, como se ha mencionado anteriormente, se adelgaza con la edad.[102] Nuestro grupo de investigación analizó la coroides de individuos sanos a través de un amplio rango de edades (de 3 a 95 años), encontrando que el perfil de grosor de la coroides era similar entre los diferentes grupos de edad, adelgazándose progresivamente, especialmente a partir de los 40.[88]

Esmaeelpour utilizó un SD-OCT (longitud de onda de 840 nm) con un protocolo de exploración en mapa que contenía 512 A-scans y 512 B-scans a través de un campo de 36º x 36º para analizar de manera automática las capas de la coroides de 45 ojos de pacientes sanos con una edad media de 44 años (de 23 a 84 años).[103] El grosor coroideo medio del área analizada fue de 228 μm y el grosor de la capa de Haller y de la capa de Sattler + coriocapilar fueron de 141 μm y de 87 μm respectivamente.

Adhi[90] estudió 24 ojos de 24 pacientes de una media de edad de 64 años. Las medidas de grosor coroideo fueron tomadas de manera manual mediante el software con el que está equipado el SD-OCT que utilizó y se alcanzó a ver correctamente el límite entre la esclerótica y la coroides en el 79% de los casos. El protocolo de imagen empleado consistió en escáneres de 1 línea centrados en la fóvea. El grosor coroideo subfoveal fue de 276 μm, el grosor de la capa de Haller subfoveal fue de 224 μm y el grosor de la capa de Sattler + coriocapilar subfoveal fue de 52 μm.

Empleando este mismo método Branchini estudió la coroides de 42 ojos de 42 pacientes sanos de una edad media de 52 años, hallando el límite entre esclerótica y coroides en el 92% de ellos.[104] Midieron de manera manual el grosor de la coroides y el de sus capas en localización subfoveal, utilizando a su vez dos puntos más de medida a 750 μm a cada lado de la fóvea. Encontraron que el grosor coroideo subfoveal de su muestra fue de 256 μm. El grosor de la capa de Haller y el de la capa de Sattler + la coriocapilar fue de 204 y 53 μm respectivamente.

En el presente estudio se analizaron 169 ojos de 169 pacientes sanos utilizando un SS-OCT, siendo la mayor muestra empleada para el estudio de las capas de la coroides hasta donde alcanza nuestro conocimiento. La edad media fue algo menos que en los otros estudios similares, siendo de 33,5 años. Por otra parte la visualización del límite entre la esclerótica y la coroides fue posible en el 100% de los casos. Las cifras obtenidas para grosor subfoveal, capa de Haller y capa de Sattler + coriocapilar (305,8, 208,6 y 87,3 μm respectivamente) son mayores que las publicadas por otros autores. Un hallazgo similar fue presentado en otra publicación previa de nuestro grupo en la que se comparó el grosor coroideo obtenido con un SS-OCT en relación al publicado por otras series que emplearon SD-OCT, obteniendo una diferencia de entorno a las 10 μm a favor de la tecnología Swept-Source.[88] Este hecho junto a que nuestra muestra es considerablemente más joven que en las otras publicaciones podría explicar la diferencia en los resultados obtenidos.

Con el objetivo de evaluar el grosor de la coroides y de sus capas a través de la mácula se añadieron 8 puntos de medida adicionales (3 en sentido nasal y 5 más en sentido temporal). Los valores medios de grosor coroideo, capa de Haller y capa

de Sattler + coriocapilar fueron de 260,1; 180,2 y 78,2 respectivamente. El perfil de grosor coroideo mostró una morfología similar entre los diferentes grupos de edad, reduciéndose progresivamente con la edad, al igual que el grosor de la capa de Haller (p<0,001). La capa de Sattler + coriocapilar mostró una tendencia hacia la reducción con la edad sin alcanzar la significación estadística (p=0,124). Nuestros modelos de regresión lineal predijeron una reducción de 0,93 μm de grosor coroideo por año de edad; 0,69 de las cuales se debieron al adelgazamiento de la capa de Haller, que fue responsable del 75% del adelgazamiento ligado a la edad de la coroides. No se hallaron diferencias relacionadas con el sexo de los pacientes ni en grosor coroideo ni en ninguna de sus capas en ninguno de los grupos. Nuestro estudio muestra que la mayoría de la pérdida de grosor debida a la edad es a expensas de los grandes vasos. Estos hallazgos en ojos sanos van en desacuerdo con los hallazgos histopatológicos en ojos con una evidente esclerosis senil, que muestran mayoritariamente una atrofia de los pequeños y medianos vasos coroideos.[102, 105]

Spaide[102] publicó que la pérdida de vasos sanguíneos coroideos asociada a la edad estaba en directa relación con la pérdida de los vasos visibles, concluyendo que es una enfermedad de pequeño vaso que afecta a la coroides. Sin embargo, sus datos no son comparables con nuestros resultados ya que Spaide sólo incluyó en su estudio a pacientes con coroides por debajo de 125 μm. Un artículo de Sarks describe únicamente dos casos cuya retinoscopia mostraba áreas bien demarcadas de esclerosis coroides que estaban en probable relación con una DMAE atrófica, mientras que en nuestro estudio sólo se analizaron pacientes sanos.[105] Este

adelgazamiento ligado a la edad podría ser un factor clave para establecer el posible papel de la coroides en multitud de patologías retinianas.

Entre las limitaciones de este estudio se puede mencionar el hecho de que las medidas del grosor coroideo fueron realizadas en todos los casos de una forma manual, por dos observadores experimentados en el análisis de imágenes de la coroides. Actualmente existe un software comercialmente disponible para el Topcon DRI OCT-1 (Ver. 9.01.003.02) que permite la segmentación automática y la medida del grosor coroideo en los modos 3D y escáner radial, sin embargo su precisión en la práctica clínica aún está por demostrar. Este trabajo incluye el primer estudio publicado sobre población infantil y el cálculo de su grosor coroideo utilizando tecnología SS-OCT. Son pocos los estudios que han sido llevados a cabo hasta la fecha en adultos de diferentes rangos de edad empleando esta plataforma.

Otra limitación de este estudio es el hecho de que sólo se estudiaron los perfiles coroideos en el plano horizontal, el uso del EE en lugar de la longitud axial, el no haber realizado correcciones según otras variables como puedan ser la paquimetría, la presión intraocular, medicación sistémica o presión arterial y la imposibilidad de determinar si los vasos de la coroides nasal son más gruesos o bien más numerosos en ojos derechos que en izquierdos. Esto se debe a que la tecnología actual no permite un análisis adecuado y preciso del grosor de los vasos de la coroides, y no hay forma de saber si se está estudiando el diámetro máximo de un vaso dada la irregularidad anatómica de los mismos.

Como otra limitación, la capa coriocapilar no pudo ser diferenciada de la capa de Sattler debido a las limitaciones en la tecnología de imagen actual descritas con anterioridad, a pesar del elevado índice de correlación intraclase.

En conclusión y según nuestros resultados podemos dar respuesta a las hipótesis iniciales planteadas afirmando que el grosor coroideo de la mácula es similar entre la población pediátrica y adulta. El perfil de grosor coroideo es distinto en la población infantil, con un grosor máximo en posición temporal. Este perfil es muy similar entre los distintos grupos de edad en la población adulta, con la coroides adelgazándose progresivamente con la edad, especialmente cuando se compara a los pacientes mayores de 40 años con adultos más jóvenes o con la población infantil. La mayor variación de grosor coroideo con la edad tiene lugar en el sector temporal.

Una inflexión en la interfaz esclero-coroidea con un adelgazamiento focal de la coroides puede considerarse como una variación de la normalidad sin significación clínica, especialmente entre la población joven. Más estudios que incluyan el área macular al completo incluyendo la inserción del músculo oblicuo inferior en su totalidad y con mayor número de pacientes serán necesarios para establecer las características finales de estas alteraciones, así como su incidencia en la población normal.

La zona nasal del perfil de grosor coroideo de la mácula de la población normal es más gruesa en ojos derechos que en ojos izquierdos. Por el contrario, el grosor subfoveal y temporal no fueron estadísticamente diferentes al comparar ambos ojos entre sí.

129

La coroides y la capa de Haller sufren un adelgazamiento progresivo con la edad y sus perfiles muestran características similares entre los diferentes grupos etarios. Este adelgazamiento asociado a la edad va a ser principalmente a expensas de la capa de Haller.

Serán necesarios más estudios para probar los resultados de esta investigación.

5. DISCUSSION

Choroidal research has always been difficult. Indocyanine green angiography (ICGA) permits visualization of choroidal vessels,[27,59] and recent advances in OCT technology have added cross-sectional information about the choroid.[72] Improved deep imaging provided by SD-OCT has permitted cross-sectional research of the choroid, increasing our knowledge of the pathophysiology and etiology of several ocular conditions. [45,57,58,60–63,66–69,73]

Longer wavelength SS-OCT prototypes (1050-1060 nm) have been used in patients improving image quality. Faster and higher quality software may overcome retinal pigment epithelium (RPE) barrier effect and movement artifacts.[74,75]

Papers on choroid thickness (CT) report a progressive choroidal thinning with age.[41,74,76–79] Margolis described 1.56 μm thinning for each year of life.[41] On the other side, Agawa[75] and Li[80] reported that correlation between CT and age did not exist in eyes with axial length < 25 mm. The effect of age on CT in children has not been studied previously.

In our series of eyes, SS-OCT allowed visualization of CT in all the cases with high quality images permitting CT determination. Mean subfoveal CT was very similar in both groups (312.9±65.3 μm in SG vs. 305.6±102.6 μm in CG) (P=0.19). Mean macular CT was slightly different (285.2±56.7 μm in SG vs. 275.2±92.7 μm in CG) (P=0.08). Subfoveal and nasal CT was similar in both groups; however temporal CT was higher in SG with statistical significance in T2 (P=0.014) and in T3 (P=0.002) and near significance in T1 (P=0.059). These data suggest that temporal CT might decrease with age and become thinner than subfoveal CT in the adult. This finding is

reinforced by the significant inverse correlation between CT and age in the whole group at T1, T2 and T3.

The results of CT in our CG are similar to those previously reported in the literature. Mean age in our CG was 53.2±15.6 years, similar to that of other series.[41,76,77] We have found reports with patient populations younger than our CG;[74,75,79,80] this information should be carefully considered due to the strong correlation found between age and CT among adults.[41]

Mean subfoveal CT in our CG (312.9±65.3 µm) is higher than those reported in other series. Margolis reported an average subfoveal CT of 287±76 µm,[41] Manjunath[77] 272±81 µm and Ouyang 297±82 µm.[79] Subfoveal CT was higher in other series: Ikuno 354±111µm;[74] Agawa 348±73 µm;[75] Branchini 337 to 347 µm;[72] Li 342±118 µm.[80] Patients in these last five series were younger than those in our CG.

Ikuno determined macular CT (instead of subfoveal CT) using two different equipments.[45] According to Ikuno, average CT is 292.7 µm (using SS-OCT) and 283.7 µm (with EDI-OCT), in a population averaged 37.6 years of age vs. 275.2 µm and 53.2 years in our series. Branchini et al. determined CT in a group of patients aged 35.2 years using three different systems. CT at N1 position was 313.3 µm with RTVue, 319.8 µm with Spectralis and 320.4 µm with Cirrus; in our CG CT was 290 µm at N1. Branchini found CT to be 335.9 µm with RTVue, 346.8 µm with Spectralis and 339.3 µm with Cirrus at T1 position; in our CG CT was 299 µm at T1. According to Ikuno,[74] average CT was 227 µm 3 mm nasal to the fovea and 337 µm at 3 mm temporal to the fovea in a group of patients averaged 39.4 years of age. In Margolis' series[41] CT was 203 µm at 2 mm nasal to the fovea and 268 µm at 2 mm temporal to the fovea

132

in a population averaged 50.4 years. In our series, CT was 205 μm at N3 (2.25 mm nasal to the fovea) and 281 μm at T3 (2.25 mm temporal to the fovea).

However, most of these determinations are very similar considering Margolis' age-correction for CT (1.56 μm reduction per year). We are unable to compare these data with those from our SG, since such data have not been previously reported. However, in our series we have not found such differences between adults and youngsters except for the choroid temporal to the fovea. The age at which subfoveal CT starts to decrease as has been suggested by some authors is still to be determined. This decline is probably related to aging vascular changes. We have found a significant correlation between macular CT and age, macular CT and spherical equivalent (SE) and between SE and subfoveal CT among the SG.

The topographic profile of CT in the CG in our series is highest in the subfoveal area, followed by the temporal and the nasal areas. This profile is similar to those previously published in other series. However, CT profile was different among the SG (highest in the temporal choroid with 320, 322 and 324 μm, followed by subfoveal choroid with 312 μm and the nasal choroid with 281, 239 and 195 μm).

OCT devices reported in the literature provide different quality of imaging, permitting a more or less adequate visualization of the line delimiting the choroid and the sclera. In our series all the patients examined by SS-OCT, showed a clearly defined, measurable posterior portion of the choroid. Measurable choroidal thickness has been reported in 74%[77] to 90%[76] of the eyes examined by Cirrus HD-OCT and in 95.8% of the eyes examined by Heildeberg EDI-OCT. Two papers comparing OCT equipment report 96.4% and 90.7% measurability.[72,81] Choroidal

visualization was better in those studies using longer wavelength equipment. The high intraclass correlation coefficient (0.91 to 0.98) for the three independent observers highlights SS-OCT accuracy in CT determination.

Age dependant thinning is a key factor to establish the role of the choroid in retinal pathology. Although Ikuno et al[74] performed a similar study in which they described the choroidal thickness in healthy Japanese subjects, their study did not include a wide variation of ages. Furthermore, the loss of SFCT predicted by our studies is of 0.852 μm per year, far from the 4.32 μm per year predicted by previous papers, reaching different conclusions.

This was the largest series to date of CT measured with SS OCT and it confirms again the accuracy with which SS OCT can measure the choroid. SS-OCT was chosen to perform this study because its characteristics allow the analysis of the choroid with more precision than previous OCT technology from a theoretical point of view. This accuracy has been shown in other papers by Copete[47] or Ruiz-Moreno,[46] using the same device. Full choroidal thickness was successfully measured in 100% of the patients of their studies. Using SS-OCT we successfully measured the choroidal thickness of 100% of the eyes in this study as well. Wei et al[82] successfully measured 93.2% of 3,468 (largest study reported to date) using Heidelberg Spectralis OCT on the EDI setting. The choice of Manjunah et al[77] was Cirrus HD OCT without EDI which was able to successfully measure the choroid in only 74% of the eyes. Yamashita[81] and Shin[83] used Topcon SD OCT and were able to image 63.3 % and 90.7% respectively. Copete et al[47] compared SD OCT and SS OCT obtaining good measurements in 70.4 and 100% respectively.

Margolis et al[41] studied a group of 54 eyes with a mean SE of -1.3 D finding a mean SFCT of 287 μm, similar to Flores-Moreno's[64] results and to Manjunath's[77] who published a mean SFCT of 272 μm in 34 eyes of 51.1-year-old patients. Xu et al[84] compared diabetic with non-diabetic patients, finding a mean SFCT of 266 μm in the control group (1,795 subjects).

As noted before, the choroid has also been studied in pediatric population with SS OCT.[46] Park et al,[85] in a recent study with pediatric subjects, find a mean SFCT of 348.4 μm in the 48 eyes studied.

In the present study the mean SFCT was found to be 301.89 μm. This figure is about 10 μm thicker than that found by other authors using SD OCT. It is likely that the introduction of pediatric eyes into the study group resulted in a slight increase in the mean SFCT. Interestingly, these results match those of Ruiz-Moreno et al, who using the same device found almost the same CT in their patient group consisting of adults only. SS-OCT may result in a CT measurement slightly greater than that seen with SD-OCT. This may be explained by the higher quality of the images and by the fact that the measures were taken from the posterior edge of the RPE to the outer aspect of the lamina fusca, rather than the outer limit of the choroidal vessels.

Ruiz-Moreno with SS OCT and Flores-Moreno with SD-OCT provide data about mean macular choroidal thickness (MCT). Ruiz-Moreno found it to be of 275 μm in adults compared to 285 μm in pediatric subjects. Flores-Moreno obtained results of 257 μm in healthy patients and of 115 μm in highly myopic patients. We found that mean MCT was 258.69 μm, similar to these authors' results. Nevertheless the present study is the first employing a subfoveal 8 mm line of the macula

compared to the 6 mm studied by other authors. This was possible due to SS-OCT technology, which provides a more robust imaging of the temporal choroid, as this 2 mm increase was performed on this sector. This may prove to be a clinically important measure as it is in the temporal sector where greater variations of CT with age take place.

We found no statistically significant difference when comparing men to women. Subjects of both sexes showed almost identical choroidal profiles with a minimal difference in the temporal sector, in which the females usually had slightly thinner choroids. Mean SFCT was 303.9 μm in men vs. 296.4 μm in women. These slight, non-statistically significant differences can be explained by the age differences of the two groups, 30.39 in men and 37.48 in women. CT was about 7 μm thicker in men, on average, but the men in this study were, on average 7 years younger. According to the correlation formulas established by this database, CT in a sex and age-matched group would like have been almost identical.

A few studies have been previously performed in adults using high penetration OCT but without comparing different age groups. We analysed CT comparing several ranges of age, with a 20-year gap. The first two age groups spanned 0 to 10 and from 10 to 20 years old. These times were selected because eye growth undergoes two phases, first until age 6 years, reaching emmetropization, and second from 7 to 19 years of age, when global expansion of the eye takes place.[86] CT profile changed in every group and the choroid measured thinner as age increases, showing statistically significant differences. This decrease was found to be progressive until 40 years old, at which point the most significant variation takes

place, from 313.9 µm in the 21-40 years old group to 264.6 µm in the 41-60 years old one (49 µm difference). Interestingly from 40 years on (41-60 vs. >60 years) the differences in CT were not found to be statistically significant in either mean MCT or SFCT. Variations when taking into account one eye per patient only (as stated by Ray et al[87]) or both were minimal, obtaining calculated decreases of 9.4 vs. 10 µm per decade in MCT and 8.5 vs. 8.87 µm per patient in SFCT.

The choroid normally is thickest in the subfoveal region decreasing slowly and progressively towards the temporal aspect and more steeply towards the optic nerve,[88,89] with a bowl-shaped contour.[90]

Adhi et al described significant alterations in choroidal morphological features in the majority of eyes with DR. They found an irregular temporal choroidoscleral interface inflection point in 8 of 9 eyes with non-proliferative DR (89%), 9 of 10 eyes with proliferative DR (90%), and 13 of 14 eyes with diabetic macular oedema (93%) compared with 0 of 24 in controls.[90] The presence of an irregular temporal choroidoscleral interface inflection contour with focal thinning of the choroid has been detected in some diseases (diabetic retinopathy and age-related macular degeneration).[73,90,91]

Dolz-Marco et al[92] reported a bilateral case of focal inferotemporal scleral bulge with a concave choroidal thinning surrounded by normal choroidal tissue. The authors hypothesized that this finding could be related to the inferior oblique muscle leading to inward compression of the choroid, not being able to study the scleral wall, as it was not entirely visible.

No anomalies in the fundus examination were found that could justify this

137

thickening in our series of patients with temporal choroidoscleral interface inflection. SS-OCT analysis did not detect any alteration in the choroid of these patients other than one inflection point. On the other hand, an image that could represent the superior edge of the insertion of the inferior oblique muscle in the sclera was identified, together with a thin, hypo-reflective line parallel to the sclera/choroid limit that could match the intra-scleral portion of the temporal long posterior ciliary artery.

The reason why retinal vessels seem to be hyper-reflective in OCT images, while choroidal vessels look hypo-reflective is related to the velocity of blood cells through them. The blood flow velocity inside choroidal vessels is much higher than that of retinal vessels. OCT imaging is based on interferometry, where an interference fringe is detected to construct the intensity of the signal. Fast speed of the blood cells makes the interference fringe vanish, thus no signal is observed inside the choroidal vessels. On the other hand blood cell speed is relatively slow in the case of retinal vascular structures, which contributes to the interference signal as a hyper-reflective signal.

Reported studies on the anatomy of the posterior aspect of the globe and the vascular and muscular structures and its relation to the sclera show that the anterior and superior limit of the posterior insertion of the inferior oblique muscle coincides with the horizontal line/meridian, within 5.7 mm of the fovea.[93]

The mean distance from the inflection point to the fovea was 4427 μm in our series and always located temporal to the fovea. The presence of the inflection point

138

is probably related to the insertion of the inferior oblique muscle, which is believed to be 5.7 mm from the fovea. The traction applied to the sclera by the tendon might cause a separation of the scleral wall leading to its deformation and a thickening of the choroid. Based on the anatomical descriptions of this region, the parallel, hypo-reflective line at this level could correspond to the intra-scleral portion of the temporal long posterior ciliary artery.

The fact that this finding is more frequent in younger healthy people, especially those under age 15, could be explained by the reduced scleral stiffness in younger age,[94] that could facilitate the deformation induced by the traction of the inferior oblique muscle tendon.

Several studies have been published about CT in healthy populations. Ding et al. analysed the CT in 210 healthy volunteers (420 eyes) with no ophthalmic disease history using EDI SD-OCT at multiple locations: SFCT and 1 mm and 3 mm temporal, nasal, superior and inferior to the fovea. However, the authors did not analyse any differences between the eyes.[78] Ikuno et al. studied CT and its profile with a SS-OCT device in 86 eyes of 43 healthy Japanese subjects as well as the correlation with axial length, refractive error and age but they also published no data concerning any differences between right and left eyes.[74]

In contrast, Chen et al.[89] reported the factors influencing topographical and inter-ocular variations in CT in a 50 healthy adult population using EDI SD-OCT. They measured SFCT and also performed CT measurements at four paramacular loci (3 mm superior, inferior, temporal and nasal to the foveal centre). They analysed the relationship between inter-ocular differences in CT. The differences in CT between

139

right eye and left eye were 1.0 μm at SFCT, 13,6 μm at nasal and -2.9 μm at temporal location, which was not statistically significant different. Of note, there was a trend towards a thicker nasal CT (14 μm) in right eyes.

When comparing these data with the series reported in this study, at the same locations (SCFT, N3 CT and T3 CT), we observed that the difference comparing right eye and left eye was 7.45 μm in mean SFCT, 1.43 μm at T3 and 14.44 μm at N3. The differences between mean nasal CT (p=0.0002), mean nasal CT in men (p=0.003) and in women (p=0.03), mean CT at each nasal location (p=0.001, 0.002 and 0.08 respectively) were statistically significant. The choroid was thicker in the right eye at every nasal location for both sexes except for women at N1 (p=0.259).

The correlation of the CT obtained by Chen et al. between eyes was strongest for SFCT (r=0.90; p<0.001, Spearman correlation test), for nasal locations was r=0.83 (p<0.001, Spearman correlation test) and weakest for temporal locations (r=0.49; p<0.001, Spearman correlation test). In our patients, the study of correlation for mean CT at SF, N3 and T3 was similar (r=0.860, 0.853 and 0.754 respectively, p<0.001; Spearman correlation test). The CT profile described in their paper is very similar to the CT profile obtained in our work comparing right eyes to left eyes.

It is difficult to explain the strong and consistent evidence that right eyes have a thicker nasal choroid than left eyes in a healthy, young population. One possibility is a differential in blood flow between the two eyes due to lack of anatomic symmetry at the aortic arch. Such asymmetry has been suggested to explain the differences in incidence/prevalence of vascular pathologies between

right eyes and left eyes with respect to metastatic bacterial endophthalmitis[95] and retinal artery occlusion.[96–99]

Choroidal circulation is generated from short posterior ciliary arteries that penetrate through the sclera around of optical nerve in a variable number between 10 and 20; so the nasal choroid studied in our cases (choroid between fovea and optical nerve), is directly supplied from these short posterior ciliary arteries. Furthermore, short posterior ciliary arteries are branches of the ophthalmic artery, which is a branch of the internal carotid artery, which is a branch of the common carotid artery.[99]

The difference generated by the fact that the origin of the right common carotid artery lays in the brachiocephalic trunk instead of emerging directly from the aorta (as the left common carotid artery) is presumably responsible of a more proximal and direct blood flow to the right carotid.[95]

Given that most of the choroidal structure is vascular tissue (the mean vessel density in outer choroid is 87%)[100], a supposed higher blood flow in the right vs. left short posterior ciliary arteries may explain why the nasal choroid is thicker in RE, as stated in our study, and as described previously by Chen et al.[89]

In the present study, as in previous papers[88] we used spherical equivalent instead of axial length determinations since the procedure is less invasive and previous indications from the literature show that refraction, which is more convenient to obtain, provides equivalent modeling capability as axial length.[101]

The choroid has been proven to become thinner with age.[102] Our research group evaluated the choroid of healthy individuals across a wide age span (3 to 95

years old) finding that macular CT profile in healthy population was similar among the different age groups, and that healthy choroid showed a trend to become thinner with age, particularly comparing adults older than 40 years to children and younger adults. These differences were not attributable to gender and greater age-related CT variations appeared in the temporal sectors.[88] Analysing our results, it can be stated that the choroid has a wide extent of normal thickness, with under 5% of healthy population presenting CT thicker than 320 μm and no differences in CT between genders.

Esmaeelpour et al. used a SD-OCT (840 nm) with a raster protocol image consisting of 512 A-scans and 512 B-scans across a 36x36º field to automatically analyse the choroidal layers of 45 healthy eyes with a mean age of 44 years (ranging from 23 to 84 years old), although using a different method.[103] Mean CT through the areas analysed was 228 μm and the thickness of the Haller's layer and Sattler's layer + choriocapillaris were 141 μm and 87 μm respectively.

Adhi et al[90] studied 24 eyes of 24 patients with a mean age of 64 years. CT measurements were manually performed using the caliper provided by the SD-OCT device and the choroid-sclera limit was well delimited in 79% of the eyes. The imaging protocol used consisted of 1-line rasters centred at the fovea. Subfoveal CT was 276 μm, subfoveal Haller's layer thickness was 224 μm and subfoveal Sattler's layer + choriocapillaris was 52 μm.

Using the same method, Branchini analysed the choroidal layers of 42 eyes of 42 patients with a mean age of 52 years, locating the choroid-sclera limit in 92% of them.[104] They manually measured CT and its layers at the subfoveal location using

two more measurement points 750 μm away from the fovea in both the nasal and the temporal sectors. They found the subfoveal CT of their sample to be of 256 μm. Haller's layer and Sattler's layer + choriocapillaris thickness were 204 and 53 μm respectively.

In the present study, 169 eyes of 169 patients were analysed using a SS-OCT device, being the largest sample analysing choroidal layers to the best of our knowledge. The mean age was lower that other studies' at 33.5 years old, while visualization of the choroidoscleral interface was possible in all of the eyes. Our figures for subfoveal CT, Haller's layer and Sattler's layer + choriocapillaris (305.8, 208.6 and 87.3 μm respectively) are larger than those presented by other authors. A similar finding was observed when in a previous paper our group compared CT measurements with other series using SD-OCT devices, with a difference of roughly 10 μm.[88] This difference and the fact that the mean age of our sample is considerably younger that that of other series could explain the different results.

In order to evaluate the choroid and its layers across the macula we added 8 more measure points to the subfoveal location (3 nasally and 5 more temporally, although N3 was not taken into account as described before). The mean values for CT, Haller's layer and Sattler's layers + choriocapillaris thickness were 260.81, 180.2 and 78.2 μm respectively. CT profile showed a similar morphology across different age groups with both CT and Haller's layer thickness decreasing significantly with age (p<0.001). Choriocapillaris plus Sattler's layer thickness showed an age-dependent reduction trend, but was not statistically significant (p=0.124). Our linear regression models led to a predicted loss of 0.93 μm per year in CT, 0.69 of those were due to

143

the thinning of Haller's layer, which explained 75% of the age-related thinning of the choroid. No differences due to gender were found in CT, or any of its layers in any age group. Our study shows that most of the age-related thinning of the choroid of normal eyes is due to the reduction of large vessels. These findings in healthy eyes disagree with histopathological findings in eyes with marked senile sclerosis, that show atrophy of small and medium vessels mostly.[102,105]

Spaide[102] stated that age-related loss of choroidal thickness was directly related to the loss of visible vessels, implying that it is a manifestation of small-vessel disease affecting the choroid. These data are not comparable to ours, as Spaide only included eyes with CT under 125 μm. Sarks' paper describes only two cases with choroidal sclerosis whose retinoscopy showed well-demarcated areas of choroidal sclerosis that are probably in relation with atrophic age-related macular degeneration, while our study analyses healthy patients.[105] This age-related choroidal thinning could be a key factor to establish the role of the choroid in retinal pathology.

Among the limitations of this study we may mention that CT had to be manually determined. There is now an automated software commercially available, Topcon DRI OCT-1 software (Ver. 9.01.003.02) for automated segmentation and thickness measurements in 3D or radial scan mode, however its accuracy in clinical practice is yet to be widely tested.

To our best knowledge this was the first report of CT determination in youngsters using SS-OCT. Few studies had been previously performed in adults using CT SS-OCT with different mean ages, and others using different methodology (no

vertical scans and no differences in CT were analysed). Our results may also differ from those previously performed with SD-OCT.

Another limitation is the fact that only the horizontal choroidal thickness profiles were studied, the use of SE instead of axial length, the fact that no correction was made for other variables such as central corneal thickness, intraocular pressure, systemic medication and blood pressure, and the impossibility to determine whether the vessels of the nasal choroid are wider in the right eye than in the left. This is due to the fact the resolution provided by the current technology does not allow a proper and accurate analysis of choroidal vessel thickness and there is no way to make sure you are analysing the largest diameter of a vessel because of the irregularity of choroidal vascularization.

As a further limitation, the choriocapillaris could not be differentiated from Sattler's layer due to the limitations imaging technology and that despite the high ICC.

In conclusion, according to our results, an answer can be given to the initial hypothesis affirming that macular CT is similar in the healthy young and adult population. CT profile is different and temporal choroid is thicker. The macular CT profile in healthy population is similar between different age groups, with the choroid in healthy eyes getting thinner with age, particularly comparing adults older than 40 years to children and younger adults. There are no differences due to gender. The greater CT variation due to age takes place in temporal sectors.

A temporal choroidoscleral interface inflection with focal thinning of the choroid can be considered a normal variation without clinical significance, especially

145

among young people. Further studies of the whole macular profile including the complete insertion of the inferior oblique muscle and with a larger number of patients will be necessary in order to establish the final characteristics of these variations and their incidence in healthy population.

The nasal area of the macular CT profile is thicker in RE when compared to LE. In contrast, subfoveal CT and temporal CT were not found to be different between eyes.

CT and Haller's layer grow progressively thinner as patients grow older and their profiles are similar between different groups of age. Age-related choroidal thinning seems to be mostly at the expense of Haller's layer. There are no differences due to gender.

Further studies would be necessary in order to confirm our results.

6. CONCLUSIONES POR OBJETIVOS

6. CONCLUSIONES POR OBJETIVOS

6.1.   CONCLUSIÓN 1

El grosor coroideo del área macular en la población pediátrica no es estadísticamente mayor que en adultos sanos. Sin embargo el perfil de la coroides no es igual, siendo las diferencias más apreciables en el sector temporal, donde hallamos el máximo grosor coroideo en niños, al contrario que en adultos, donde la coroides más gruesa se halla bajo la fóvea.

6.2.   CONCLUSIÓN 2

Según nuestros resultados el perfil de grosor coroideo macular es similar entre los diferentes grupos de edad. La coroides se adelgaza progresivamente con la edad, especialmente a partir de los 40 años. Las mayores variaciones tienen lugar en el sector temporal de la mácula. No existen diferencias en relación al sexo de los pacientes.

6.3.   CONCLUSIÓN 3

Hallamos una inflexión en la interfaz esclero-coroidea temporal, que puede ser considerada como una variación normal sin significación clínica, especialmente frecuente entre la población joven.

6.4.   CONCLUSIÓN 4

Según nuestros resultados existe una diferencia estadísticamente significativa entre el grosor coroideo macular de el ojo derecho y el ojo izquierdo. Por otra parte, el

148

grosor coroideo subfoveal y temporal no son diferentes cuando comparamos los dos ojos entre sí.

6.5. CONCLUSIÓN 5

El grosor de la coroides y el de la capa de Haller se adelgazan de manera progresiva con la edad, pero sus perfiles de grosor mantienen una forma similar cuando comparamos diferentes grupos de edad. La mayoría del adelgazamiento de la coroides parece ser a expensas del adelgazamiento de la capa de Haller. No se hallaron diferencias en relación al sexo de los pacientes.

6.6. CONCLUSIÓN 6

El área de luz vascular y el porcentaje de vasos/área total disminuye con la edad, mientras que el área estromal se mantiene estable.

6. CONCLUSIONS

CONCLUSION 1

Macular choroidal thickness in the pediatric population is not significantly thicker than that of healthy adults. Differences are more remarkable in the temporal side of the fovea.

CONCLUSION 2

To our knowledge, this is the first population study of CT of healthy eyes across a broad range of age groups using SS-OCT. As has been determined using spectral-domain OCT, CT decreases with advancing age, especially after age 40. There were no differences due to gender. The greatest CT variation takes place in temporal sectors.

CONCLUSION 3

Temporal choroidoscleral interface inflection or S-shaped profile of the choroidoscleral interface with focal thinning of the choroid can be considered a normal variation without clinical significance, especially in younger populations.

CONCLUSION 4

To the best of our knowledge, this is the first report suggesting thicker macular nasal choroid in the RE compared with the LE. In contrast, subfoveal CT and temporal CT were not found to be different between eyes.

CONCLUSION 5

According to our results, CT and Haller's layer grow progressively thinner as patients grow older and their profiles are similar between different groups of age. Age-related choroidal thinning seems to be mostly at the expense of Haller's layer. There were no differences due to gender.

CONCLUSION 6

The luminal area and the percentage of vascular/total area decrease with increasing age while stromal area remains stable.

7. FUTURO

7. FUTURO

7.1   ESTUDIO DE LA CORIOCAPILAR MEDIANTE ANGIOGRAFÍA OCT

Ya ha sido comentado que la capa coriocapilar es la que finalmente nutre y ayuda en el metabolismo de las estructuras de la retina más externa. Hay multitud de estudios histopatológicos que hablan de cómo una pobre circulación coroidea puede ser un factor de riesgo para el desarrollo de enfermedades oculares tales como la DMAE y la retinopatía diabética. La mejoría en las técnicas de imagen de la vascularización coroidea podría ayudar a la detección precoz de una la reducción de perfusión coriocapilar, lo que podría ser un buen marcador temprano para diversas enfermedades de la retina y la coroides.

La OCTa es una técnica no invasiva que permite la obtención de imágenes de la vascularización retiniana y de la superficie coroidea mediante un promedio de multitud de B-scans tomados en una misma posición. Se genera una imagen a partir de los componentes dinámicos de estos cortes (los glóbulos rojos del interior de los vasos sanguíneos), mientras que el tejido estático es sustraído para darnos una imagen final en la que sólo se aprecia el contenido de los vasos.

Aunque la coriocapilar se ha intentado estudiar utilizando OCTa basada en tecnología SD-OCT, la pobre penetración de esta longitud de onda a través del EPR ha limitado su utilidad clínica. Sin embargo, los prototipos más recientes de SS-OCT con longitudes de onda de entorno a 1050 nm y mayor penetración tisular permiten visualizar de una manera más clara esta capa de la coroides, y permiten ver como su patrón vascular varía en función de la zona estudiada, mostrando una mayor

densidad vascular en el área foveal y mostrando un patrón más difuso hacia la periferia.[106,107]

7.2 ÓPTICA ADAPTATIVA OCT

La óptica adaptativa OCT (OA-OCT) es una nueva tecnología que permite una captura mejorada de las estructuras microscópicas de la retina y de la vascularización coroidea que se encuentran habitualmente limitadas por las aberraciones que reducen la actual resolución trasversal de los sistemas de OCT. Gracias a la combinación de la gran resolución trasversal de la óptica adaptativa y la gran resolución vertical de la OCT, se consigue la imagen más precisa de todas las técnicas de imagen *in vivo* para estructuras celulares.[108]

Aunque ya se ha empleado para el estudio de las vascularización retiniana, la coroidea implica mayores dificultades al estar bajo el EPR, que dispersa la señal, impidiendo la obtención de imágenes de buena calidad.[108] Estos problemas se han solucionado recientemente utilizando la OA-OCT Doppler, mejorando el contraste de la coriocapilar, las arteriolas y las vénulas de la capa de Sattler.[109] Así, esta nueva técnica de imagen se podría utilizar para el estudio y la detección de alteraciones en las redes de la coriocapilar sin la necesidad de utilizar productos de contraste.

Sin embargo, esta técnica por el momento requiere un estudio en mayor profundidad para poder relacionar sus hallazgos con el conocimiento histopatológico actual y dado que muestra importantes limitaciones como el pequeño campo de trabajo estudiado, el elevado tiempo requerido para la toma de la imagen y la facilidad a la hora de generar artefactos que esto conlleva.

7.3 OCT DE CAMPO AMPLIO

Las imágenes de campo amplio para OCT que se habían obtenido hasta los últimos años de conseguían a base de usar protocolos de imagen destinados a áreas extra maculares y a hacer montajes de las imágenes a posteriori.[110]

Utilizando tecnología SD-OCT, los sistemas Spectralis (Heidelberg Engineering, Heidelberg, GERMANY) han incrementado su longitud máxima de B-scan desde los 9 mm gracias al uso de lentes de 30º hasta los 15 mm gracias a la adaptación de las lentes de 50º, anteriormente limitadas a la captura de imagen de autofluorescencia y de angiografías. La última generación de OCT con tecnología Swept-Source nos ofrece la posibilidad de capturar imágenes B-scan que pueden alcanzar los 12 mm de longitud, llegando según algunas publicaciones hasta los 100º de ángulo de visualización de la retina.[57]

7.4 ANGIOGRAFÍA CON VERDE DE INDODIANINA DE CAMPO ULTRA-AMPLIO

La tecnología de angiografía de campo amplio ya había mostrado su utilidad para la captura de imágenes de AF, sobretodo para la evaluación del grado de isquemia o no-perfusión periférica en pacientes con retinopatía diabética y otras enfermedades vasculares de la retina.

Una publicación reciente en la que los autores utilizan un sistema Optos modificado (Optos PLC, Dunfermline, SCOTLAND) para la obtención de imágenes de AVI de campo ultra-amplio, llegando hasta los 200º de campo.[111] Sería de esperar que técnicas como ésta puedan resultar útiles a la hora de incrementar nuestro

conocimiento sobre la coroides periférica y mejorar la detección, seguimiento y

tratamiento de patologías como la VCP, la CSC y las MNV.[111]

8. RESUMEN

8. RESUMEN

Objetivos: Empleando la tomografía de coherencia óptica Swept-Source (SS-OCT):

- Evaluar el grosor coroideo (GC) en la población infantil.

- Determinar el perfil del GC en población sana.

- Analizar las características morfológicas de la interfase coroides-esclerótica.

- Determinar la diferencia interocular en el perfil del GC macular.

- Estudiar el GC y sus variaciones con la edad, así como la morfología y cambios de las tres capas anatómicas de la coroides.

- Analizar la densidad de la coroides de la población sana.

Material y Métodos: Los criterios de inclusión fueron: mejor agudeza visual corregida entre 20/20 y 20/25, equivalente esférico (EE) entre ±3 dioptrías (D) y ausencia de enfermedades sistémicas u oculares. Las medidas y determinaciones fueron realizadas por dos o tres investigadores independientes y enmascarados según el caso, con un prototipo SS-OCT (Topcon Co., Japón).

Para el estudio de la población infantil se realizó un estudio comparativo transversal no intervencionista del área macular de 83 ojos de 43 pacientes pediátricos (<18 años). El GC macular se determinó independientemente por 3 observadores manualmente a intervalos de 750 μm midiendo la distancia desde el borde posterior del epitelio pigmentario de la retina (EPR) hasta la unión coroides-esclerótica, a lo largo de una línea de 4500 μm centrada en la fóvea. El GC pediátrico se comparó con el de 75 ojos de 50 voluntarios adultos sanos (≥18 años).

Para el estudio del perfil coroideo y la morfología de la interfase esclerótica-coroides se hizo un estudio transversal, no intervencionista de 276 ojos. Dos investigadores de manera independiente y enmascarada analizaron las características morfológicas de la interfase coroides-esclerótica, clasificando su contorno y forma como cóncavo (bowl-shaped) o inflexión (S-shaped) y midieron de forma manual el GC en posición subfoveal desde el límite posterior del EPR hasta la interfase esclerótica-coroides. Se realizaron tres mediciones cada 1000 μm nasal a la fóvea, y cinco más en sentido temporal a la misma. Los sujetos estudiados fueron estratificados en 5 grupos de edad.

Para buscar la posible existencia de diferencias en el GC entre ambos ojos se realizó un estudio transversal, no intervencionista en 140 ojos de 70 pacientes sanos con diferencias interoculares ≤0,25D. El perfil de la coroides macular se creo midiendo manualmente el GC subfoveal (GCSF) y realizando 3 mediciones más cada 1000 μm en sentido nasal y otras 5 en sentido temporal a la fóvea.

Para el análisis de las capas de la coroides se realizó un análisis retrospectivo de un subgrupo de 169 ojos de 169 sujetos. Dos observadores determinaron el GC macular horizontal y de la capa de Haller en posición subfoveal; se repitió este procedimiento cada 1000 μm en dirección nasal y temporal a la fóvea obteniendo 9 mediciones por ojo.

Para en análisis de la evolución de la densidad vascular de la coroides se llevó a cabo un estudio transversal, no intervencionista sobre 136 ojos de 136 pacientes. El análisis del estroma y de los vasos coroideos se realizó mediante una segmentación y una binarización automática empleando algoritmos validados.

159

Resultados: La edad media fue 10±3 años en la población pediátrica vs. 53±16 en la adulta (P<0,001). El equivalente esférico medio no fue diferente (P=0,06) entre los grupos. El GCSF medio fue de 312,9±65,3 μm en la población pediátrica vs. 305,6±102,6 μm en la adulta (P=0,19). El GC macular medio fue de 285,2±56,7 μm en la población pediátrica vs. 275,2±92,7 μm en la adulta (P=0,08). La distribución del GC fue distinto entre las poblaciones. La coroides temporal resultó ser más gruesa en la población pediátrica (320, 322 y 324 μm; P=0,002, P=0,001 y P=0,06 respectivamente), seguido por la subfoveal (312 μm) y la nasal (281, 239 y 195 μm).

En la población sana el GCSF medio fue de 301,89±80,53 μm (95%: 292,34 a 311,43). El GC macular medio fue de 258,69±64,59 μm (95%: 251,04 a 266,35). No se hallaron diferencias de grosor entre hombres y mujeres. El GCSF medio de los diferentes grupos estudiados fue de 325,6±51,1 μm (0 a 10 años), 316,7±90,1 μm (11 a 20 años), 313,9±80,3 μm (21 a 40 años), 264,6±79,3 μm (41 a 60 años) y 276,3±88,8 μm en mayores de 60 respectivamente (P<0,001; ANOVA). El GC macular medio fue de 286,0±43,5 μm, 277,7±68,2 μm, 264,0±61,9 μm, 223,4±62,2 μm y 229,7±66,1 μm respectivamente (P<0,001; ANOVA). El GC fue estadísticamente diferente entre los diferentes grupos etarios.

La presencia de inflexión coroideo-escleral fue identificada en 12,8% de los ojos. El GC en este punto fue de 372,1±76,8 μm y la distancia media a la fóvea fue de 4427,3±627,9 μm. Nueve pacientes mostraron esta inflexión en ambos ojos. No se hallaron cambios en el perfil retiniano en ninguno de los casos. La edad media de los pacientes con inflexión fue de 16±19 años vs. 36±25 años en el grupo de contorno

cóncavo (P=0,001). El GC temporal a 4000 y 5000 μm de la fóvea fue mayor en el grupo de contorno cóncavo.

En el estudio de las diferencias entre ojos la edad media fue de 25,4±19,9 años. El EE medio fue de 0,18±1,37. El GC macular medio fue mayor en ojos derecho que en izquierdos, (228,11±69,23 μm vs. 212,27±62,71 μm; P=0,0002). El GCSF medio y el GC macular temporal medio no fueron diferentes entre ambos ojos. No hubo diferencias en EE entre ojos derechos e izquierdos. El GC nasal medio también fue mayor en ojos derechos independientemente del género (hombres P=0,003 y mujeres p=0,03).

El grosor subfoveal de la capa de Haller fue 215,47±67,70 μm (207,30-227,86) y el de la capa de Sattler + coriocapilar fue 87,31±40,40 μm (83,38-95,65). No se hallaron diferencias significativas en ninguna de las capas al comparar hombres y mujeres. El perfil de GC fue similar entre los diferentes grupos de edad; el GC y de la capa de Haller disminuyó progresivamente con la edad (P=0,002). La capa de Sattler + coriocapilar mostró esta tendencia hacia el adelgazamiento, sin alcanzar la significación estadística (P=0,124).

El porcentaje de vascularización de la coroides fue de 54,40±8,35 %. El área coroidea, vascular y el porcentaje de vascularización coroidea fueron mayores en el grupo de <18 años que en el de >18 años (p<0,001). El área estromal no fue diferente (p=0,46). De la misma manera el área coroidea, vascular y el porcentaje de vascularización coroidea fueron diferentes en los 5 grupos de edad (p<0.001), mientras que no se hallaron diferencias en el área estromal (p=0.71).

Conclusiones: El GC macular pediátrico no es significativamente más grueso que el de adultos sanos. Las diferencias son más destacables en la zona temporal. El GC disminuye con la edad, especialmente después de los 40 años. No hay diferencias relacionadas con el género. Las mayores variaciones de GC tienen lugar en los sectores temporales de la coroides. La inflexión coroideo-esclerótica temporal o perfil S-shaped con adelgazamiento focal de la coroides puede ser considerado una variante normal sin significación clínica, especialmente en la población joven. Existe un mayor GC macular nasal en ojos derechos en comparación con los izquierdos, mientras que el GCSF y el grosor temporal no fue diferente entre los dos ojos. El perfil de la coroides, Haller y Sattler + coriocapilar son similares entre diferentes grupos de edad; las dos primeras se adelgazan de manera progresiva con la edad. El área luminal y el porcentaje de área vascular/área total disminuyen con la edad, mientras que el área estromal permanece estable.

8. SUMMARY

Objectives: While using Swept-Source optical coherence tomography (SS-OCT):

- Study choroidal thickness of healthy pediatric population.

- Study the choroidal thickness profile of healthy population.

- Study the morphologic characteristics of the choroid-sclera interface.

- Study interocular differences regarding the macular choroidal thickness profile.

- Study choroidal thickness, its variations with age and the changes that appear within its three layers.

- To analyse the vascular density of the choroid in a healthy population.

Material y Methods: Inclusion criteria were: Best corrected visual acuity between 20/20 and 20/25, spherical equivalent (SE) between ±3 diopters (D) and absence of systemic or ocular diseases. Measures were performed by 2 or 3 independent, masked observers using a SS-OCT prototype (Topcon Co. Japan).

To study pediatric population, a cross-sectional, non-interventional study was carried out on 83 eyes from 43 underage patients (<18 years old). Macular choroidal thickness was independently determined by 3 different observers who performed manual measures at 750 μm intervals, measuring the distance between the posterior edge of the RPE and the choroid-sclera junction through a 4500 μm fovea-centred line-scan. Pediatric choroidal thickness was compared to that of 75 eyes from 50 healthy, adult volunteers.

A cross-sectional, non-interventional study of 276 eyes was performed to analyse the choroidal thickness profile and the morphology of the choroid-sclera interface. Two independent, masked observers studied these characteristics and classified the shape into concave (bowl-shaped) or inflection (S-shaped), manually measuring choroidal thickness from the posterior edge of the RPE and the choroid-sclera junction under the fovea. They performed 8 more measures every 1000 μm towards temporal and nasal sectors. Analised subjects were stratified into 5 age groups.

A cross-sectional, non-interventional study was performed using 140 eyes from 70 patients with interocular differences of SE < 0.25 D to analyse interocular differences of choroidal thickness.

A retrospective analysis of 169 eyes from 169 patients was performed to study choroidal layers. Two independent, masked observers determined choroidal thickness, Haller's layer thickness and Sattler's layer + choriocapillary thickness under the fovea. They performed 8 more measures every 1000 μm towards temporal and nasal sectors.

A cross-sectional, non-interventional study was performed on 136 eyes from 136 to analyse the possible age-related changes regarding the percentage of vascularization of the choroid. Choroidal stroma and vessel area analysis involved automated segmentation and binarization using validated algorithms.

Results: Mean age was 10±3 years old in pediatric population vs. 53±16 in the adult group (P<0.001). SE was not different between groups (P=0.06). Mean subfoveal

164

choroidal thickness (SFCT) was 312.9±65.3 µm in pediatric population vs.

305.6±102.6 µm in adults (P=0.19). Mean macular choroidal thickness (MCT) was

285.2±56.7 µm in pediatric population vs. 275.2±92.7 µm in adults (P=0.08).

Choroidal thickness profiles were different between both groups. Temporal choroid

was shown to be thicker in pediatric subjects (320, 322 and 324 µm; P=0.002,

P=0.001 y P=0.06 respectively), followed by subfoveal thickness (312 µm) and nasal

(281, 239 y 195 µm).

Healthy population showed a mean SFCT of 301.89±80.53 µm (95%: 292.34

to 311.43). Mean MCT was 258.69±64.59 µm (95%: 251.04 to 266.35). There were

no statistically significant differences between men and women regarding choroidal

thickness. Mean SFCT in the different groups studied was 325.6±51.1 µm (0 to 10),

316.7±90.1 µm (11 to 20), 313.9±80.3 µm (21 to 40), 264.6±79.3 µm (41 to 60) and

276.3±88.8 µm (>60) respectively (P<0.001; ANOVA). Mean MCT was 286.0±43.5

µm, 277.7±68.2 µm, 264.0±61.9 µm, 223.4±62.2 µm and 229.7±66.1 µm respectively

(P<0.001; ANOVA). MCT was statistically different between different age groups.

The presence of a temporal choroidoscleral interface inflection was identified

in 12.8% of the eyes. The mean choroidal thickness was 372.1±76.8 µm and the

average distance from the inflection point to the fovea was 4427.3±627.9 µm. Nine

patients showed an inflective profile in both eyes. No changes in the retinal profile

were found in any of these cases. The mean age of the patients with an inflective

profile was 16±19 years (range 4 to 82) vs. 36±25 years (range 3 to 95) in the group

with a concave contour (p=0.001). The temporal choroidal thickness at 4,000 and

5,000 µm from the fovea was thicker in the group with a concave contour.

In the interocular difference study mean age was 25.4±19.9 years (4 to 75). The mean SE was 0.18±1.37 D (-3 to +3). Mean macular nasal CT was thicker in the right eye (RE) than in the left eye (LE), (228.11±69.23 μm vs. 212.27±62.71 μm; p= 0.0002; Student t test paired data). Mean SFCT and mean temporal CT were not different between RE and LE. No statistically significant differences were observed comparing SE in the RE vs. LE. Mean nasal CT by gender, was also thicker in the RE vs. LE. At each nasal determination CT in the RE was thicker than LE (p= 0.001, p= 0.0002 and p= 0.008 respectively).

Mean subfoveal thickness for Haller's layer was 215.47 ± 67.70 mm (95% confidence interval: 207.30–227.86) and mean subfoveal thickness for choriocapillaris plus Sattler's layer was 87.31 ± 40.40 mm (95% confidence interval: 83.38–95.65). No significant differences were found due to gender. Choroidal thickness profile was similar between groups with choroidal thickness and Haller's layer thickness decreasing with age (P = 0.002).

The percentage of choroidal vascularity was 54.40±8.35 %. Choroid area, vascular region and percentage of choroidal vascular density were statistically higher in the <18-year-old group vs. >18-year-old group (p<0.001). Stromal region was not different (p=0.46). In the same way, choroid area, vascular region and percentage of choroidal vascular density between the five age groups was statistically different (p<0.001), while stromal region was not (p=0.71).

Conclusions: Mean MCT in pediatric population is not statistically thicker than that of healthy adults. Differences are more remarkable in temporal sectors. Choroidal

thickness is reduced with age, especially after age 40. There are no gender-related differences. Greatest variations in choroidal thickness take place in temporal sectors. Temporal choroidoscleral interface inflection or S-shaped profile of the choroidoscleral interface with focal thinning of the choroid can be considered a normal variation without clinical significance, especially in younger populations. Nasal macular choroid is thicker in the RE compared with the LE. In contrast, subfoveal CT and temporal CT were not found to be different between eyes. CT and Haller's layer grow progressively thinner as patients grow older and their profiles are similar between different groups of age. Age-related choroidal thinning seems to be mostly at the expense of Haller's layer. The luminal area and the percentage of vascular/total area decrease with increasing age while stromal area remains stable.

9. BIBLIOGRAFÍA

9. BIBLIOGRAFÍA

1.   Guyer DR, Schachat AP GW. The choroid: structural considerations. In: Ryan

      SJ, ed. *Retina*. 4th ed. Philadelphia: Elsevier Mosby; 2006:33-34.

2.   Ramrattan RS, van der Schaft TL, Mooy CM, de Bruijn WC, Mulder PG, de Jong

      PT. Morphometric analysis of Bruch's membrane, the choriocapillaris, and the

      choroid in aging. *Invest Ophthalmol Vis Sci*. 1994;35:2857-2864.

3.   Kiel JW. *The Ocular Circulation*. San Rafael (CA); 2010.

4.   Sellheyer K. Development of the choroid and related structures. *Eye (Lond)*.

      1990;4:255-261.

5.   Mrejen S, Spaide RF. Optical coherence tomography: imaging of the choroid

      and beyond. *Surv Ophthalmol*. 2013;58:387-429.

6.   Mund M, Rodrigues M, Fine B. Light and electron microscopic observations on

      the pigmented layers of the developing human eye. *Am J Ophthalmol*.

      1972;73:167-182.

7.   Hogan MJ, Zimmerman LE. *Ophthalmic Pathology, an Atlas and Textbook*. 2nd

      ed. Philadelphia: Saunders; 1962.

8.   Booij J, Baas D, Beisekeeva J, Gorgels T, Bergen A. The dynamic nature of

      Bruch's membrane. *Prog Retin Eye Res*. 2010;29:1-18.

9.   Korte G, D'Aversa G. The elastic tissue of Bruch's membrane. Connections to

      choroidal elastic tissue and the ciliary epithelium of the rabbit and human

      eyes. *Arch Ophthalmol*. 1989;107:1654-1658.

10.   Blaauwgeers H, Holtkamp G, Rutten H, et al. Polarized vascular endothelial

      growth factor secretion by human retinal pigment epithelium and localization

of vascular endothelial growth factor receptors on the inner choriocapillaris.

Evidence for a trophic paracrine relation. *Am J Pathol*. 1999;155:421-428.

11. Nickla DL, Wallman J. The multifunctional choroid. *Prog Retin Eye Res*.

2010;29:144-168.

12. Lutjen-Drecoll E. Choroidal innervation in primate eyes. *Exp Eye Res*.

2006;82:357-361.

13. Hayreh SS. Hayreh SS. The blood supply of the optic nerve head and the

evaluation of it - myth and reality. *Prog Retin Eye Res*. 2001;20:563-593.

14. Wangsa-Wirawan N, Linsenmeier R. Retinal oxygen: fundamental and clinical

aspects. *Arch Ophthalmol*. 2003;121:547-557.

15. Friedman E. Choroidal blood flow. Pressure-flow relationships. *Arch

Ophthalmol*. 1970;83:95-99.

16. Kiel J, van Heuven W. Ocular perfusion pressure and choroidal blood flow in

the rabbit. *Invest Ophthalmol Vis Sci*. 1995;36:579-585.

17. Fujiwara T, Imamura Y, Giovinazzo V, Spaide R. Fundus autofluorescence and

optical coherence tomographic findings in acute zonal occult outer

retinopathy. *Retina*. 2010;30:1206-1216.

18. Mundt G, Hughes W. Ultrasonics in ocular diagnosis. *Am J Ophthalmol*.

1956;41:488-498.

19. Oksala A. The Clinical Value of Time-Amplitude Ultrasonography. *Am J

Ophthalmol*. 1964;57:453-460.

20. Goldberg RE, Sarin LK. Experiences with Ultrasonography. *Am J Ophthalmol*.

1966;61:1497-1502.

21. Yannuzzi LA, Ober MD, Slakter JS, et al. Ophthalmic fundus imaging: today and beyond. *Am J Ophthalmol*. 2004;137:511-524.

22. Goldberg MF, Hodes BL. Ultrasonographic diagnosis of choroidal malignant melanoma. *Surv Ophthalmol*. 1977;22:29-40.

23. Flower R, Hochheimer B. Clinical infrared absorption angiography of the choroid. *Am J Ophthalmol*. 1972;3:458-459.

24. Hyvarinen L, Maumenee AE, George T, Weinstein GW. Fluorescein angoigraphy of the choriocapillaris. *Am J Ophthalmol*. 1969;67:653-666.

25. Novotny H, Alvis D. A method of photographing fluorescence in circulating blood of the human eye. *Tech Doc Rep SAMTDR USAF Sch Aerosp Med*. 1960;60-82:1-4.

26. MacLean A, Maumenee A. Hemangioma of the choroid. *Am J Ophthalmol*. 1960;50:3-11.

27. Stanga PE, Lim JI, Hamilton P. Indocyanine green angiography in chorioretinal diseases: indications and interpretation: an evidence-based update. *Ophthalmology*. 2003;110:13-15.

28. Piccolino FC, Borgia L, Zinicola E, Iester M, Torrielli S. Pre-injection fluorescence in indocyanine green angiography. *Ophthalmology*. 1996;103:1837-1845.

29. Coscas F, Stanescu D, Coscas G, Soubrane G. Feeder vessel treatment of choroidal neovascularization in age-related macular degeneration. *J Fr d'Ophthalmolgie*. 2003;26:602-608.

30. Craandijk A, Van Beek C. Indocyanine green fluorescence angiography of the

choroid. *Br J Ophthalmol*. 1976;70:377-385.

31.   Mori K, Gehlbach P, Yoneya S, Shimizu K. Asymmetry of choroidal venous

vascular patterns in the human eye. *Ophthalmology*. 2004;111:507-512.

32.   Guyer D, Yannuzzi LA, Slakter JS. Digital indocyanine-green videoangiography

of occult choroidal neovascularization. *Ophthalmology*. 1994;101:1727-1737.

33.   Lim J, Aaberg TS, Capone AJ, Sternberg PJ. Indocyanine green angiography-

guided photocoagulation of choroidal neovascularization associated with

retinal pigment epithelial detachments. *Am J Ophthalmol*. 1997;123:524-532.

34.   Reichel E, Duker J, Puliafito C. Indocyanine green angiography and choroidal

neovascularization obscured by hemorrhage. *Ophthalmology*. 1995;102:1871-

1876.

35.   Shiraga F, Shiragami C, Matsuo T, Al E. Identification of ingrowth site of

idiopathic subfoveal choroidal neovascularization by indocyanine green

angiography. *Ophthalmology*. 2000;107:600-607.

36.   Staurenghi G, Orzalesi N, La Capria A, Aschero M. Laser treatment of feeder

vessels in subfoveal choroidal neovascular membranes. A revisitation using

dynamic indocyanine green angiography. *Ophthalmology*. 1998;105:2297-

2305.

37.   Huang D, Swanson E, Lin C, Schuman J, Stinson W, Chang W. Optical

coherence tomography. *Science (80-)*. 1991;254:1178-1181.

38.   Drexler W, Fujimoto J. State-of-the-art retinal optical coherence tomography.

Prog Retin Eye Res. 2008;27:45-88.

39.   de Amorim Garcia Filho C, Yehoshua Z, Gregori G, Puliafito CA, Rosenfeld PJ.

Optical coherence tomography. In: Ryan SJ, ed. *Retina*. 5th ed. Elsevier

Saunders; 2013:82-110.

40. Spaide R, Koizumi H, Pozzoni M. Enhanced depth imaging spectral-domain

optical coherence tomography. *Am J Ophthalmol*. 2008;146:496-500.

41. Margolis R, Spaide RF. A pilot study of enhanced depth imaging optical

coherence tomography of the choroid in normal eyes. *Am J Ophthalmol*.

2009;147:811-815.

42. Huber R, Adler D, Srinivasan V, JG. F. Fourier domain mode locking at 1050 nm

for ultra-high-speed optical coherence tomography of the human retina at

236,000 axial scans per second. *Opt Lett*. 2007;32:2049–2051.

43. Unterhuber A, Povazay B, Hermann B, Sattmann H, Chavez-Pirson A, Drexler

W. In vivo retinal optical coherence tomography at 1040 nm-enhanced

penetration into the choroid. *Opt Express*. 2005;13:3252–3258.

44. Lim H, de Boer J, Park B, Lee E, Yelin R, Yun S. Optical frequency domain

imaging with a rapidly swept laser in the 815-870 nm range. *Opt Express*.

2006;14:5937–5944.

45. Ikuno Y, Maruko I, Yasuno Y, et al. Reproducibility of retinal and choroidal

thickness measurements in enhanced depth imaging and high-penetration

optical coherence tomography. *Invest Ophthalmol Vis Sci*. 2011;52:5536-5540.

46. Ruiz-Moreno J, Flores-Moreno I, Lugo F, Ruiz-Medrano J, Montero J, M. A.

Macular choroidal thickness in normal pediatric population measured by

Swept-Source Optical Coherence Tomography. *Invest Ophthalmol Vis Sci*.

2012;54:353-359.

47. Copete S, Flores-Moreno I, Montero J a, Duker JS, Ruiz-Moreno JM. Direct comparison of spectral-domain and swept-source OCT in the measurement of choroidal thickness in normal eyes. *Br J Ophthalmol*. 2014;98:334-338.

48. Ruiz-Medrano J, Flores-Moreno I, Montero JA, Duker JS, Ruiz-Moreno JM. Morphologic features of the choroidoscleral interface in a healthy population using swept-source optical coherence tomography. *Am J Ophthalmol*. 2015;160:596-601.

49. Podoleanu AG, Dobre GM, Cucu RG, Rosen RB. Sequential optical coherence tomography and confocal imaging. *Opt Lett*. 2004;29:364-366.

50. Motaghiannezam R, Schwartz D, Fraser S. In vivo human choroidal vascular pattern visualization using high-speed swept-source optical coherence tomography at 1060 nm. *Invest Ophthalmol Vis Sci*. 2012;53:2337–2348.

51. Mohler KJ, Draxinger W, Klein T, et al. Combined 60° Wide-Field Choroidal Thickness Maps and High-Definition En Face Vasculature Visualization Using Swept-Source Megahertz OCT at 1050 nm. *Invest Ophthalmol Vis Sci*. 2015;56:6284.

52. Alasil T, Ferrara D, Adhi M, et al. En face imaging of the choroid in polypoidal choroidal vasculopathy using swept-source optical coherence tomography. *Am J Ophthalmol*. 2015;159:634-643.

53. Sohrab M, Wu K, Fawzi A. A pilot study of morphometric analysis of choroidal vasculature in vivo, using en face optical coherence tomography. *PLoS One*. 2012;7:e48631.

54. Savastano MC, Lumbroso B, Rispoli M. In Vivo Characterization of Retinal

Vascularization Morphology Using Optical Coherence Tomography Angiography. *Retina*. 2015;35:2196-2203.

55.   de Carlo TE, Bonini Filho M, Chin AT, et al. Spectral-Domain Optical Coherence Tomography Angiography of Choroidal Neovascularization. *Ophthalmology*. 2015;122:1-11.

56.   Jia Y, Tan O, Tokayer J, et al. Split-spectrum amplitude de- correlation angiography with optical coherence tomography. *Opt Express*. 2012;20:4710-4725.

57.   Imamura Y, Fujiwara T, Margolis R, Spaide R. Enhanced depth imaging optical coherence tomography of the choroid in central serous chorioretinopathy. *Retina*. 2009;29:1469-1473.

58.   Maruko I, Iida T, Sugano Y, Ojima A, Sekiryu T. Subfoveal choroidal thickness in fellow eyes of patients with central serous chorioretinopathy. *Retina*. 2011;31:1603-1608.

59.   Yannuzzi LA. Indocyanine green angiography: a perspective on use in the clinical setting. *Am J Ophthalmol*. 2011;151:745-751.

60.   Chung SE, Kang SW, Lee JH, Kim YT. Choroidal thickness in polypoidal choroidal vasculopathy and exudative age-related macular degeneration. *Ophthalmology*. 2011;118:840-845.

61.   Koizumi H, Yamagishi T, Yamazaki T, Kawasaki R, Kinoshita S. Subfoveal choroidal thickness in typical age-related macular degeneration and polypoidal choroidal vasculopathy. *Graefes Arch Clin Exp Ophthalmol*. 2011;249:1123-1128.

62.   Ueta T, Obata R, Inoue Y, et al. Background comparison of typical age-related
       macular degeneration and polypoidal choroidal vasculopathy in Japanese
       patients. *Ophthalmology*. 2009;116:2400-2406.

63.   Chen W, Wang Z, Zhou X, Li B, Zhang H. Choroidal and photoreceptor layer
       thickness in myopic population. *Eur J Ophthalmol*. 2012;22:590-597.

64.   Flores-Moreno I, Lugo F, Duker JS, Ruiz-Moreno JM. The relationship between
       axial length and choroidal thickness in eyes with high myopia. *Am J
       Ophthalmol*. 2013;155:314-319.

65.   Fureder W, Krauth MT, Sperr WR, J. Evaluation of angiogenesis and vascular
       endothelial growth factor expression in the bone marrow of patients with
       aplastic anemia. *Am J Pathol*. 2006;168:123-130.

66.   Fujiwara T, Imamura Y, Margolis R, Slakter JS, Spaide RF. Enhanced depth
       imaging optical coherence tomography of the choroid in highly myopic eyes.
       Am J Ophthalmol. 2009;148:445-450.

67.   Aoyagi R, Hayashi T, Masai A, et al. Subfoveal choroidal thickness in multiple
       evanescent white dot syndrome. *Clin Exp Optom*. 2012;95:212-217.

68.   Channa R, Ibrahim M, Sepah Y, et al. Characterization of macular lesions in
       punctate inner choroidopathy with spectral domain optical coherence
       tomography. *J Ophthalmic Inflamm Infect*. 2012;2:113-120.

69.   Say EAT, Shah SU, Ferenczy S, Shields CL. Optical coherence tomography of
       retinal and choroidal tumors. *J Ophthalmol*. 2011;2011:385058.

70.   Shields CL, Pellegrini M, Ferenczy SR, Shields JA. Enhanced depth imaging
       optical coherence tomography of intraocular tumors: from placid to seasick to

rock and rolling topography--the 2013 Francesco Orzalesi Lecture. *Retina*.

2014;34:1495-1512.

71. Shields CL, Perez B, Materin MA, Mehta S, Shields JA. Optical coherence

tomography of choroidal osteoma in 22 cases: evidence for photoreceptor

atrophy over the decalcified portion of the tumor. *Ophthalmology*.

2007;114:53-58.

72. Branchini L, Regatieri C, Flores-Moreno I, Baumann B, Fujimoto J, Duker J.

Reproducibility of Choroidal Thickness Measurements Across Three Spectral

Domain Optical Coherence Tomography Systems. *Ophthalmology*.

2012;119:119-123.

73. Manjunath V, Goren J, Fujimoto JG, Duker JS. Analysis of choroidal thickness in

age-related macular degeneration using spectral-domain optical coherence

tomography. *Am J Ophthalmol*. 2011;152:663-668.

74. Ikuno Y, Kawaguchi K, Nouchi T, Yasuno Y. Choroidal thickness in healthy

Japanese subjects. *Invest Ophthalmol Vis Sci*. 2010;51:2173-2176.

75. Agawa T, Miura M, Ikuno Y, et al. Choroidal thickness measurement in healthy

Japanese subjects by three-dimensional high-penetration optical coherence

tomography. *Arch Clin Exp Ophthalmol*. 2011;249:1485-1492.

76. Ho J, Branchini L, Regatieri C, Krishnan C, Fujimoto JG, Duker JS. Analysis of

normal peripapillary choroidal thickness via spectral domain optical coherence

tomography. *Ophthalmology*. 2011;118:2001-2007.

77. Manjunath V, Taha M, Fujimoto JG, Duker JS. Choroidal thickness in normal

eyes measured using Cirrus HD optical coherence tomography. *Am J*

Ophthalmol. 2010;150:325-329.

78. Ding X, Li J, Zeng J, et al. Choroidal thickness in healthy Chinese subjects. *Invest Ophthalmol Vis Sci*. 2011;52:9555-9560.

79. Ouyang Y, Heussen FM, Mokwa N, et al. Spatial distribution of posterior pole choroidal thickness by spectral domain optical coherence tomography. *Invest Ophthalmol Vis Sci*. 2011;52:7019-7026.

80. Li X, Larsen M, Munch I. Subfoveal choroidal thickness in relation to sex and axial length in 93 danish university students. *Investig Opthalmology Vis Sci*. 2011;52:8438-8441.

81. Yamashita T, Yamashita T, Shirasawa M, Arimura N, Terasaki H, Sakamoto T. Repeatability and reproducibility of subfoveal choroidal thickness in normal eyes of Japanese using different SD-OCT devices. *Investig Opthalmology Vis Sci*. 2012;53:1102-1107.

82. Wei W, Xu L, Jonas J, et al. Subfoveal choroidal thickness: the Beijing Eye Study. *Ophthalmology*. 2013;120:175-180.

83. Shin J, Shin Y, Cho H, Lee B. Measurement of choroidal thickness in normal eyes using 3D OCT-1000 spectral domain optical coherence tomography. *Korean J Ophthalmol*. 2012;26:255-259.

84. Xu J, Xu L, Du KF, et al. Subfoveal choroidal thickness in diabetes and diabetic retinopathy. *Ophthalmology.* 2013;120:2023-2028.

85. Park K-A, Oh SY. Choroidal thickness in healthy children. *Retina*. 2013;33:1971-1976.

86. Ishii K, Iwata H, Oshika T. Quantitative evaluation of changes in eyeball shape

in emmetropization and myopic changes based on elliptic fourier descriptors. *Investig Opthalmology Vis Sci*. 2011;52:8585-8591.

87. Ray W, O'Day D. Statistical analysis of multi-eye data in ophthalmic research. *Investig Opthalmology Vis Sci*. 1985;26:1186-1188.

88. Ruiz-Medrano J, Flores-Moreno I, Peña-García P, Montero JA, Duker JS, Ruiz-Moreno JM. Macular choroidal thickness profile in a healthy population measured by swept-source optical coherence tomography. *Invest Ophthalmol Vis Sci*. 2014;55:3532-3542.

89. Chen FK, Yeoh J, Rahman W, Patel PJ, Tufail A, Da Cruz L. Topographic variation and interocular symmetry of macular choroidal thickness using enhanced depth imaging optical coherence tomography. *Invest Ophthalmol Vis Sci*. 2012;53:975-985.

90. Adhi M, Brewer E, Waheed NK, Duker JS. Analysis of morphological features and vascular layers of choroid in diabetic retinopathy using spectral-domain optical coherence tomography. *JAMA Ophthalmol*. 2013;131:1267-1274.

91. Regatieri C V, Branchini L, Carmody J, Fujimoto JG, Duker JS. Choroidal thickness in patients with diabetic retinopathy analyzed by spectral-domain optical coherence tomography. *Retina*. 2012;32:563-568.

92. Dolz-Marco R, Gallego-Pinazo R, Lopez-Galvez MI, et al. Focal Inferotemporal Scleral Bulge With Choroidal Thinning: A New Observation on High-Penetration Optical Coherence Tomography. *Retina*. 2015;35:600-602.

93. Siam ALH, El-Mamoun TA, Ali MH. A restudy of the surgical anatomy of the posterior aspect of the globe: an essential topography for exact macular

buckling. *Retina*. 2011;31:1405-1411.

94. Pallikaris IG, Kymionis GD, Ginis HS, Kounis GA, Tsilimbaris MK. Ocular rigidity in living human eyes. *Invest Ophthalmol Vis Sci*. 2005;46:409-414.

95. Greenwald MJ, Wohl LG, Sell CH. Metastatic bacterial endophthalmitis: a contemporary reappraisal. *Surv Ophthalmol*. 1986;31:81-101.

96. Hayreh SS, Zimmerman MB. Amaurosis fugax in ocular vascular occlusive disorders: prevalence and pathogeneses. *Retina*. 2014;34:115-122.

97. Leavitt JA, Larson TA, Hodge DO, Gullerud RE, J. The incidence of central retinal artery occlusion in Olmsted County, Minnesota. Am ;. *Am J Ophthalmol*. 2011;152:820-823.

98. Hayreh SS, Podhajsky PA, Zimmerman MB. Retinal artery occlusion: associated systemic and ophthalmic abnormalities. *Ophthalmology*. 2009;116:1928-1936.

99. Harris A, Kagemann L, Cioffi GA. Assessment of human ocular hemodynamics. *Surv Ophthalmol*. 1998;42:509-533.

100. Shorab M, Wu K, Fawzi AA, et al. A pilot study of morphometric analysis of choroidal vasculature in vivo, using en face optical coherence tomography. *PLoS One*. 2012;7:e48631.

101. Ruiz-Medrano J, Flores-Moreno I, Pena-Garcia P, Montero J, Duker JS, Ruiz-Moreno J. Author Response: Choroidal Thickness and Axial Length. *Invest Ophthalmol Vis Sci*. 2014;55:5055-5055.

102. Spaide R. Age-related choroidal atrophy. *Am J Ophthalmol*. 2009;147:801-810.

103. Esmaeelpour M, Kajic V, Zabihian B, et al. Choroidal Haller's and Sattler's Layer Thickness Measurement Using 3-Dimensional 1060-nm Optical Coherence

Tomography. *PLoS One*. 2014;9:e99690.

104.   Branchini L, Adhi M, Regatieri C, et al. Analysis of Choroidal Morphologic

Features and Vasculature in Healthy Eyes Using Spectral-Domain Optical

Coherence Tomography. *Ophthalmology*. 2013;120:1901-1908.

105.   Sarks S. Senile choroidal sclerosis. *Br J Ophthalmol*. 1973;57:98-109.

106.   Kolb JPJ, Klein T, Kufner CLC, Wieser W, Neubauer AAS, Huber R. Ultra-

widefield retinal MHz-OCT imaging with up to 100 degrees viewing angle.

Biomed Opt Express. 2015;6:1534-1552.

107.   Reznicek L, Klein T, Wieser W, et al. Megahertz ultra-wide-field swept-source

retina optical coherence tomography compared to current existing imaging

devices. *Graefe's Arch Clin Exp Ophthalmol = Albr von Graefes Arch für Klin

und Exp Ophthalmol*. 2014;252:1009-1016.

108.   Torti C, Povazay B, Hofer B, et al. Adaptive optics optical coherence

tomography at 120,000 depth scans/s for non-invasive cellular phenotyping of

the living human retina. *Opt Express*. 2009;17:19382-19400.

109.   Kurokawa K, Sasaki K, Makita S, Hong Y-J, Yasuno Y. Three-dimensional retinal

and choroidal capillary imaging by power Doppler optical coherence

angiography with adaptive optics. *Opt Express*. 2012;20:22796-22812.

110.   Mori K, Kanno J, Gehlbach PL, Yoneya S. Montage Images of Spectral-Domain

Optical Coherence Tomography in Eyes with Idiopathic Macular Holes.

Ophthalmology. 2012;119:2600-2608.

111.   Klufas MA, Yannuzzi NA, Pang CE, et al. Feasibility and clinical utility of ultra-

widefield indocyanine green angiography. *Retina*. 2015;35:508-520.